Investigation into the Effects of Tool Geometry and Metal Working Fluids on Tool Forces and Tool Surfaces during Orthogonal Tube Turning of Aluminum 6061 Alloy

by

Prajwal Swamy Sripathi

A thesis submitted to the Graduate Faculty of
Auburn University
in partial fulfillment of the
requirements for the Degree of
Master of Science

Auburn, Alabama
December 18, 2009

Keywords: metal cutting, metal working fluids, cutting parameters

Approved by

Lewis N Payton, Chair, Associate Research Professor of Mechanical Engineering
J T Black, Professor Emeritus of Industrial and Systems Engineering
Robert L Jackson, Associate Professor of Mechanical Engineering

Abstract

Orthogonal Metal Cutting has evolved as a significant way of analyzing the mechanics involved in the art of metal cutting. An orthogonal tube turning apparatus was constructed and validated. The instrument was used to investigate the effects of back rake angle, uncut chip thickness and cutting environments on the tool forces generated during tube turning. Surface roughness was used to parameterize tool surface finish for cutting each factor level combination of the experiment. This work empirically documents the variation of tool forces and tool surface roughness under the influence of various cutting parameters. Force ratios and shear plane angles are calculated using the classical metal cutting equations, analyzing the behavioral patterns and interdependence of cutting forces, tool surface roughness and shear angle.

Acknowledgements

It is with profound gratitude that I would like to thank my advisor Dr. Lewis N Payton for his incredible support and guidance. I am highly indebted to him for his continuous encouragement, advice and suggestions involving my academic course work and research. His support also includes funding for this research.

I would like to convey my heartfelt thanks to Dr. J T Black for supporting me with my academics and research throughout my schooling at Auburn University. His constant encouragement, motivation and counseling have been major factors responsible for the successful completion of my work.

I would also like to thank Dr. Robert L Jackson for his advice and encouragement with my research work. Thanks to XYRIS4000CL Taicaan and John McBride at the University of Southampton for lending the Taicaan confocal Laser Proflometer used to make the measurements.

Special thanks to Namo Pankaj Vijayakumar for his invaluable assistance and patience in helping me carry out my experiments. I would also like to thank my colleagues Sakthivael Kandaswaamy, Suresh Muthusamy, Alan Dunlavy, John David Jenkins and Eileen Vega Ortiz for their support, advice, guidance and suggestions with my work.

Finally, words alone cannot express the thanks I owe to my parents Mr. Sripathi N G and Mrs. Sujatha H and to my sister Pruthvi Sripathi for their invaluable support and guidance, special thanks to them for being a never ending source of inspiration in my life.

Table of Contents

List of Figures

List of Tables

Nomenclature

F_c Cutting Force; Force component acting in direction of motion of tool.

F_t Thrust Force; Force component acting in direction nomal to shear plane.

F Frictional Force upon Chip

N Normal Force upon Chip

μ Friction Co efficient

F_s Shear Force on the Plane

F_n Normal Force on the Plane

t Uncut Chip Thickness (also referred to as Feed Rate)

t_c Cut Chip Thickness

t/t_c Chip Thickness Ratio

A_s Area of the Shear Plane

τ_s Shear Stress on the Shear Plane

α Rake Angle

β Friction Angle

φ Shear Plane Angle

ψ Shear Front Angle

V Cutting Velocity

Vc Chip Velocity

Vs Shear Velocity

HPs Specific Horse Power

CHAPTER 1

INTRODUCTION

The process of material removal is one of the most extensively used mechanical processes in the industry. The material removal is by a cutting edge in oblique machining processes such as drilling, milling, turning, shaping where in most of these cases the cutting edge is not perpendicular to the cutting motion. In order to simplify the mathematical models, a two force component process called orthogonal machining has been developed and used extensively by metal cutting researchers. M.E.Merchant [1] in 1944 defined the orthogonal tube turning process as characterized by following assumptions,

- The plane of the cutting tool is parallel to the plane of the material being cut.
- The cutting velocity vector and the cutting edge are perpendicular, with the width of the cutting tool more than the width of the work piece.
- The plane of the cutting edge is perpendicular to the direction of motion, generating a plane surface as the work moves beyond the tool with a constant depth of cut.
- The cutting edge is perfectly sharp and has no contact on the clearance face.
- There is relative motion between work and tool with continuous chip formation with no built up edge formation.
- The shear and normal stress along the shear plane and the tool are uniform.

Researchers use orthogonal machining for research purposes since it is easy to model and obtain the required forces. Orthogonal machining is usually performed [2] on

1. Metal plates at low speed
2. Tube turning at moderate speed
3. Plate turning at high speed

Figure 1 shows the motion of the tool and the force system involved in the oblique machining. It can be modified to form a tube turning orthogonal system as in Figure 2 for the ease of understanding, modeling and analyzing the force components.

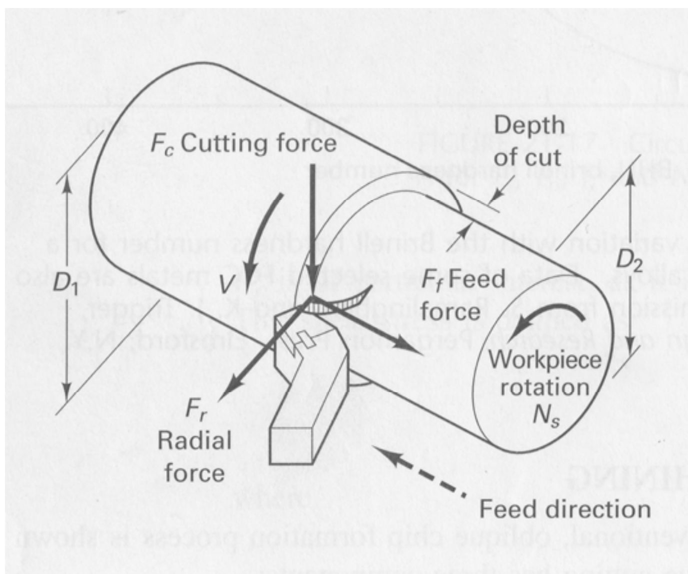

Figure 1: Oblique Machining [2]

F_c = Cutting Force; F_t = Thrust Force; F_r = Radial Force; V = Velocity of Cut; t = Uncut Chip Thickness; t_c = Cut Chip Thickness; V_c = Cut Chip Velocity.

The process chip formation is influenced by various parameters including workpiece material, cutting tool material, feed rate, cutting speed, tool rake angle, depth of cut and cutting environment. Extensive research has been carried out in order to understand the effects of these parameters on the cutting forces and tool wear.

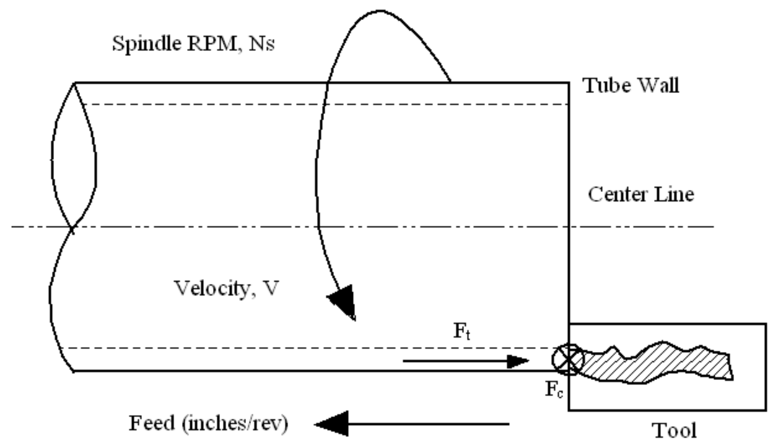

Figure 2: Orthogonal Tube Turning (Top View)

Orthogonal tube turning experiments have also been carried out to measure the variables such as chip geometry, chip thickness, cutting forces, cutting temperatures from which one can calculate shear plane angle, strain and strain rate.

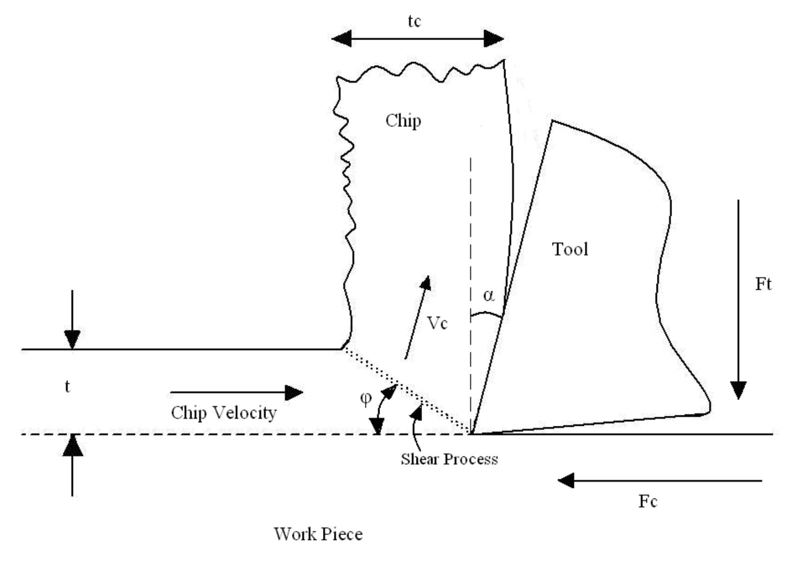

Figure 3: Orthogonal Metal Cutting Model

Historically, numerous models have been proposed for the parametric evaluation of the mechanisms of chip formation detailed in Figure. 2 including the force system involved in cutting process, the shear plane angle, φ and the tool wear. None of the models successfully explains the variation of tool forces and tool wear mechanism under the influence of different cutting parameters. The following work will address the construction and validation of an orthogonal tube turning set up on a 2 axis HAAS TL 42 lathe at Auburn University in order to explore the effects of cutting parameters like rake angle α, feed rate and cutting environment on the tool forces,surface roughness and shear angle.

CHAPTER 2

SCOPE AND OBJECTIVES

The main aim of the experiment was to develop a better understanding of the force system involved in the Orthogonal Tube Turning process, which seems to be the least well studied of the orthogonal turning experimental setups. The variation of these forces under different cutting environments and the progressive tool surface roughness were studied to develop an alternative yet efficient cooling system at the tool chip interface where almost all the energy produced by the plastic deformation of the material is converted into heat. The objectives of the experiment included:

1) A comprehensive review of the available orthogonal turning processes to include:
    a. Previous force measurements.
    b. Previous tool surface measurements.
2) Construct an experimental set up capable of accomplishing following goals:
    a. Measure the cutting forces generated during tube turning.
    b. Measure the tool surface roughness under different cutting conditions.
    c. Calculate the chip thickness ratio and onset of shear plane angle.
    d. Validate statistical repeatability and statistical sensitivity of the experiments.
    e. Achieve a statistical sampling power of 95% with 5 replications.
3) Develop a better understanding of the orthogonal tube turning process.
4) Design an experiment using ANOVA with the orthogonal tube turning equipment.
5) Compare resulting data to previous model.

CHAPTER 3

LITERATURE REVIEW

Overview

The principle of orthogonal machining is to observe variations in the metal cutting process for different parameters during the using a 2 dimensional geometry rather than the regular 3 dimensional geometry called oblique machining used in manufacturing environments. Orthogonal machining geometries can be attained utilizing a mill, a shaper or a lathe. In the lathe orthogonal machining can be done on a tube at normal speeds and on a disc at very high speeds with the tool feed in the direction of facing. The tool in both cases is wider than the piece being machined.

The tube to be machined is fastened firmly within the chuck. The tool is mounted on a dynamometer which is used for tube machining to measure the forces involved in the machining. The tool feeds perpendicular to the tube wall to generate a cutting force and a normal (or thrust) force. The tool's direction of motion eliminates the radial force or brings it down to near zero. The tube can be created from a solid through a grooving operation in order to increase the rigidity. This allows the use of a tailstock to support the center of the workpiece. This set-up is commonly done with high tensile strength materials such as steel, sacrificing long duration runs. Figure 3 shows a schematic of orthogonal tube turning on a lathe [2]. The jaws may be insulated to protect the work.

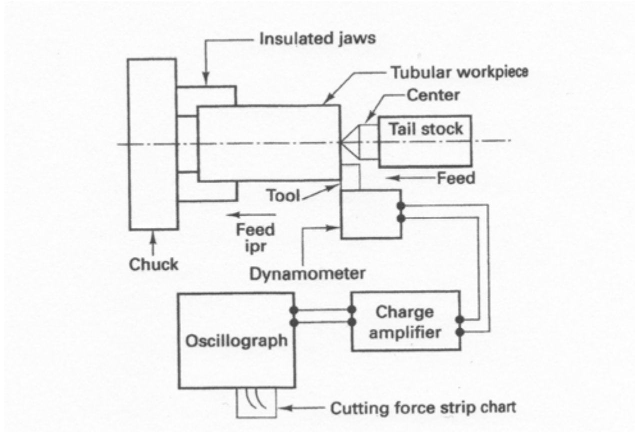

Figure 4: Orthogonal Tube Turning [2]

Dr. M.E. Merchant's [1] classic force diagram for orthogonal machining is depicted in Figure 4. In Figure 4, the cutting force F_c is the force generated by the motion of the work piece with respect to the tool and thrust force F_t is the force generated perpendicular to the point of contact of the tool and work piece. Fc and Ft form the resultant force R. These forces are measured with the dynamometer. The resultant force can be resolved into two components; the shearing force along the onset of shear plane, F_s, and a force normal to the onset of shear plane, F_n. The resultant force can also be resolved into F, the force parallel to the rake face and N, a force normal to the tool face. The onset of shear plane angle is represented as φ and the friction angle as β [3]. The cutting force and the thrust force are easily captured by the dynamometer setup shown in Figure 3.

Figure 5 summarizes the papers reviewed chronologically within this chapter by broad subject area for the reader. This should facilitate area reviews by future researchers as well. The papers reviewed within this work helped frame and support the objectives of this thesis. A detailed discussion of the many orthogonal machining models is precluded here but available through other sources [3, 22].

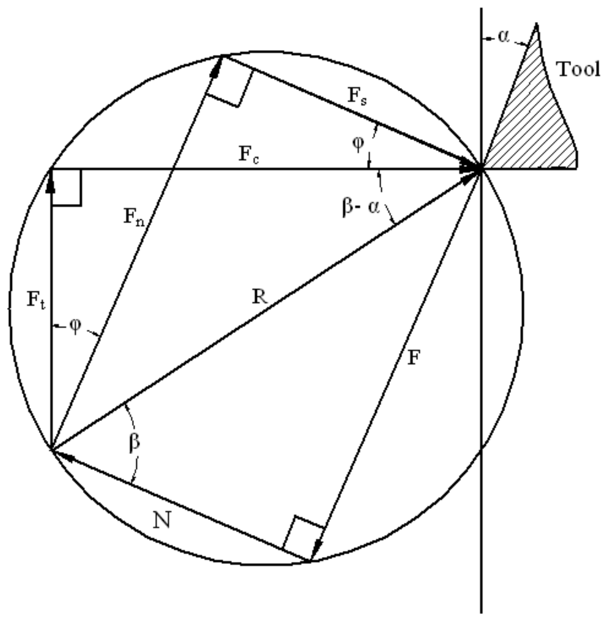

Figure 5: Merchant Circle diagram illustrating the Orthogonal Force System

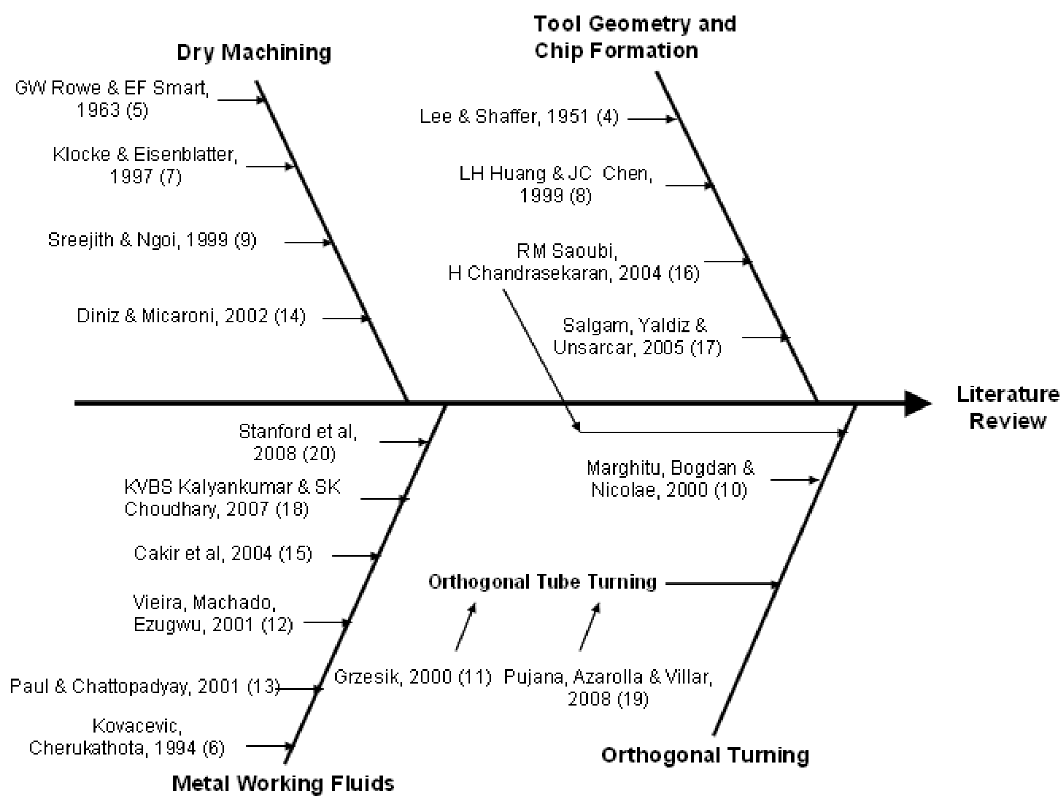

Figure 6: Summary of papers by keywords for this literature review

Chronological Review of Papers

The forces involved in machining processes are affected by parameters like feed, cutting speed, tool rake angle, depth of cut and cutting environment. An instrument designed to collect Orthogonal Tube Turning data must yield results that are consistent with the published literature observations as the experimentalist varies the cutting parameters (feed, tool rake, etc) and environment (dry, wet, etc).

Lee and Shaffer [4] in 1951 developed a slip line theory in which the chip formation is considered where the forces exerted by the tool are transmitted to the shear plane and in two dimensions; shear plane is the cut along which the tangential velocity is discontinuous. By applying this theory a plastic zone is assumed to exist within the chip bounded by shear plane, tool face and an imaginary boundary across which no stress is transmitted. This state can be represented on a Mohr's circle where the circle passes through the origin and the radius of the circle is equal to the shear strength since it assumes that the shear stress and normal stress are zero along the imaginary boundary. The angle between the slip line and the tool face depends on the friction on the tool face. It is assumed that sticking happens when the friction angle is larger than 45^o.

Rowe and Smart [5] in 1963 conducted experiments to show the importance of oxygen in dry machining environment. To examine this, machining was carried out in a vacuum chamber and was compared against oxygen environment. They used an 18^o rake, 6^o clearance high speed steel tool and a depth of cut 0.003 inch/rev on 0.15% carbon steel. Experiments revealed that the pure oxygen provides lower cutting forces when compared to a vacuum chamber or a normal atmosphere. It is also explained that a jet of oxygen directed at the cutting tool edge decreases the cutting force as against the atmospheric air.

Kovacevic, Cherukathota and Mazurkiewicz [6] in 1994 evaluated the effectiveness of high pressure water jet assisted cooling system in terms of cutting force, surface finish and tool wear during milling a stainless steel tubing. Water jets were delivered at high pressure through a nozzle onto a tool chip interface through the tool rake face. The tool forces tend to decrease drastically with the increase in water pressure. A smooth tool chip contact surface was achieved with the help of water jet cooling because of the absence of high shearing forces as compared to flood coolant. The reduction in tool wear was observed due to the reduced tool chip interface resulting from the fragmentation of the chip by the impinging jet.

Klocke and Eisenblatter [7] in 1997 presented the dry machining techniques for cast iron, steel, super alloys and titanium. The work presented a deterministic way of using the cutting parameters to reduce heat generated at the tool chip interface by reducing the friction. The control of chip formation was found to be of prime importance as it has significant effects on machining temperature.

Huang and Chen [8] in 1999 found that the temperature and force involved in machining increased with the increase in depth of cut and contact length of the tool/chip interface. They also found that the change in force due to the change in contact length of the tool chip interface is accompanied by the change in shear angle to match the change in resultant force. It is further explained that the shear angle becomes small as the deformation of the chip reduces thus reducing the cutting forces.

Sreejith and Ngoi [9] in 1999 presented the significance of dry machining in the near future and the cutting tool requirements for the same. It is stated that the cutting fluids has been greatly reduced due to the increase in use of mist coolant lubrication which is found to cause serious respiratory effects on the operator. This study insists on the use of cemented carbide, ultra-hard tool materials such as diamond and cubic boron nitride which produces better machined surfaces with remarkable increase in tool life due to the extremely high "hot" hardness of the tool materials.

Marghitu, Bogdan and Nicolae [10] in 2000 proposed a non-linear dynamics approach for the analysis of cutting and thrust force data obtained during orthogonal turning processes. They conducted turning operations on various materials like aluminum, ductile cast iron and grey cast iron. After applying several non-linear dynamic tools to determine the type of time evolution in terms of periodicity or non-periodicity of the forces, it was concluded that the orthogonal turning of aluminum work pieces is more stable than ductile cast iron and grey cast iron and produces a stable force response.

Grzesik [11] in 2000 investigated the influence of thin hard coatings on frictional behavior during the orthogonal turning process. During the experiment he was able to observe a visual difference at the tool chip contact area for different friction forces and was more pronounced in TiC/TiN coatings. The reduction in the friction forces suggested that the energy required in overcoming friction and shearing is less, where as the tangential force decreased intensively with increase in cutting speed. The reduction of friction force is probably due to an intensive thermal softening in the shearing zone. The reduction of contact area at higher speeds can intensify the thermal softening of the material. Two mechanisms that influence he contact stress were clarified in this research. One is reduction of the contact area and the other is intense thermal softening of the work at the interface. He also concluded that the interplay between mechanical stress at rake and thermal energy between the chip and tool is a key factor influencing the surface temperature of the tool.

Vieira, Machado and Ezugwu [12] in 2001 studied the cooling ability of different cutting fluids in comparison with dry machining. During the machining of AISI 8640 steel bars using carbide inserts an increase in the tool life was achieved under dry machining conditions as compared to other synthetic coolant environments. This was explained by the fact that dry machining generated higher cutting temperature leading to decrease in shear strength of the work material thus reducing the power consumption and eventually causing a reduction in tool wear. However their recorded surface roughness values under various cutting environments showed a random behavior with time.

Paul and Chattopadhyay [13] in 2001 investigated the beneficial effects of cryogenic cooling over dry and wet machining. They used liquid nitrogen jets on the tool wear surface and they found the forces involved in machining were less and the surface finish was better as against dry machining.

Diniz and Micaroni [14] in 2002 conducted experiments to remove the use of cutting fluid from a finish turning process without harming the tool life by increasing the feed and tool nose radius and decreasing the cutting speed. In turning a 1045 steel using carbide inserts under large feeds, tool life for dry cutting gets closer to that of wet turning where in synthetic oil with 6% concentration in water was used. With the increase in feed, heat generated at the tool chip interface increased, but the surface area on the tool to dissipate this heat also increased. This also resulted in decrease in specific cutting force. It is further concluded that with the increase in tool nose radius, the surface area dissipating the heat increases making the cooling of cutting zone not so necessary.

Cakir et al [15] in 2004 investigated the effects of cutting fluids to provide quantitative results about the cutting force, thrust force and the surface roughness. A 5% emulsion type cutting fluid was used as liquid coolant and compressed oxygen, nitrogen and carbon dioxide gas stored in cylinders at their normal temperatures were used. They used tubes ending with nozzles and fitted with suitable pressure regulators to direct the gases and the coolant at the cutting edge of the tool. The response curve of the mean cutting force and the thrust force showed that all gaseous and flood coolant is different from the dry cutting and also increases with increase in feed. Later Cakir analyzed the response of the shear plane angle under varying depth of cut. This showed an appreciable increase in the shear angle in the gaseous and flood coolant environment leading to smaller shear area and reduced cutting forces as compared to dry cutting environment. Although the effect of feed was obvious on the surface roughness of the machined parts the investigation concluded that the dry machining produced the highest value of roughness then wet machining.

Saoubi and Chandrashekaran [16] in 2004 investigated the effect of tool micro-geometry and temperature on coated tools. During their investigation they found that machining parameters chosen has an effect on temperature. An increase in cutting speed or feed resulted in the increase in the temperature. It was noted that the maximum temperature moved closer to the tip of the tool as cutting speed increased and away as the feed increased. The material hardness as well had an effect on the temperature. This may be explained by the fact that harder the materials, smaller will be the plastic deformation zone and the size of tool chip contact length.

Saglam, Yaldiz and Unsacar [17] in 2005 investigated the effect of tool geometry on the cutting forces and tool temperature. During machining large amount of energy is converted into heat energy considerably on the shear plane, rake face and clearance face. In orthogonal machining, the cutting is assumed to be uniform along the cutting edge; hence it is a two dimensional plane strain deformation. The cutting forces are exerted only in the direction of velocity and uncut chip. Rake angle determines the tool/chip contact area. They found that with the increase in the rake angle from 0^o up to 20^o has a positive effect on the tool by increasing the shear plane angle causing the reduction in the force system. But increasing beyond a point affects the tool's performance and accelerates tool wear. Smaller positive rake angles leaves a better finish but excessive positive angle weakens the tool causing tool breakage. The optimal rake angle was obtained as 12^o.

Kalyankumar and Choudhury [18] in 2007 investigated the effects of cryogenic cooling on tool wear and high frequency dynamic cutting forces generated during high speed machining of stainless steel. They observed from their experiments that the cutting force decreased with increase in cutting speed since the co-efficient of friction at the tool chip interface decreases and the shear plane angle increases, decreasing the area of shearing. They also found that the increase in feed and depth of cut increased the cutting force. Due to the increase in depth of cut and feed, the material removal rate also increases eventually the rate of plastic deformation and hence the cutting force increases. With the increase in cutting speed, higher cutting temperature and shortened contact area were observed. As a result the temperature concentration moved towards the tip of the tool resulting in the reduction of tool strength and increased tool wear. They concluded that the cutting force and tool wear was considerably less using the cryogenic environment compared to a dry environment as well as tool wear.

Pujana, Azarolla and Villar [19] in 2008 developed an in-process high speed photography for orthogonal turning to measure strain and strain rates. The work piece was micro-scale grid printed by the process of photochemical milling. They calculated the strain and strain rate manually based on the grid pattern. It was observed that the strain decreased with an increase in cutting speed and shear angle. They also noted that the chip topology for the working conditions they chose were not uniform. The chip formation of 42CrMo4 they observed was defined as a random process between serrated, transitional and continuous chip.

Stanford, Lister and Kibble [20] in 2008 studied the effects of cutting forces and tool wear under different cutting conditions. The behavior of the responses were derived by using a 4% dilution semi synthetic flood coolant, compressed air (20% oxygen at 0.27 MPa), Nitrogen gas (6% oxygen at 0.27 MPa) and liquid nitrogen and eventually compared against dry cutting. Plain carbon steel with UTS of 217 MPa was machined on a CNC turning center with a constant depth of cut of 1.2 mm and a feed rate of 0.1inch/rev under different cutting environments. Results show that the cutting force and the thrust force decreases with the use of flood coolant and liquid nitrogen as compared to the other gaseous environments and dry machining. Also the use of flood coolants showed a significant increase in the shear plane angle as compared to dry and gaseous environment cutting. It was observed that compressed air and nitrogen environment produced significantly thicker chips which can be confirmed by smaller shear angle and longer shear plane. Stanford et al further discusses the behavior of the crater wear and flank wear and concludes that although all the environments show significant wear, the dry cutting environment produces the highest level of wear. According to their experiments the best performing environment with considerably less wear is produced when flood coolant is used and lowest density of work piece adherence at the crater face and the flank edge is achieved. It is also explained that the use of nitrogen environment would assist in the reduction of notch wear reducing oxidation and providing better finish of the machined component.

One of the early advantages which drove metal cutting research was an interest in the power required by a machine to remove a certain "swept volume". Using the classic Merchant force diagram for example, total energy per unit time can be calculated by the product of primary cutting force, F_c, and the velocity of the cut, V. Due to the fact that many parameters can be varied during the cutting process that affects the total energy consumed, this energy is normalized by dividing it by the rate at which the material is removed. The material removal rate for a tube is the product of area being cut and the velocity perpendicular to the area at which the material is removed. Considering the thickness of uncut chip, t and the width of the tube wall, the energy per unit time or specific energy, u, is calculated by,

$$u = \frac{F_c.V}{t.w.V} = \frac{F_c}{t.w}$$

Specific energy can be partitioned into 4 components (a) Shear energy per unit volume, (b) Friction energy per unit volume, (c) Kinetic energy per unit volume and (d) Surface energy per unit volume. Specific energies can be used to calculate the power/volume/time (specific horsepower) and are available for most engineering material. They are a measure of the difficulty involved in machining a particular material and are sometimes used to model a given material's machinability.

Summary

The parametric effects upon measured results discussed within this literature review are summarized in Table 1. Any newly constructed instrument must yield results consistent with these historical results.

Parameter	Change	Cutting Force	Thrust Force	Chip Thickness	Wear	Shear Angle
Feed, t	Increase	Increase	Increase	Increase	Increase	Increase
Rake Angle (0-20)	Increase	Decrease	Decrease	Decrease	Decrease	Increase
Negative Rake Angle (< 0)	Increase	Increase	Increase	Increase	Increase	Decrease
Cutting Speed, v	Increase	Decrease	Decrease	Decrease	Increase	Decrease
Width of Cut, w	Increase	Increase	Increase	Increase	Increase	Decrease
Compressed Air	On	Increase	Increase	Increase	Decrease	Increase
Metal Working Fluid	On	Decrease	Decrease	Decrease	Decrease	Increase
Contact Length	Increase	Increase	Increase	Increase	Increase	Increase

Table 1: Summary of Variation of Response with Input Parameters.

.

CHAPTER 4

DESCRIPTION OF EQUIPMENT

This chapter documents the materials, equipment and software used to conduct the experimental research. Below is the list of the machine tools and instruments used to construct an orthogonal tube turning setup, the materials used in the experiments and further to carryout the data analysis.

- HAAS Two Axis Lathe (Model TL-2)
- KISTLER Three Component Dynamometer (Type 9257A)
- KISTLER Charge Amplifier (Model 5004)
- NATIONAL INSTRUMENTS DAQ device (NI USB-6008, with Digital I/O channels and a 32-bit counter)
- LABVIEW 8.2 Data Acquisition Software
- HSS Stick Tools (¾” x ¾” x 5”), ground to appropriate angles
- Aluminum 6061 Alloy Tubing (3” OD with wall thickness 1/8”)
- Nitrogen Cylinder supplied by Air Gas with Pressure Regulator
- VORTEC Cold Air Gun
- Commercial Spray Coolant Generator
- TaiCaan XYRIS series Surface Profiler with a LT-8010 Sensor head, LT-V201 Camera Unit and a LT-8105 Controller unit
- HARIG 618 AUTOMATIC Surface Grinder

Figure 7: HAAS Two Axis Lathe

The final experimental setup consists of a HAAS two axis lathe with a conventional tool post being replaced by a custom tool post to hold the HSS tool in a way that the force in the radial direction is reduced to zero. A three component KISTLER dynamometer is mounted on a steel plate which in turn is mounted onto the lathe bed in position of the conventional tool post. A custom made Aluminum tool post is fastened onto the Dynamometer so that the complete load on the tool holder will be transmitted to the dynamometer. An aluminum 6061 alloy tube is held firmly in the chuck for machining.

Control Validation of the Two Axis HAAS Lathe

The HAAS (Model TL-2) lathe features an option where the spindle rotations are input in revolutions per minute and feed is input in inches per revolution. Validation of feed in a lathe is of prime importance yet difficult with feed being in inches per revolution; hence to make it easier, the spindle speed was multiplied with feed to convert feed in terms of inches per minute.

A feed rate of 0.001 inches per revolution was chosen with a rpm of 100. The feed in terms of inches per minute is 0.1 inch/minute. To validate the X-Axis, the lathe was run and the time taken for the tool post to travel 0.1 inches were recorded with the help of a stop watch. The lathe took 60, 60 and 61 seconds on the first, second and third trial respectively. For Z-Axis, same steps were followed and the time taken for carriage to move 0.1 inches were recorded. The lathe took 62, 60 and 61 seconds respectively. Considering the fact that the stopwatch is being operated by a human, human error has to be taken into account during switching on and off the stopwatch and hence conclude that the lathe is validated for the expected feed rate. The lathe has an inbuilt feature to adjust the RPM according to the work piece radius in order to maintain the specified SFM.

Figure 8: KISTLER 9257A 3 Component Dynamometer

A calibrated 3 axis dynamometer collected the force data exterted on the tool in cutting, normal and radial directions.

Figure 9: KISTLER Charge Amplifiers (Model 5004)

Dual mode charge amplifiers were used to amplify the piezo electic output of the dynamometer.

Figure 10: National Instruments USB 6008

The output signal from the amplifiers is converted to digital voltage signals using a NI USB 6008 module and LabVIEW 8.2 software.

Figure 11: Vortec Cold Air Gun

A cold air gun usually used for spot cooling when machining plastics is used to achieve cold compressed air environment in this experiment.

Figure 12: Kool Mist Spray Coolant Generator

A spray coolant generator capable of producing a mist environment with the mixture of compressed air and water soluble synthetic coolant is used. Manufacturers recommended settings were used through out.

Figure 13: TaiCaan XYRIS Series Surface Profiler with a LT-8010 Sensor head, LT-V201 Camera Unit and a LT-8105 Controller unit.

Unit was graciously loaded to Auburn University by XYRIS4000CL Taicaan and John McBride at the University of Southampton. This Confocal Laser Profilometer was used for measuring the surface roughness of the tool

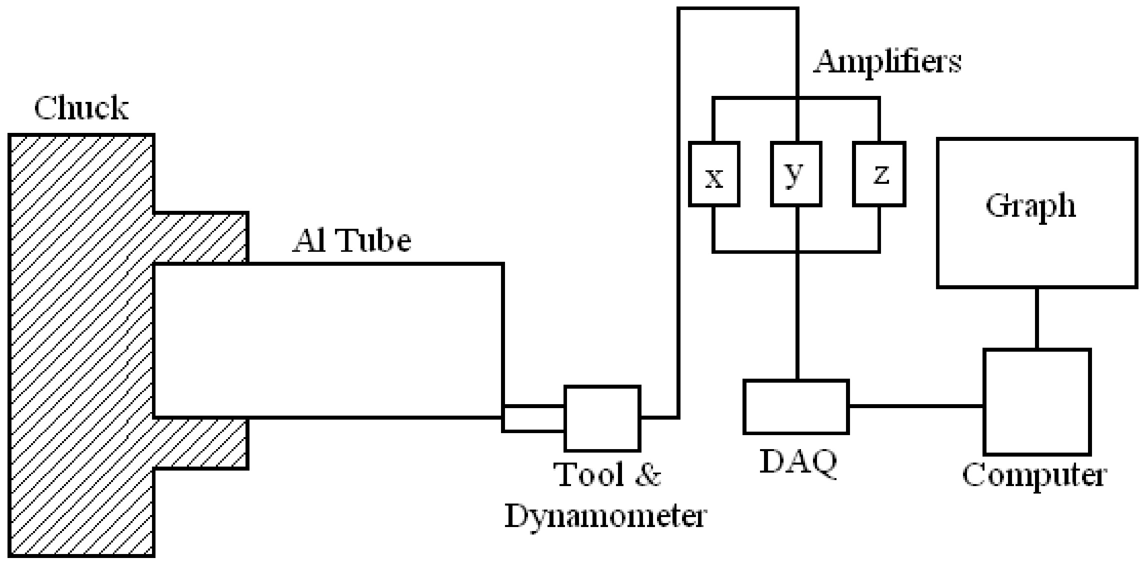

Figure 14: Overall Network Schematic of the Experimental Set up

The forces exerted on the tool are effectively delivered to the dynamometer which sends the piezo-electric signals to the charge amplifiers. The charge amplifiers amplify the signals and are traferred to a digital input/output DAQ system. The DAQ system converts the voltage signals to the force signals with the aid of labview computer software which displays the variation of forces with time.

CHAPTER 5

CONSTRUCTION OF THE ORTHOGONAL TUBE TURNING APPARATUS

The Auburn University instrument was designed with an objective to study the response of the tool force system, tool surface roughness and the shear angle behavior under the influence of various cutting parameters and environments during the orthogonal tube turning process on a HAAS two axis CNC lathe modified to carry out orthogonal tube turning. The basic geometry of the tube turning is as shown in Figure 19.

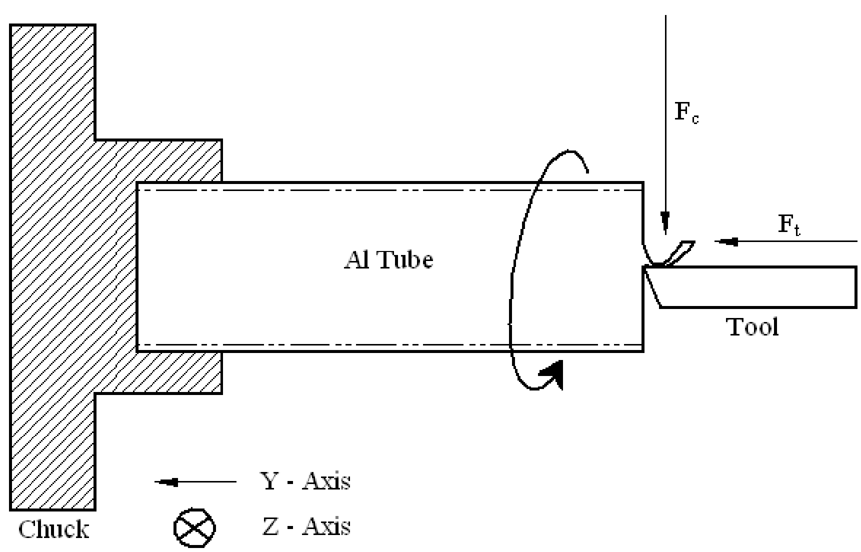

Figure 15: Geometry of Orthogonal Tube Turning

The KISTLER 3 component dynamometer is mounted on a steel plate and in turn is bolted down onto the lathe in the position of the tool post. A custom made tool holder machined using an aluminum alloy with a slot exactly sufficient to seat a ¾ inch tool is mounted onto the dynamometer in way that the total base area of the tool post is seated completely on the dynamometer surface to achieve total load transfer from the tool to the dynamometer. The tool holder consists of top and bottom blocks with bolts to clamp down the tool. The bottom block is bolted down to the dynamometer where as the top block is adjustable using four 2 ½ inch long, ¼ - 20 bolts at each edge to facilitate the tool change as shown in Figure 21.

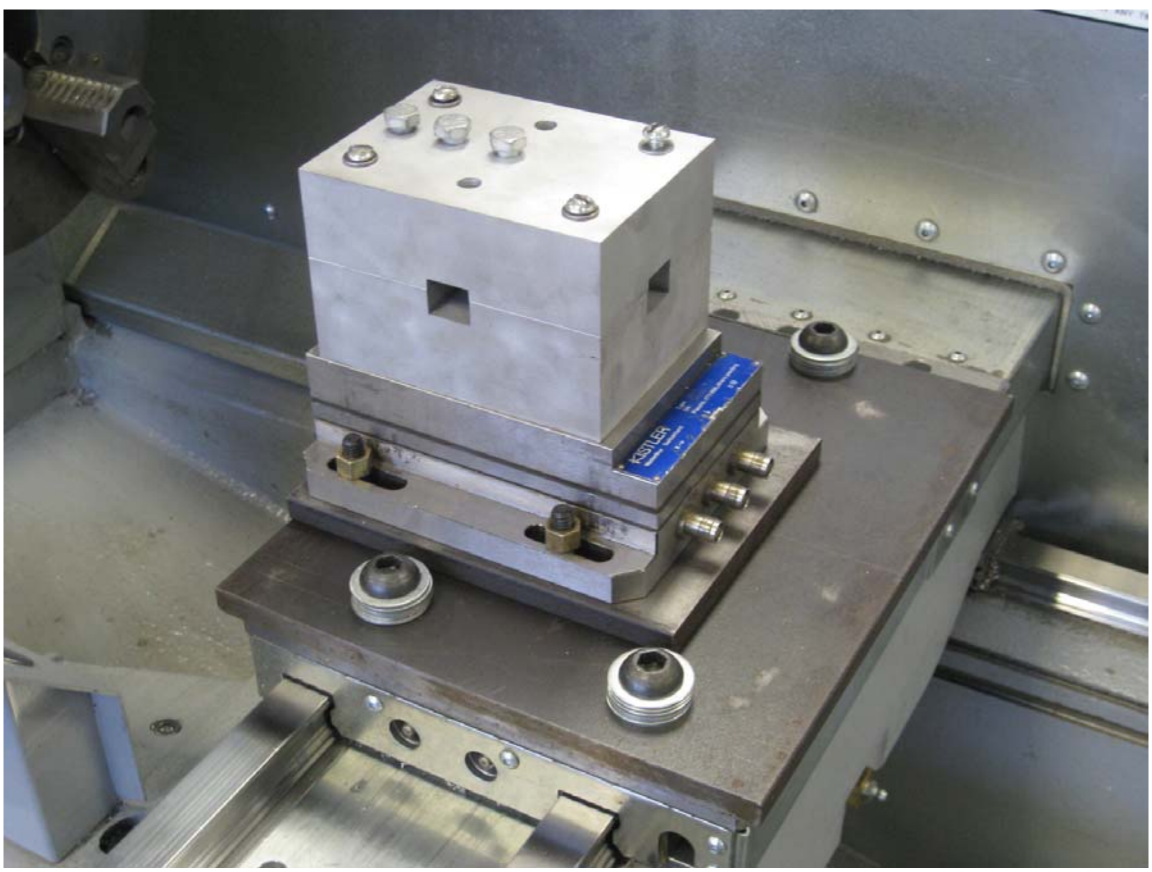

Figure 16: Dynamometer and Tool Holder Mounting Assembly

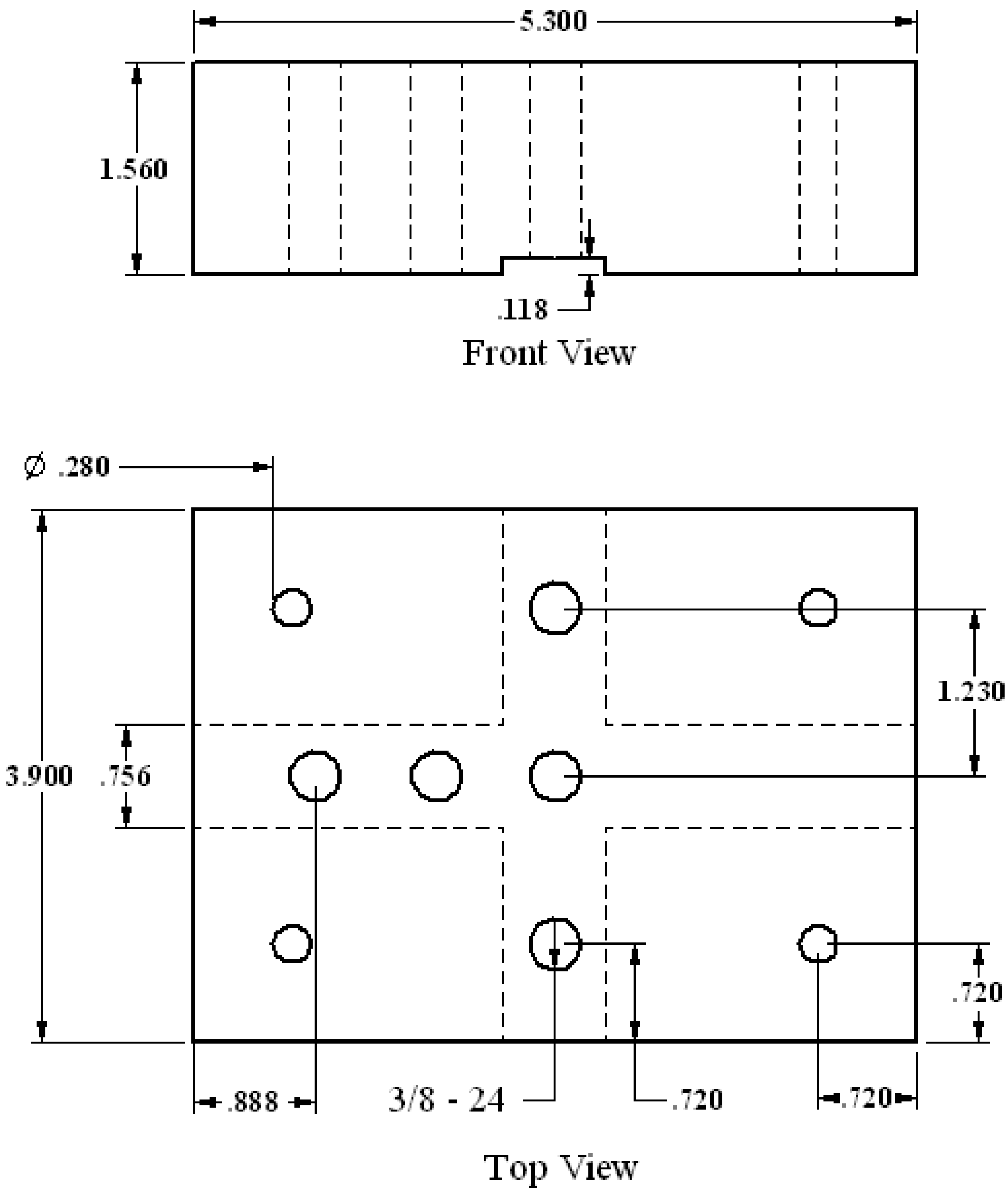

Figure 17: Top block of the Tool Holder.

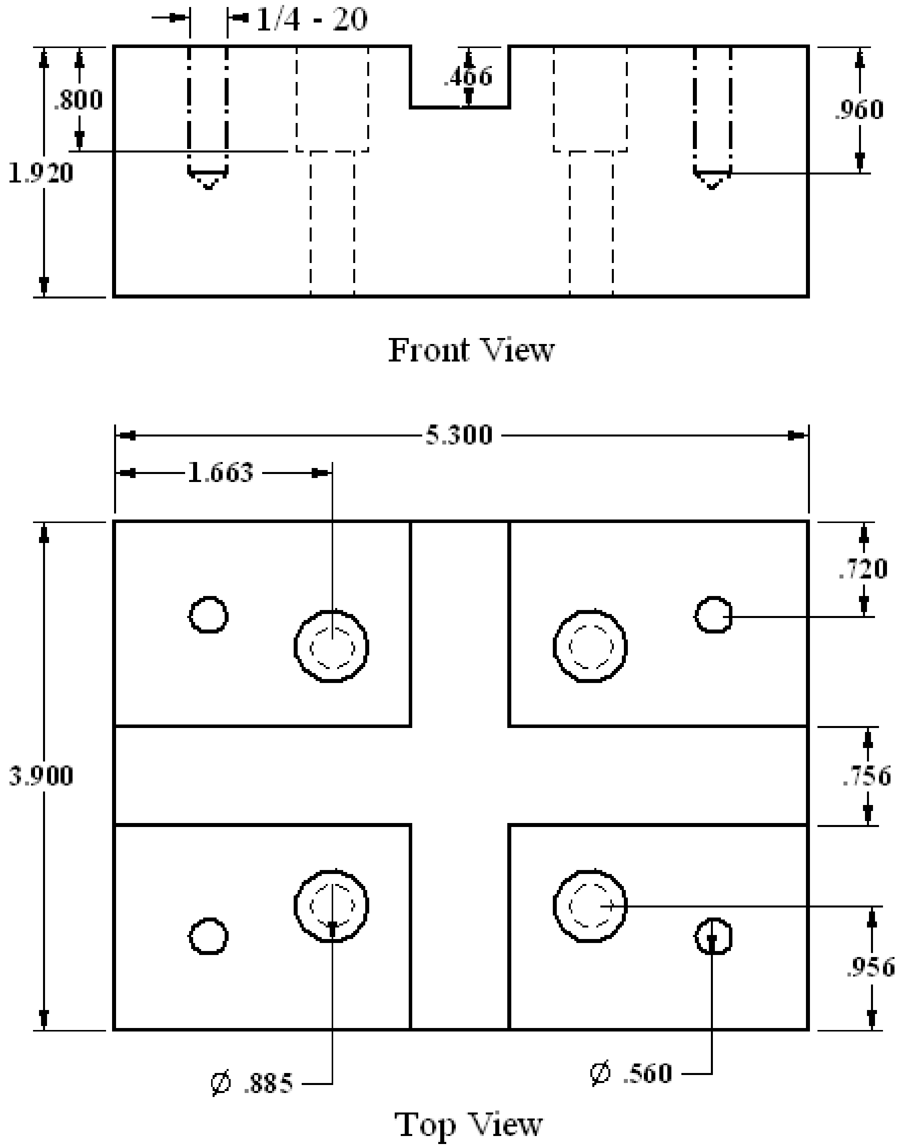

Figure 18: Bottom block of the Tool Holder.

The x, y and z output from the dynamometer which is in the form of an electric charge were connected to KISTLER 5004 charge amplifiers for signal amplification. The sensitivity and the linearity of the charge amplifiers are adjusted according to the manufacturer's calibration certificate (Appendix A). The amplifiers convert the electric charge from the piezoelectric transducer into a higher voltage, more sensible output. The output voltages from the charge amplifiers are then connected to the National Instruments (NI) USB - 6008 which has 12 digital input/output (DIO) channels and a 32-bit counters with a full speed USB interface.

Figure 19: Charge Amplifiers and USB DAQ system module connected to the LABVIEW 8.2 system software

The software interface for NI USB – 6008 is LABVIEW which reads out the force signals. The outputs of the Kistler Amplifiers are converted into cutting and normal force data by the software. The block diagram of the Lab View program used to convert the electrical signals to the force data is shown in Figure 24.

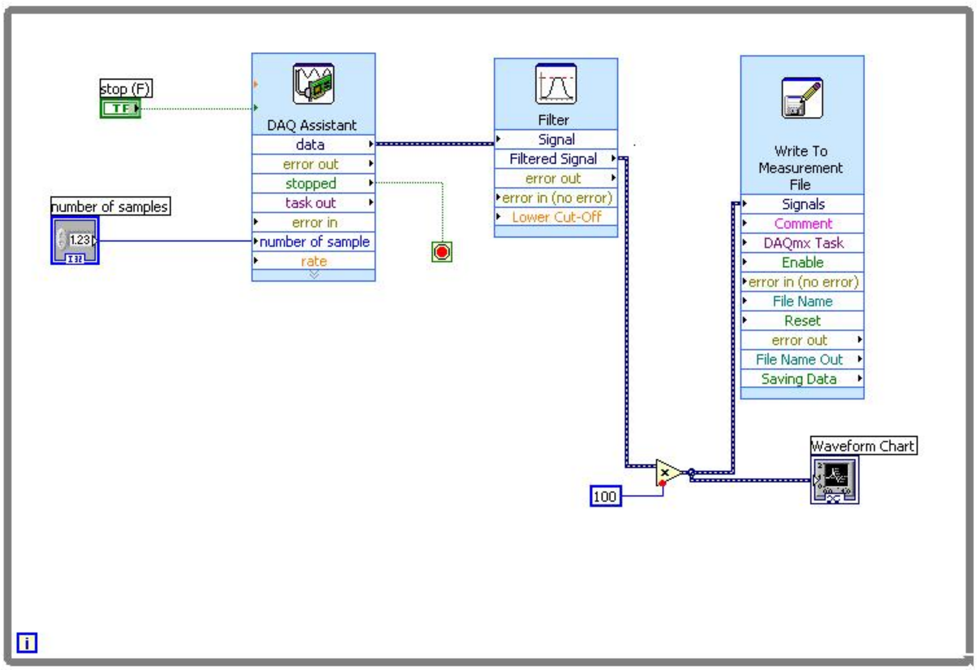

Figure 20: Block Diagram of the program in LABVIEW 8.2 Software

The DAQ assistant receives the signals from the amplifiers which are sent to the filtering block. These filtered signals are recorded in a measurement file and a waveform chart is displayed.

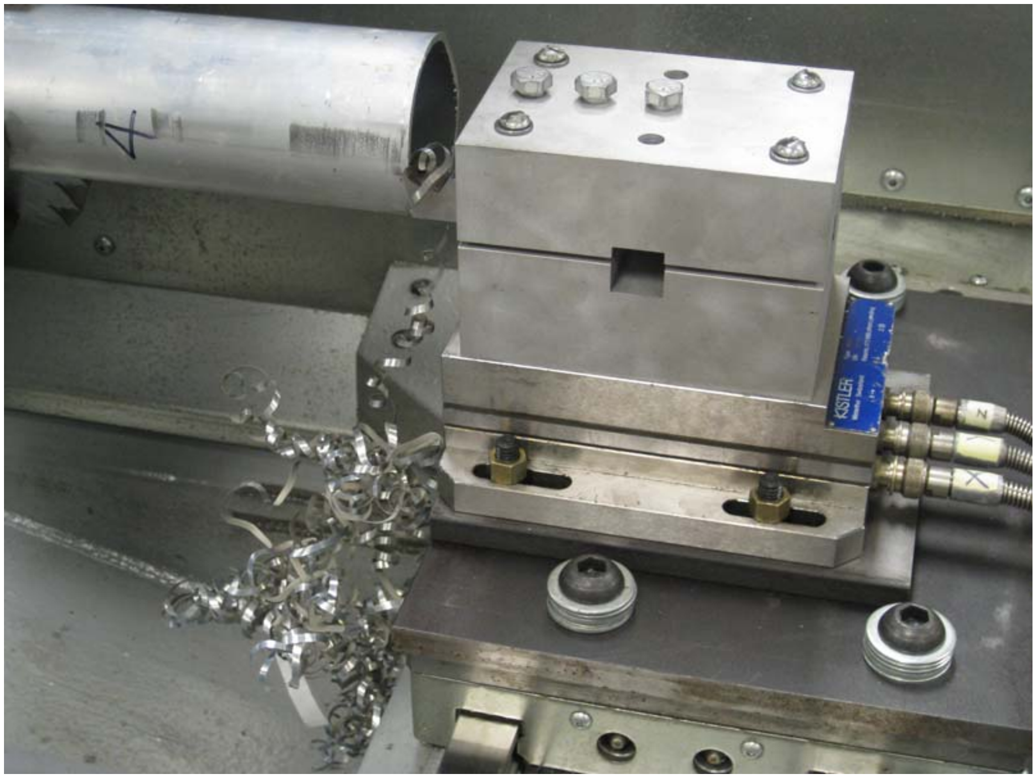

Figure 21: Dry Machining

Enviromental Controls

As mentioned in the literature review, it is desirable for a number of reasons to study the environmental effects upon the cutting process. Four different environments have been prepared initially for experiments at Auburn University using dry (or hard) turning with no applied gases or coolants, cold compressed air, gaseous nitrogen and commercially available water based spray coolants.

The dry machining is done at the atmospheric temperature without the aid of any apparatus to dissipate the heat generated at the tool chip interface. The tool mounted on the tool holder plunges into the material in the direction of the axis of the spindle rotation. A canned cycle for constant feed was used and the total material to be cut was calculated so that the tool cuts exactly for 60 seconds under all different feeds. This is the basic setup described by Figures (19) and (25).

Figure 22: Turning at Cold Compressed Air Environment with Vortex Air Gun

To achieve a cold compressed air environment a Vortex air gun with a nozzle is used to direct the cold air generated by the air gun to the tool chip interface. The Vortex air gun is designed to keep plastics cold and hard during machining so that they do not melt into the harder, hot tool. The inlet of the air gun is connected to a compressed air main bus through a pressure regulator. The compressed air enters the cylindrical generator which is proportionately larger than the hot tube where it causes the air to rotate. This rotating air is forced down on the inner walls of the hot tube at speeds reaching 1,000,000 rpm. At the end of the hot tube, a small portion of this air exits through a needle valve as hot air exhaust. The remaining air is forced back through the center of the incoming air stream at a slower speed. The heat in the slow moving air is transferred to the fast moving incoming air. This super cooled air flows through the center of the generator and exits through the cold air exhaust port. The nozzle connected to the exhaust port directs the cold air over the cutting zone. The pressure of the compressed air before it enters the cold air gun is maintained at 75 psi. Temperatures down to -70 degrees Fahreinheit are routinely achieved at the outlet to the nozzle.

Figure 23: Turning at Nitrogen Gas Environment

A Nitrogen cylinder with a suitable pressure regulator was used to generate a continuous directed flow of nitrogen gas at high pressure over the cutting zone at the tool chip interface. The outlet from the pressure regulator was connected to a suitable nozzle and clamped to a magnetic stand which can be seated on the lathe bed conveniently to adjust the direction of the gas flow. The pressure at the regulator was maintained at 75 psi and the outlet nozzle used for the nitrogen is same as the one used to direct cold compressed air at the cutting zone.

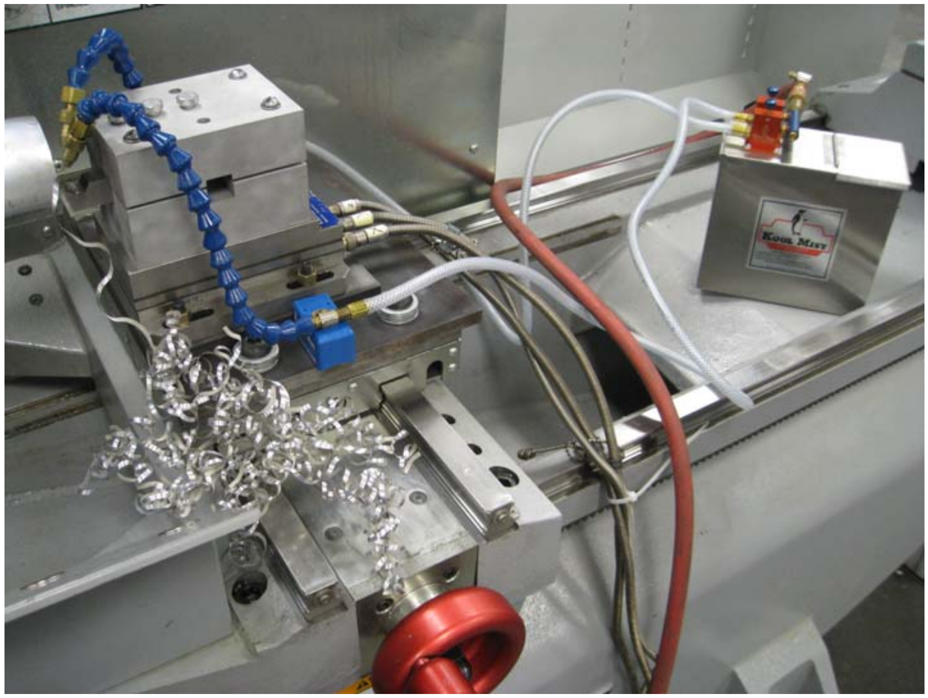

Figure 24: Turning at Spray Coolant Environment

A commericially available, popular cool mist environment was obtained using a spray coolant generator which basically consists of a steel tank with a siphon line immersed in the tank. The outlet of the siphon is connected to the valve fitted with an inlet and an outlet port. The inlet line is connected to the compressed air line fitted with a suitable pressure regulator maintained at 75 psi. The tank is filled with 1:40 ratio commericially available synthetic coolant and water. The compressed air entering the valve creates the suction in the siphon and a mist of spray coolant and compressed air is sprayed over the cutting zone. The coolant tank as supplied by the manufacturer has two outlet ports for the spray coolant and both the outlets are connected to separate nozzle and directed at the tool chip interface from either sides as shown in Figure 29. These are the manufacturer's recommended "ideal" settings. All components in the system were "new" out of the box and undamaged.

The continuous chips obtained during all different runs under various environments and various cutting parameters are collected and stored for analysis purposes as will be described later.

Tool Surface Roughness Measurements:

The average surface roughness of a tool face can be mapped using a confocal laser profilometer. A tool to be scanned was placed under the scanner so that the laser beam is projected above the surface of the tool and travels 3 mm in the x-direction so as to just stop at the edge of the tool and jump to the next line for scanning. Adjusting the area of the surface to be profiled is aided by a camera to position and preview the area to be scanned. The tool path of the laser over the profiled surface is as shown in figure 26.

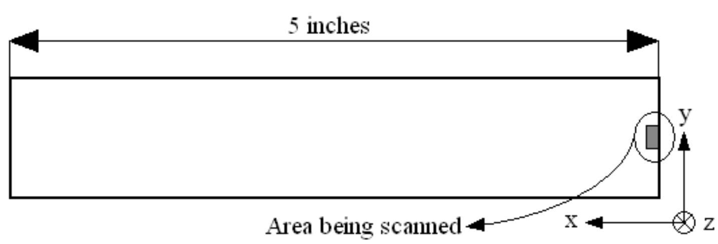

Figure 25: Area being scanned on top face of a ¾ x ¾ x 5 inch tool

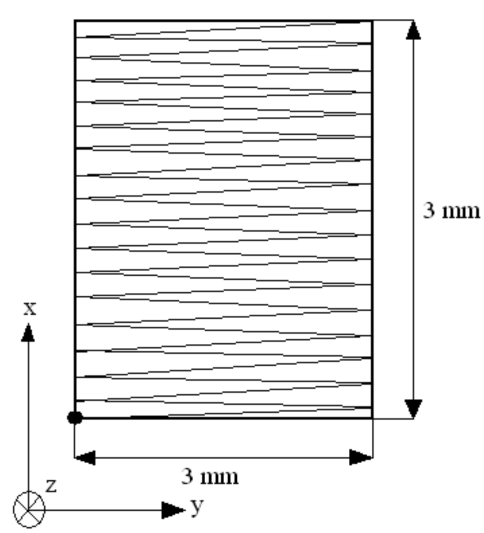

Figure 26: Laser Beam Path

The TAICAAN software used was programmed to scan 101 points in x direction (3 mm) and 101 points in y direction (3 mm) resulting in 10201 data points for each tool profiled. The number of points to be scanned can be varied depending upon the accuracy of the roughness value needed. The resolution of the instrument is evaluated as 0.1 µm according to manufacturer specifications.

The readout represents the height of the surface being profiled (in mm) from the tip of the laser probe. This profile data was used to calculate the root mean square deviation of the profile from the mean line. Suppose z_1, z_2, z_3... z_n represents the height variation of the surface from the laser tip, Root mean square deviation is defined as,

$$R_q = \sqrt{\frac{z_1^2 + z_2^2 + z_3^2 \ldots\ldots\ldots\ldots z_n^2}{n}}$$

The 'R_q' value calculated as above is a direct measure of the surface roughness. The same tool after being used for 300 seconds on a tube turning setup was used to map the profile again. The used tool is placed below the laser beam. With the aid of the camera unit, the position of the tool is adjusted to scan the same 3mm x 3mm area scanned for the unused tool. This was achieved through carefully positioning the tool by observing the light spot at the edge of the tool as shown in figure below. Before scanning the tool, the laser path is previewed using the camera multiple times to make sure the laser beam travel path is not crossing the edge of the tool and is over the light spot where tool wear is expected to be remarkable.

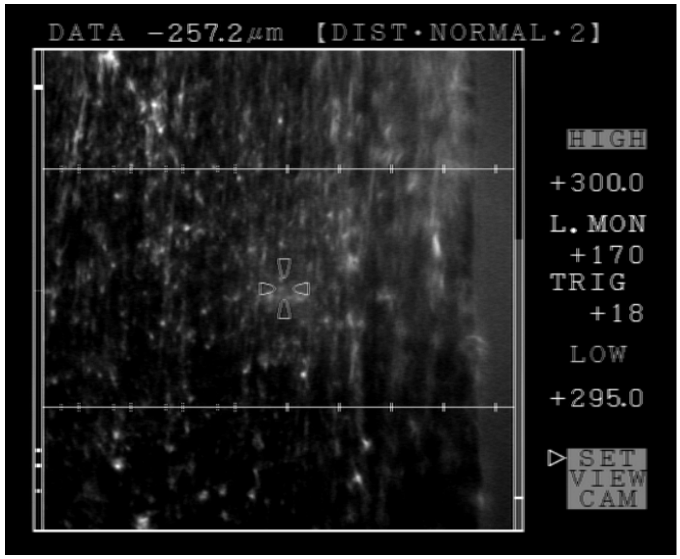

Figure 27: Enlarged camera view of the cutting edge.

This way the tool is profiled and subsequently the root mean square deviation is calculated. After obtaining the average surface roughness for new tool ($(R_q)_{new}$) and for the used tool ((R_q)used) the effective surface roughness of the tool face is calculated as the difference in the surface roughness values of used and new tool.

$$\Delta R_q = (R_q)_{new} - (R_q)_{used}$$

CHAPTER 6

INSTRUMENT VALIDATION AND SAMPLE SIZE DETERMINATION

Having constructed the Orthogonal Tube Turning (OTT) instrument, it is necessary to validate the instrument for repeatability, sensitivity and standard deviation in order to design and determine the statistical power of the response data. The instrument repeatability requires one set of tests to establish that for a given set of conditions, the same result is returned. A second series of tests to validate that the instrument is capable of measuring an actual change is then required in order to prove the instrument is not always returning the same (potentially false) result. Finally, in order to determine the confidence one can place in the results at a given factor level combination of experimentation, one must establish the standard deviation of the instrument.

Repeatability Test

For the purpose of instrument repeatability, three data sets were considered each with five runs carried out on different days over a period of time at dry environment with a 0^{o} rake angle tool and a constant feed of 0.001 inch. The standard spindle rpm was used and the force data was saved in a MS Excel file for analysis. The dynamometer records a response reading for every 0.01 seconds, so for 60 seconds of cut a total of 6000 readings are recorded. The initial 10 seconds are disregarded during which the tool is deflected during the onset of the force occurs and response curve stabilizes. Table 3 and Table 4 shows the average and the standard deviation values of the thrust force and the cutting force data under each run.

Thrust Force Data						
Run No.	Data Set 1		Data Set 2		Data Set 3	
	Mean	Std Deviation	Mean	Std Deviation	Mean	Std Deviation
Run 1	178.7172	6.6239	185.3432	3.1193	175.1395	3.5045
Run 2	175.5777	7.9548	177.0952	7.7615	17.6127	3.3581
Run 3	175.7445	6.5045	178.2868	2.1636	173.0687	6.6251
Run 4	173.5154	4.3147	176.9404	2.1055	177.4118	3.0499
Run 5	178.1167	1.8644	174.6758	1.7307	177.2100	1.7704

Table 2: Thrust Force Data for Instrument Validation

Cutting Force Data						
Run No.	Data Set 1		Data Set 2		Data Set 3	
	Mean	Std Deviation	Mean	Std Deviation	Mean	Std Deviation
Run 1	172.4828	6.9405	179.2302	4.0760	168.4391	3.0778
Run 2	171.1007	7.5971	172.5878	7.3604	166.7893	3.3153
Run 3	174.1149	6.3800	176.8490	2.3010	178.2868	6.2337
Run 4	170.2533	4.4802	173.8834	2.1370	168.8458	3.0956
Run 5	175.4985	1.9894	171.2168	1.8795	169.6373	1.9405

Table 3: Cutting Force Data for Instrument Validation

The mean and standard deviation values of the cutting force and thrust force is used to conduct a 2 sample t-test using the MINITAB 15 statistical software to determine the repeatability of the instrument. The test was conducted with a null hypothesis that the two means were equal. The t-test was conducted for force values between two data sets with different combination available between the three data sets for an average time interval of 50 seconds. The comparison between different data set combinations and their respective p-values are given in Table 5. The p-values of the t-tests under all different combinations conclude that the cutting force and thrust force responses are equal at 95% confidence interval and hence the data sets are repeatable since all tests were conducted under the same cutting conditions.

Data Set Combination	P – Value		95% Confidence Interval		Remarks
	Thrust	Cutting	Thrust	Cutting	
Data 1 vs. Data2	0.337	0.281	Equal	Equal	Repeatable
Data 1 vs. Data3	0.615	0.354	Equal	Equal	Repeatable
Data 2 vs. Data3	0.219	0.124	Equal	Equal	Repeatable

Table 4: Repeatability Test Analysis

Sensitivity Test

The experiment was conducted at the same dry environment using a 0^{o} rake tool under two different feeds of 0.001 and 0.002 inches in order to force variation in the response. Three different data sets were collected with each data set comprising of five replicates. The mean of the thrust and cutting force data for an average cutting time of 50 seconds is recorded and is shown in Table 6 and Table 7.

Thrust Force Data (N)						
Run No.	Data Set 1		Data Set 2		Data Set 3	
	0.001” D1F1	0.002” D1F2	0.001” D2F1	0.002” D2F2	0.001” D3F1	0.002” D3F2
Run 1	178.7172	248.7989	185.3432	241.3228	175.1395	240.6577
Run 2	175.5777	240.2342	177.0952	240.373	170.6697	239.6734
Run 3	175.7445	236.3356	178.2868	233.2487	173.0687	240.4760
Run 4	173.5154	239.5938	176.9404	240.9454	172.2748	235.7926
Run 5	178.1167	240.2020	174.6758	237.1459	173.2100	237.4057

Table 5: Thrust Force Data for Sensitivity Test

Cutting Force Data (N)						
Run No.	Data Set 1		Data Set 2		Data Set 3	
	0.001” D1F1	0.002” D1F2	0.001” D2F1	0.002” D2F2	0.001” D3F1	0.002” D3F2
Run 1	172.4828	268.7188	179.2302	265.6712	168.4391	259.0863
Run 2	171.1007	265.9970	172.5878	266.5099	166.7893	266.4834
Run 3	174.1149	266.5493	176.8490	264.6484	178.2868	270.369
Run 4	170.2533	265.4674	173.8834	266.5676	168.8458	262.2706
Run 5	175.4985	268.2023	171.2168	260.7075	169.6373	265.3257

Table 6: Cutting Force Data for Sensitivity Test

MINITAB was again utilized to compare paring of data. The t-tests conducted on the data sets under various combinations show that the change in feed has an influence over the cutting and thrust force response and the two means of the data sets are not equal thereby rejecting the null hypothesis. The P-values are calculated and is presented in the Table 8. This shows that the instrument is capable of detecting a change in the cutting parameter and hence was determined to be sensitive to change in variables.

Data Set Combination	P - Value		95 % Confidence Interval		Remarks
	Thrust	Cutting	Thrust	Cutting	
D1F1 vs. D1F2	0.000	0.000	Not Equal	Not Equal	Sensitive
D1F1 vs. D2F2	0.000	0.000	Not Equal	Not Equal	Sensitive
D1F1 vs. D3F2	0.000	0.000	Not Equal	Not Equal	Sensitive
D2F1 vs. D1F2	0.000	0.000	Not Equal	Not Equal	Sensitive
D2F1 vs. D2F2	0.000	0.000	Not Equal	Not Equal	Sensitive
D2F1 vs. D3F2	0.000	0.000	Not Equal	Not Equal	Sensitive
D3F1 vs. D1F2	0.000	0.000	Not Equal	Not Equal	Sensitive
D3F1 vs. D2F2	0.000	0.000	Not Equal	Not Equal	Sensitive
D3F1 vs. D3F2	0.000	0.000	Not Equal	Not Equal	Sensitive

Table 7: Sensitivity Test Analysis

Standard Deviation of the Instrument

The standard deviation of the instrument is given by the sum of the sensitivity of the dynamometer and the sensitivity of the NI USB 6008. The sensitivity of the dynamometer is estimated to be +/- 10 N by the manufacturer (KISTLER) and the sensitivity of the USB module is +/- 1 N (National Instruments). So the standard deviation of the instrument can be determined as 11 N under normal atmospheric conditions. The standard deviation values of the thrust force and cutting force presented in Table 3 and Table 4 is compared with the standard deviation of the instrument and was found to be less than 11 N which is a good measure for the accuracy and sensitivty of the experimental set up.

Determination of Sample Size

The sample size necessary to obtain reportable results is of prime importance during the planning stage of the experiments. Sample size is dictated by how accurate you must be, or how large a margin of error you can tolerate. The larger your sample size, the more sure you can be that their averages truly reflect the population. Power analysis can either be done before or after the data is collected. A power analysis was conducted prior to the research study to determine an appropriate sample size to achieve adequate power.

Statistical power is the capability of the analysis to detect a difference which actually exists between two sets of data or the ability that the test will reject a false null hypothesis to avoid Type II error. A Type II error is the error of not rejecting a null hypothesis when it is not true and increases with decreases with increase in power.

Using the previously collected data from the repeatability and sensitivity analysis, the minimum number of replicates necessary to achieve a statistical power of 95% was calculated using the MINITAB software. The output of the software is shown in Figure 30 and is evaluated that a sample size of 5 yields in achieving 95% statistical power which is more than our target power.

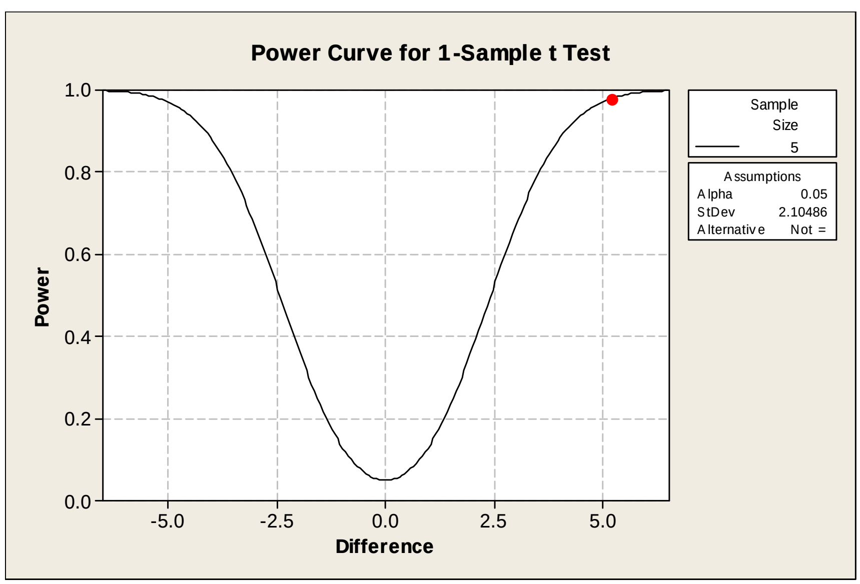

Figure 28: Power Curve to achieve 95% Statistical Power

CHAPTER 7

STATISICAL DESIGN OF EXPERIMENT (DOE)

The orthogonal tube turning experiment was mainly designed to study the variation of tool forces, tool surface roughness and shear angle with varying input parameters. The input parameters were decided based upon the literature, trial runs and experience. The different parameters involved in the experiments are presented in Table 9 and are further discussed in this chapter.

Parameter	Value
Spindle RPM, N_s	640 rpm
Tool Material	HSS T-56
Sample Material	Aluminum – 6061 (54.5 HRB)
Width of Cut (tube wall), w	0.125 inches
Environment	Dry, Cold Compressed Air, Nitrogen and Spray Coolant.
Tool Rake Angle, α	-10^o, 0^o, 15^o 30^o
Uncut Chip Thickness, t_1	0.001, 0.002, 0.003, 0.004,0.005 inches
Total Time for each Run	60 seconds
Cutting Speed, v	500 SFPM

Table 9: Input Parameters for Tube Turning Experiment

The spindle RPM was calculated based on a cutting speed of 500 sfpm considering the hardness and the geometrical dimensions of the alloy and was determined to be 640 RPM according to the Metals Handbook [21]. RPM calculations are shown in Appendix B.

The properties of Aluminum 6061-T6 are well documented and considering the ease of availability and cost, this alloy was selected for all the experimental purposes. The tube used in this set up was a 3 inch diameter 6061 alloy with a wall thickness of 0.125 inch. Usually the tubes were machined to be a maximum of 9 inches long to avoid the deflection of the work from the chuck. It was decided to use hollow tubes with no supporting tailstock in order to permit long periods of heavy chip cutting.

The effects of atmospheric temperature and humidity are neglected while measuring the responses or while calculating the results, although it should be noted that the lab temperarture and humidity are well controlled by the environmental system. A piece of HSS tool stock with ¾ inch x ¾ inch x 5 inches is used for all the cutting operations on the lathe. The work piece was machined along the circumference of the tube using the HSS tool. Precise rake angles are ground into the tools as discussed later.

The hardness of Aluminum 6061 was measured using a Rockwell Hardness Tester HR 150A. The indentation for plastic deformation was by 1/16" ball and a HRB scale was used. The standard and the sample were tested alternately to find the deviation from the exact value and the data is presented in Table 2. The average hardness of the sample is determined to be 54.5 HRB, as would normally be expected of a T6 tempered piece of aviation grade general purpose aluminum (AL 6061). All aluminum was obtained from the same manufacturer and the same production batch.

Standard = 91.0 B Scale	
Major Load = 100 Kg, Minor Load = 10 Kg	
Indenter = 1/16 inch ball	
Standard = 90.5	Standard = 91.0
Specimen 1 Trial 1 = 54.5	Specimen 2 Trial 2 = 54.5
Standard = 90.5	Standard = 91.0
Specimen 1 Trial 2 = 54.5	Specimen 3 Trial 1 = 54.0
Standard = 91.0	Standard = 91.5
Specimen 2 Trial 1 = 55.0	Specimen 3 Trial 2 = 54.5
	Standard = 91.5

Table 9: Evaluation of Hardness of Aluminum 6061

In order to compare the behavior of the responses under various environments, four different cutting environments were chosen. Dry machining with out the aid of any kind of cooling mechanism, Cold compressed air environment obtained by a vortex air gun to direct a continuous supply of cold air at the tool chip interface, Nitrogen environment with the aid of the gas cylinder fitted with a suitable pressure regulator and lastly Cool Mist Environment using a spray coolant generator fitted with a splitter and directed onto the tool chip interface. An argon environment was disregarded after the trial runs since no significant changes in the responses were observed.

Historically, the variation of the tool forces and the tool wear is largely attributed to the tool rake angle. In order to investigate the influence of the tool geometry, four different rake angles were selected and the tools were machined to -10^o, 0^o, 15^o and 30^o so as to obtain data over a wide range of varying rake angles. The 0^o tool is commonly used in industries because of their superior tool life and rigidity [22]. The selected rake angles are machined onto the HSS tools using a surface grinder. The normal range of tool rake angles (-5 to 15 degrees) is well represented by the 0 and 15 degree tools. The

-10 and +30 degree tools represent an extreme outer range and are not commonly used values except within academia.

Traditionally, the selection of feed is also of prime importance as this decides the variation of tool forces significantly and also determines the chip thickness ratio. During the trial runs the possible optimum feeds were determined to be 0.001, 0.002, 0.003, 0.004 and 0.005 inches/revolution. Any feed after 0.005 inch/rev led to an increase in the disfiguration of the chip and a feed of 0.008 inch/rev resulted in smoke which could have burnt the tool or would have caused severe damage to the machine tool if carried out. Traditionally, lathe operators consider a 0.005 inch/rev cut as a “heavy” roughing cut. A finishing cut of 0.0005/rev to 0.0010/rev is quite common in industry because of the superior finish produced.

The HSS tools are machined using a HARIG 618 Automatic surface grinder as in Figure 19 to the required rake angles. An angular milling machine vice which can be swiveled to 45 degrees in both the directions was used. The angular vise is held on the magnetic bed of the grinding machine. The tool is held in the vice and is swiveled to the required angle. A dial gauge is run over the surface of the vice to make sure that the vice is gripped parallel to the machine reference. The tool is then machined with a slow feed rate and depth of cut to achieve high quality surface and reduce surface roughness. The vice is swiveled to prepare multiple -10^{o}, 0^{o}, 15^{o} and 30^{o} tools. During the trial runs it was also established that up to a certain limit the length of the tool protruding out of the tool holder does not make any significant difference with the responses measured (i.e., the tool is stiff). The clearance angle of all the tools was measured to be 15^{o}.

Figure 29: Machining a 30 degree tool on a HARIG 618 Automatic Surface Grinder

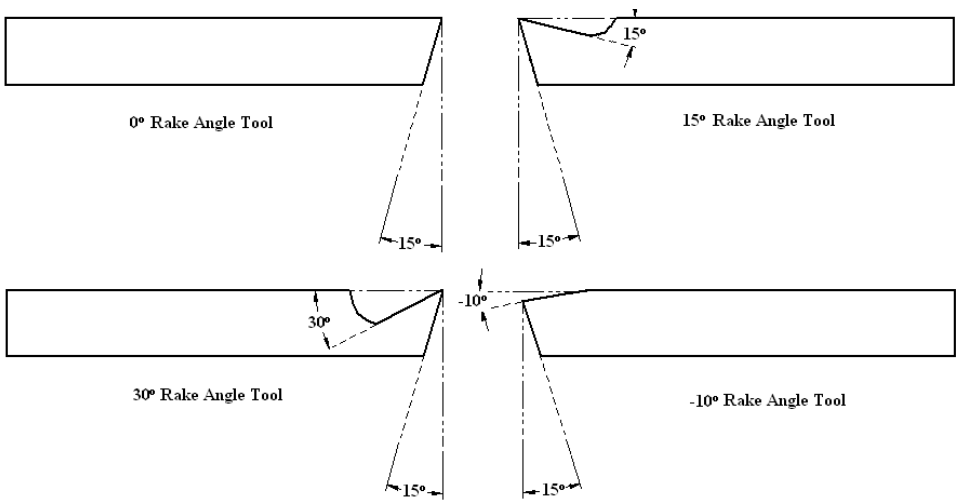

Figure 30: Selected Rake Angles machined on a square section HSS tool

The Aluminum tubing measuring 72 inches as obtained by the supplier is cut into tubes of 9 inch length on a Horizontal band saw and the faces are sanded on a vertical belt sander to make them flat and burrs if any are removed using a deburring tool. A small experiment was conducted during the trial runs to determine if there is any significant change in the force response based on the length of the tube protruding outside the chuck. It is concluded that the length of this protrusion has very negligible effect on the forces and hence can be disregarded.

The experiments are designed at various factor level combinations as shown in Table 10. Each factor level combination comprises of 5 replicates leading to 100 runs under each environment which amounts to 400 runs over a range of four different environments, four different rake angle and five different feeds.

The cutting force and thrust force responses at all possible factor level combination is recorded. Each factor level combination uses a new tool machined to required rake angle. So assuming that the material is being cut for a total of 60 seconds under each cut, every tool was used for 300 seconds to obtain 5 replicates. The used tool was then stored for surface roughness analysis using the confocal laser profilometer. The aluminum chips obtained under each run was labeled accordingly and stored for chip thickness measurement to aid in shear angle calculations.

Design of Experiment		
Environment	Rake Angle	Feed (inches)
Dry	-10^o	0.001
Cold Compressed Air	0^o	0.002
Nitrogen	15^o	0.003
Spray Coolant	30^o	0.004
		0.005

Table 10: Factor Level Combinations of the Principal Experiment.

CHAPTER 8

RESULTS AND DISCUSSION

The designed experiment as discussed in Chapter 7 consists of large number of runs at various factor level combinations. Four different cutting environments, four different rake angles and five different feeds were used resulting in 80 different factor level combinations each with five replicates amounting to 400 total runs. The cutting force and thrust force data are initially saved as MS excel files for ease of calculations. A typical graph of variation of cutting tool forces with time is as shown below.

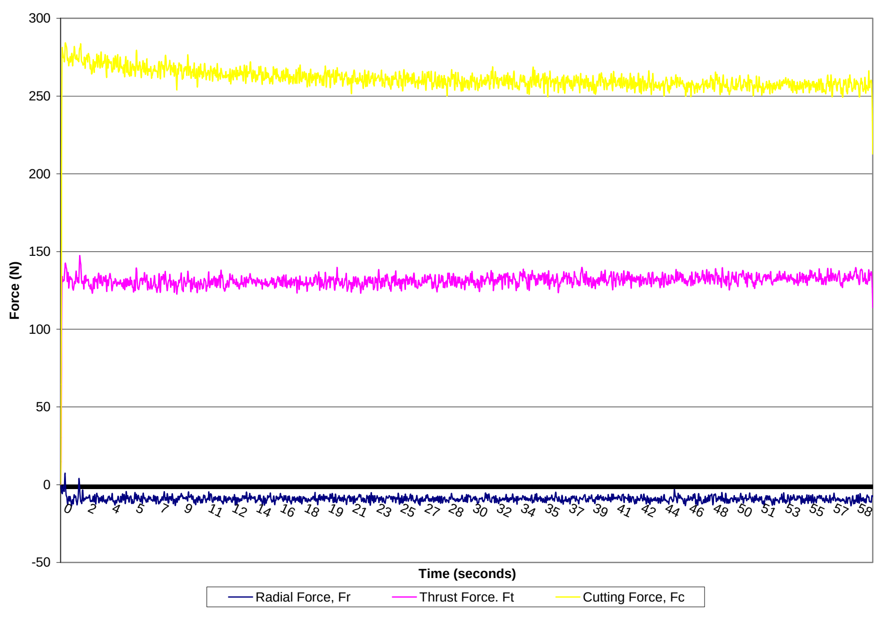

Figure 31: Variation of Tool forces with time.

Further the used tools are measured for surface roughness estimation using a laser confocal profilometer and the data is saved in .txt format. The uncut chip thickness is measured at 5 different locations along the continuous chip and is saved for shear angle calculations. The observed experimental data are tabulated to facilitate further calculations as in Table 11.

Run	Rake Angle	Feed	Run	Thrust Force, Ft (N)	Cutting Force, Fc (N)
1	-10	0.001	Run 1	177.7517	175.9930
2	-10	0.002	Run 1	251.7904	263.4748
3	-10	0.003	Run 1	310.3103	335.1369
4	-10	0.004	Run 1	356.3264	412.3702
5	-10	0.005	Run 1	407.1834	474.6960

Table 11: Example Thrust Force and Cutting Force Raw Data (Appendix C)

Based on the observed cutting force and thrust force data, the friction force (F), normal force (N), shearing force along the shear plane (Fs) and a force normal to the shear plane (F_n) is calculated and the corresponding force ratios are derived.

The cutting forces, shear angle, friction angle and shear stress calculations are based on the classical equations presented in Table 12 as first developed by Merchant (1).

Data	Symbol	Units	Equations
Chip Thickness Ratio	r_c	none	$r_c = \frac{t_1}{t_2}$
Friction Force	F	N	$F = F_c.\sin\alpha + F_t.\cos\alpha$
Normal Force	N	N	$N = F_c.\cos\alpha - F_t.\sin\alpha$
Friction Co-efficient	μ	none	$\mu = \frac{F}{N}$
Shear Force on Shear Plane, Merchant	(F_s) M	N	$(F_s)M = F_c.\cos\phi - F_t.\sin\phi$
Normal Force on Shear Plane, Merchant	(F_n) M	N	$(F_n)M = F_c.\sin\phi - F_t.\cos\phi$
Area of Shear Plane	A_s	$inch^2$	$A_s = \frac{t_1.w}{\sin\phi}$
Shear Stress on Shear Plane	τ_s	MPa	$\tau_s = \frac{F_s}{A_s}$
Shear Plane Angle	φ	degree	$\phi = \arctan\left(\frac{r\cos\alpha}{1 - r\sin\alpha}\right)$
Friction Angle	β	degree	$\beta = \arctan\left[\frac{F}{N}\right]$

Table 12: Equations used to calculate results from the Force Response and Chip Thickness Data (also discussed in Appendix D)

Table 13 and Table 14 show examples of the various forces, force ratios and shear stress calculations. The complete set of experimental force calculations, surface roughness, shear angle and shear stress calculations are presented in Appendix D and Appendix E. All calculations are the factor level average of the 5 replicates meaning that the average of each of the run is averaged to obtain the following data.

Run No.	Friction Force (F)	Normal Force (N)	F/N Ratio	Fs (Merchant)	Fn (Merchant)	Fs/Fn (Merchant)
1	144.4904	204.1855	0.7076	154.0374	-155.9893	-0.9875
2	184.1773	177.2929	1.0388	177.2929	-184.1773	-0.9626
3	177.9254	180.9517	0.9833	180.9517	-177.9254	-1.0170
4	189.0791	181.1614	1.0437	181.1614	-189.0791	-0.9581
5	194.3560	185.0437	1.0503	185.0437	-194.3560	-0.9521

Table 13: Example of Force Ratio Calculations from Appendix (E)

<table>
<tr><th>Run No.</th><th>Roughness (microns)</th><th>t/tc</th><th>Phi (degrees)</th><th>Beta (degrees)</th><th>As (in2)</th><th>τ_s (Mpa)</th></tr>
<tr><td>1</td><td rowspan="5">154.942318</td><td rowspan="5">0.121892</td><td rowspan="5">6.704454207</td><td>35.2848498</td><td rowspan="5">0.001070683</td><td rowspan="5">254.3531778</td></tr>
<tr><td>2</td><td>46.09109792</td></tr>
<tr><td>3</td><td>44.5168538</td></tr>
<tr><td>4</td><td>46.22510005</td></tr>
<tr><td>5</td><td>46.40603269</td></tr>
<tr><td>6</td><td rowspan="5">161.1517652</td><td rowspan="5">0.162259</td><td rowspan="5">8.83393002</td><td>33.70095615</td><td rowspan="5">0.001627911</td><td rowspan="5">248.960118</td></tr>
<tr><td>7</td><td>43.80856404</td></tr>
<tr><td>8</td><td>44.03211179</td></tr>
<tr><td>9</td><td>43.9692226</td></tr>
<tr><td>10</td><td>43.64414797</td></tr>
</table>

Table 14: Example of Surface Roughness, Shear Angle and Shear Stress Calculation Data from Appendix F

Variation of Thrust Force (F_t) with Environment, Rake angle and Feed

Statistical analysis of the thrust force (F_t) was conducted using the GLM (general linear module) of MINITAB 15. The main effects plot indicates that environment has a relatively less effect on this result. The thrust force decreases greatly with increasingly positive rake angles. The thrust force increases sharply as the depth of cut or feed is increased.

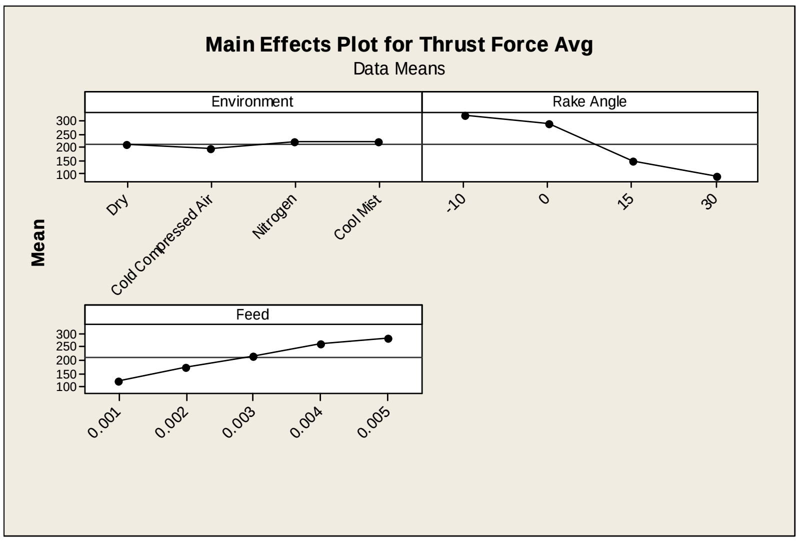

Figure 32: Main Effect Plot for Thrust Force response (Minitab 15)

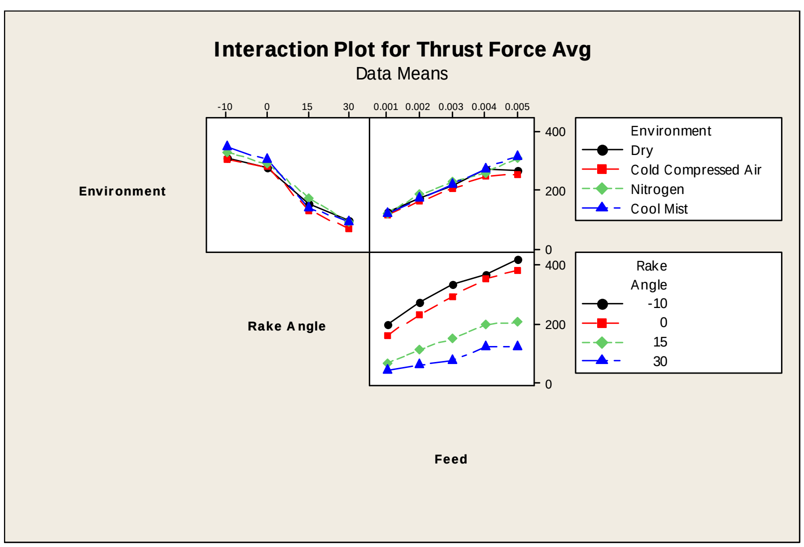

Figure 33: Interaction Plot for Thrust Force response (Minitab 15)

General Linear Model: Thrust Force versus Environment, Rake Angle, Feed

Factor	Type	Levels	Values
Environment	fixed	4	Dry, Cold Compressed Air, Nitrogen, Cool Mist
Rake Angle	fixed	4	-10, 0, 15, 30
Feed	fixed	5	0.001, 0.002, 0.003, 0.004, 0.005

Analysis of Variance for Thrust Force Avg, using Adjusted SS for Tests

Source	DF	Seq SS	Adj SS	Adj MS	F	P
Environment	3	38078	38078	12693	559.98	0.000
Rake Angle	3	3693229	3693229	1231076	54313.14	0.000
Feed	4	1439297	1439297	359824	15874.88	0.000
Environment*Rake Angle	9	34456	34456	3828	168.91	0.000
Environment*Feed	12	40228	40228	3352	147.90	0.000
Rake Angle*Feed	12	175989	175989	14666	647.03	0.000
Environment*Rake Angle*Feed	36	153141	153141	4254	187.68	0.000
Error	320	7253	7253	23		
Total	399	5581673				

S = 4.76091   R-Sq = 99.87%   R-Sq(adj) = 99.84%

Table 15: ANOVA Table for Thrust Force response (Minitab 15)

The Analysis of Variance (ANOVA) of the thrust force response indicates that the Rake Angle has by far the dominant effect on this force with an F-statistic of 54,313. The feed factor is second in significance with an F-statistic of 15,874. The interaction of the rake angle and feed outperforms the environment in terms of the F-statisic.

This result can be interpreted as follows. A sharper tool plunges into the work and can form a chip piece with considerably less force required than a blunt tool. The thrust force increases with the increase in feed. Turning using a sharper tool is more likely to reduce the thrust force than just decreasing the feed. The main effects of environment achieve significance but are less than the effect of rake angle and feed on the thrust force. It can also be observed from the main effect plot that the drop in thrust force is more rapid from 0^o to 15^o as compared to other trends.

Variation of Cutting Force (F_c) with Environment, Rake angle and Feed

Statistical analysis of the Cutting force (F_c) was conducted using the GLM (general linear module) of MINITAB 15. The main effects plot indicates that environment has a relatively less effect on Cutting force but decreases considerably with increasing positive rake angles. The cutting force greatly increases as the depth of cut or feed is increased.

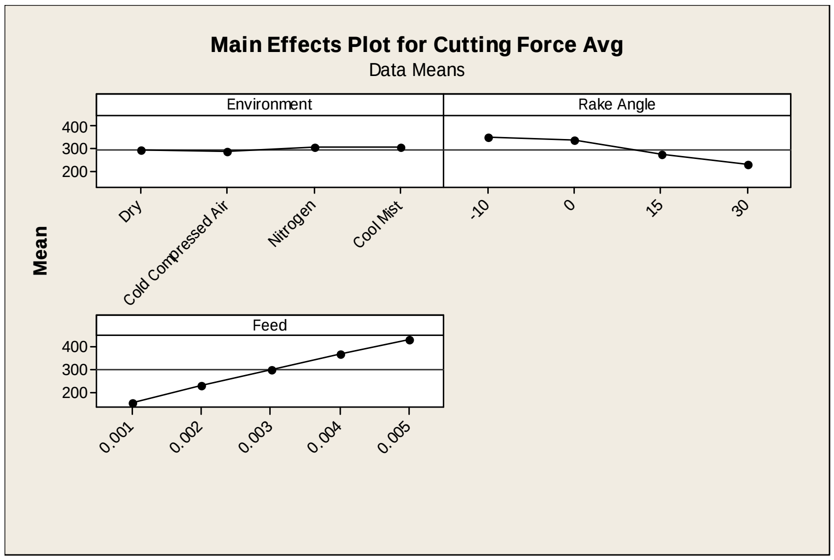

Figure 34: Main Effect Plot for Cutting Force response (Minitab 15)

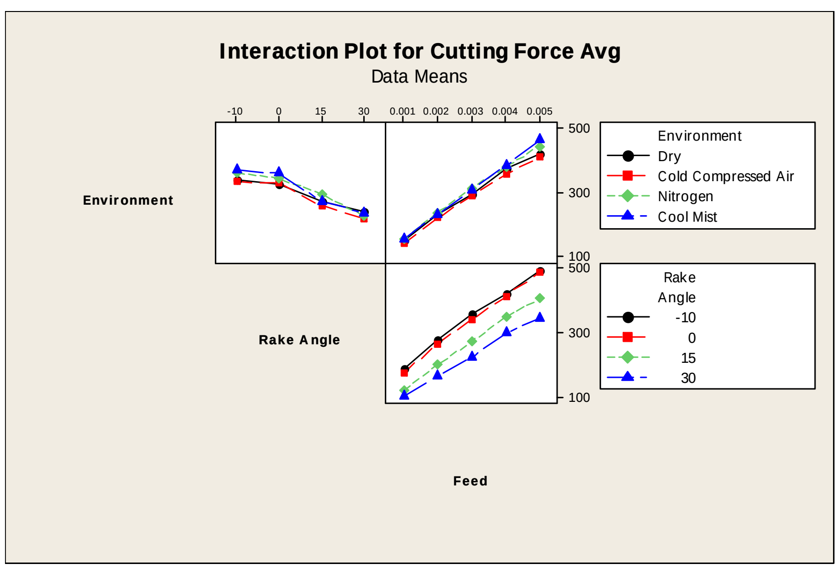

Figure 35: Interaction Plot for Cutting Force response (Minitab 15)

General Linear Model: Cutting Force versus Environment, Rake Angle, Feed

Factor	Type	Levels	Values
Environment	fixed	4	Dry, Cold Compressed Air, Nitrogen, Cool Mist
Rake Angle	fixed	4	-10, 0, 15, 30
Feed	fixed	5	0.001, 0.002, 0.003, 0.004, 0.005

Analysis of Variance for Cutting Force Avg, using Adjusted SS for Tests

Source	DF	Seq SS	Adj SS	Adj MS	F	P
Environment	3	38297	38297	12766	662.04	0.000
Rake Angle	3	970355	970355	323452	16774.39	0.000
Feed	4	4097534	4097534	1024384	53125.13	0.000
Environment*Rake Angle	9	27001	27001	3000	155.59	0.000
Environment*Feed	12	17951	17951	1496	77.58	0.000
Rake Angle*Feed	12	36005	36005	3000	155.60	0.000
Environment*Rake Angle*Feed	36	35516	35516	987	51.16	0.000
Error	320	6170	6170	19		
Total	399	5228829				

S = 4.39118   R-Sq = 99.88%   R-Sq(adj) = 99.85%

Table 16: ANOVA Table for Cutting Force response (Minitab 15)

The Analysis of Variance (ANOVA) of the cutting force response indicates that the significant main effect of feed on this force with an F-statistic of 53125. The rake angle is the next most significant factor with an F-statistic of 16774. The effect of environment outperforms the interaction of feed and rake angle in terms of the F-statistic

The cutting force is the force in the direction of the work motion against the tool. The increase in feed demands more energy for the plastic deformation of the material thus consuming more power leading to larger cutting force responses. The simple effect also shows the decrease in cutting force with decrease in feed. Turning at a lower feed is more likely to reduce the cutting force than just using a sharper tool. The main effects of environment achieve significance but are less than the individual effect of rake angle and feed on the cutting force. It is also to be noted that the increase in cutting force is close to linear with the increase in feed.

Variation of Friction Force (F) with Environment, Rake angle and Feed

Statistical analysis of the Friction force (F) was conducted using the GLM (general linear module) of MINITAB 15. The main effects plot indicates that cold compressed air environment showed a reduction in the friction force as compared to other environments. Friction force decreases greatly with increasing positive rake angles. The friction force greatly increases as the depth of cut or feed is increased.

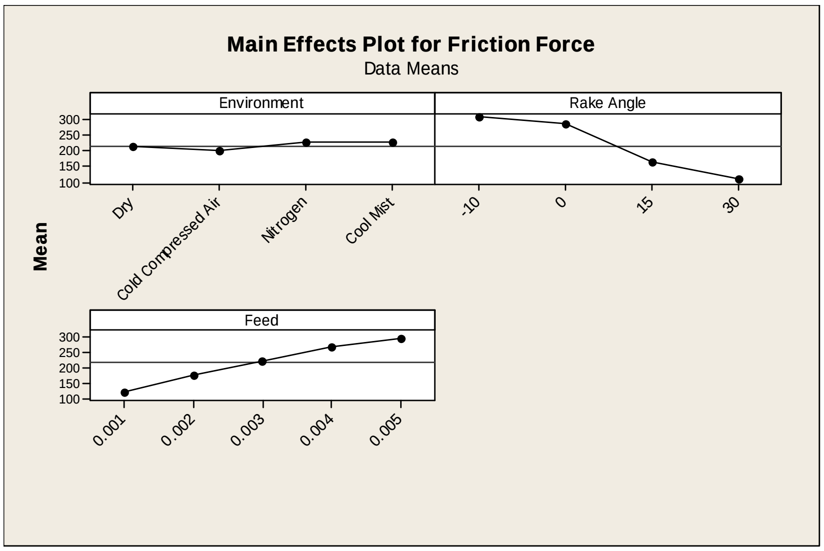

Figure 36: Main Effect Plot of Friction Force data (Minitab 15)

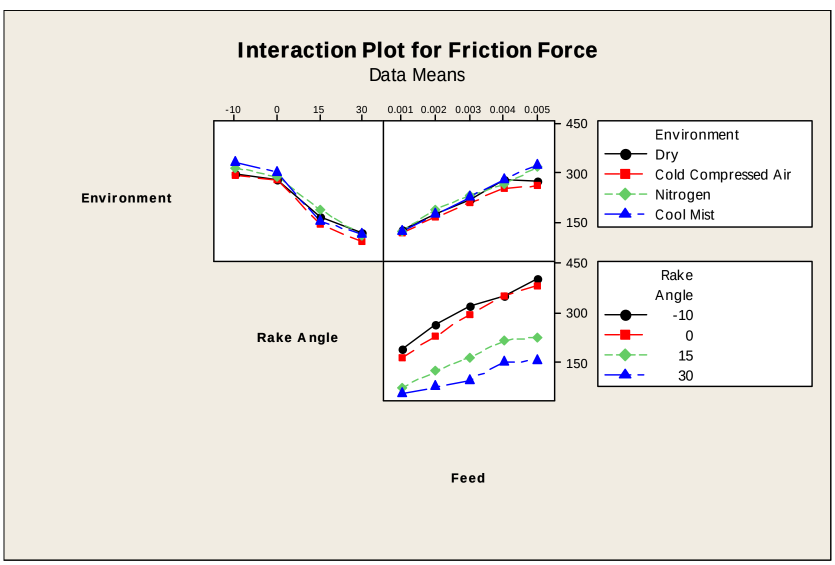

Figure 37: Interaction Plot for Friction Force data (Minitab 15)

General Linear Model: Friction Force versus Environment, Rake Angle, Feed

Factor	Type	Levels	Values
Environment	fixed	4	Dry, Cold Compressed Air, Nitrogen, Cool Mist
Rake Angle	fixed	4	-10, 0, 15, 30
Feed	fixed	5	0.001, 0.002, 0.003, 0.004, 0.005

Analysis of Variance for Friction Force, using Adjusted SS for Tests

Source	DF	Seq SS	Adj SS	Adj MS	F	P
Environment	3	38329	38329	12776	11.99	0.000
Rake Angle	3	2807437	2807437	935812	878.55	0.000
Feed	4	1547405	1547405	386851	363.18	0.000
Environment*Rake Angle	9	35399	35399	3933	3.69	0.000
Environment*Feed	12	41267	41267	3439	3.23	0.000
Rake Angle*Feed	12	118045	118045	9837	9.24	0.000
Environment*Rake Angle*Feed	36	154762	154762	4299	4.04	0.000
Error	320	340856	340856	1065		
Total	399	5083501				

S = 32.6370   R-Sq = 93.29%   R-Sq(adj) = 91.64%

Table 17: ANOVA Table for Friction Force (Minitab 15)

The calculated friction force response was subjected to Analysis of Variance (ANOVA) and the result shows a significant main effect of rake angle upon the force response with an F-statistic of 878. The feed factor is second in significance with an F-statistic of 363. The environment has very little effect on the friction force response when compared to rake angle and feed in terms of F-statistic.

The pattern of the findings during the analysis of the friction force is same as the ones observed for thrust force response. A rapid decrease in friction force values occur for a rake angle between 0^o to 15^o. The friction force is considerably less when cutting using a sharper tool. Also the increase in feed causes an increase in friction force due to the increase in energy consumed to cause the plastic deformation of the work piece.

Variation of Normal Force (N) with Environment, Rake angle and Feed

Statistical analysis of the Normal force (N) was conducted using the GLM (general linear module) of MINITAB 15. The main effects plot indicates that the Environment has very little effect on the normal force response as compared to the other parameters. A considerable decrease in normal force is observed with the increasing positive rake angles. The Normal force greatly increases as the depth of cut or feed is increased.

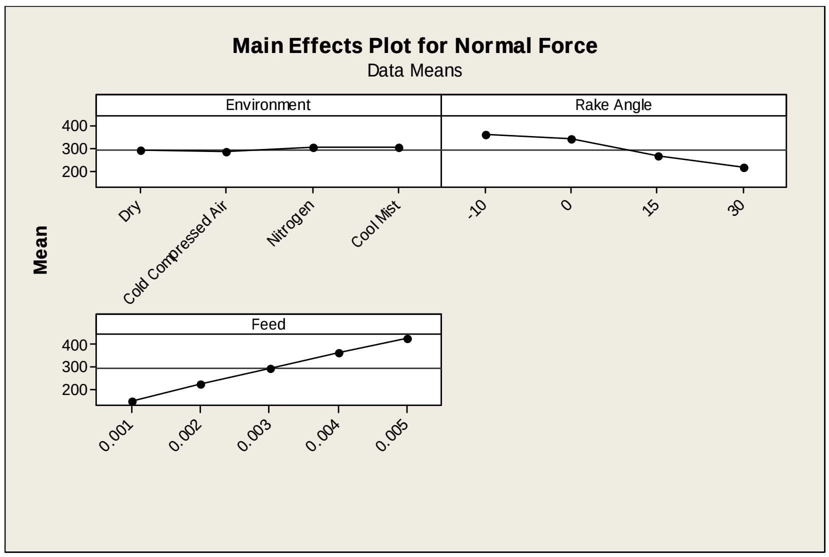

Figure 38: Main Effect Plot of Normal Force response (Minitab 15)

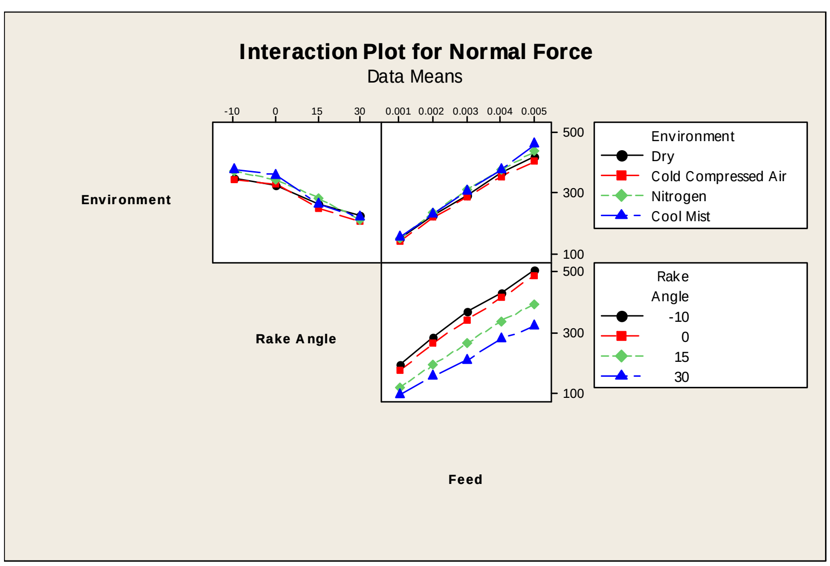

Figure 39: Interaction Plot for Normal Force response (Minitab 15)

General Linear Model: Normal Force versus Environment, Rake Angle, Feed

Factor	Type	Levels	Values
Environment	fixed	4	Dry, Cold Compressed Air, Nitrogen, Cool Mist
Rake Angle	fixed	4	-10, 0, 15, 30
Feed	fixed	5	0.001, 0.002, 0.003, 0.004, 0.005

Analysis of Variance for Normal Force, using Adjusted SS for Tests

Source	DF	Seq SS	Adj SS	Adj MS	F	P
Environment	3	36553	36553	12184	20.68	0.000
Rake Angle	3	1354337	1354337	451446	766.05	0.000
Feed	4	3967380	3967380	991845	1683.05	0.000
Environment*Rake Angle	9	26064	26064	2896	4.91	0.000
Environment*Feed	12	17871	17871	1489	2.53	0.003
Rake Angle*Feed	12	56526	56526	4711	7.99	0.000
Environment*Rake Angle*Feed	36	29600	29600	822	1.40	0.072
Error	320	188580	188580	589		
Total	399	5676911				

S = 24.2758   R-Sq = 96.68%   R-Sq(adj) = 95.86%

Table 18: ANOVA Table for Normal Force response (Minitab 15)

The calculated normal force response was subjected to Analysis of Variance and the result shows that feed has by far the dominant effect on this force with an F-statistic of 1683. The tool rake angle is second in significance with an F-statistic of 766. Environment does have very little effect on the normal force response but is negligible when compared to individual effects of rake angle and feed.

The pattern of the findings during the analysis of the normal force is same as the ones observed for cutting force response. The increase in feed causes an increase in normal force due to the increase in energy consumed to cause the plastic deformation of the work piece. It is also to be noted that the combined effect of environment, rake angle and feed fails to achieve significance on the normal force response with an F-statistic of 1.40 and $p > 0.001$. The main effect curve for increase in normal force with increase in feed is close to linear however rake angle too has a considerable effect resulting in reduced normal force when using a sharper tool.

Variation of F/N Ratio with Environment, Rake angle and Feed

Statistical analysis of the F/N Ratio was conducted using the GLM (general linear module) of MINITAB 15. The main effects plot indicates that the Environment has almost constant effect on this force ratio. F/N ratio is found to abruptly decrease with the increasing rake angle. An appreciable decrease in F/N ratio is observed with the increase in depth of cut or feed.

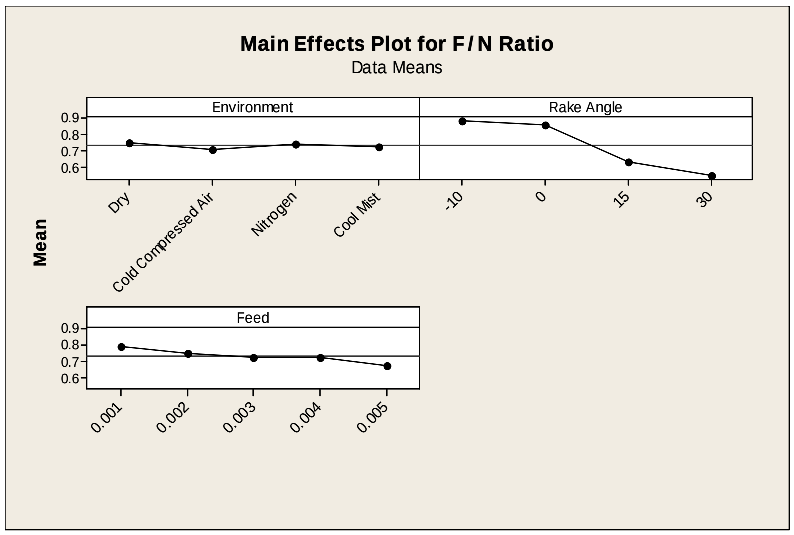

Figure 40: Main Effect Plot of F/N Ratio (Minitab 15)

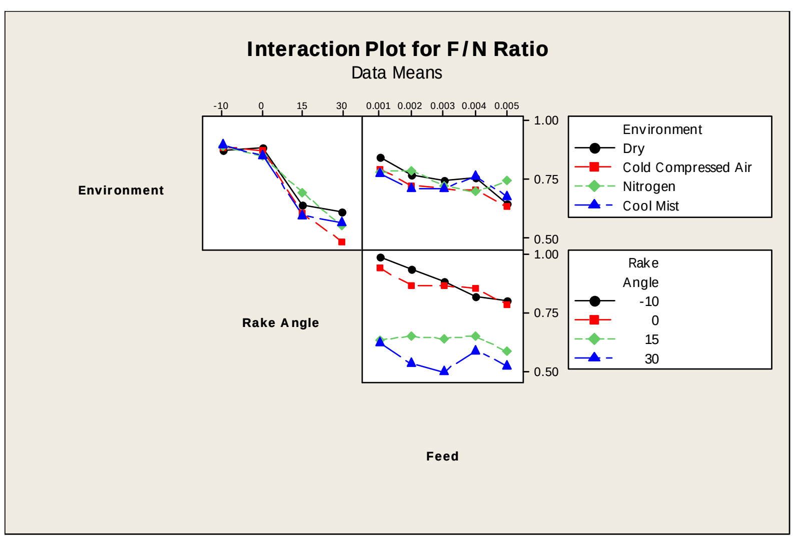

Figure 41: Interaction Plot for F/N Ratio (Minitab 15)

General Linear Model: F/N Ratio versus Environment, Rake Angle, Feed

Factor	Type	Levels	Values
Environment	fixed	4	Dry, Cold Compressed Air, Nitrogen, Cool Mist
Rake Angle	fixed	4	-10, 0, 15, 30
Feed	fixed	5	0.001, 0.002, 0.003, 0.004, 0.005

Analysis of Variance for F/N Ratio, using Adjusted SS for Tests

Source	DF	Seq SS	Adj SS	Adj MS	F	P
Environment	3	0.10326	0.10326	0.03442	0.71	0.546
Rake Angle	3	8.31765	8.31765	2.77255	57.31	0.000
Feed	4	0.62511	0.62511	0.15628	3.23	0.013
Environment*Rake Angle	9	0.28728	0.28728	0.03192	0.66	0.745
Environment*Feed	12	0.27026	0.27026	0.02252	0.47	0.934
Rake Angle*Feed	12	0.37164	0.37164	0.03097	0.64	0.807
Environment*Rake Angle*Feed	36	1.01625	1.01625	0.02823	0.58	0.974
Error	320	15.48097	15.48097	0.04838		
Total	399	26.47244				

S = 0.219950   R-Sq = 41.52%   R-Sq(adj) = 27.08%

Table 19: ANOVA Table for F/N Ratio (Minitab 15)

Analysis of Variance (ANOVA) of F/N Ratio indicates that the rake angle has by far the dominant effect on this force ratio with an F-statistic of 57. The environment and feed fail to attain significance on F/N ratio with their p values being greater than 0.001.d

Also the effect of the interaction between environment, rake angle and feed has no significance on the F/N ratio. The interaction plot obtained shows that with a 30^o rake angle tool a much lower F/N ratio is obtained than compared to a 0^o, 15^o or a -10^o tool. Also a drastic decrease in F/N ratio is observed between rake angles of 0^o to 15^o.

Variation of Shear Force along Shear Plane (F_s) with Environment, Rake and Feed

Statistical analysis of the Shear force along the shear plane (F_s) was conducted using the GLM (general linear module) of MINITAB 15. The main effects plot indicates that the effect of environment on the shear force is nearly a constant. Shear force decreases appreciably with increasing positive rake angles. The Shear force greatly increases as the depth of cut or feed is increased.

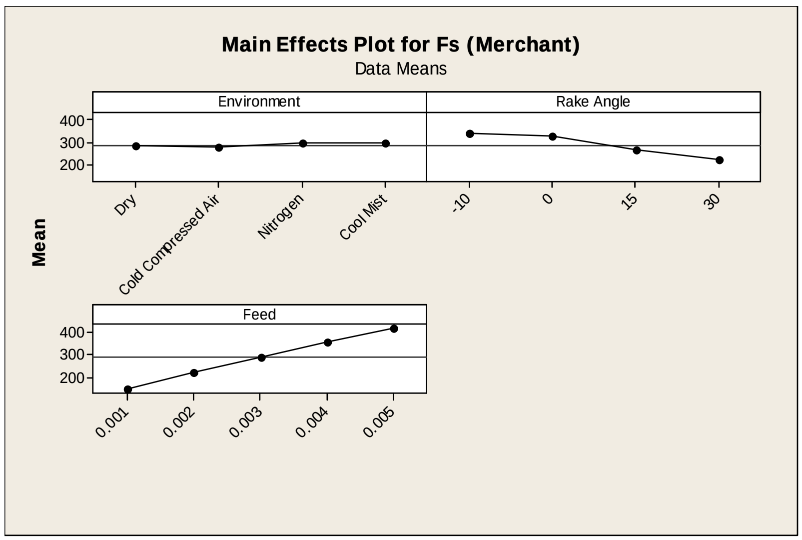

Figure 42: Main Effect Plot of Shear Force along Shear Plane (Minitab 15)

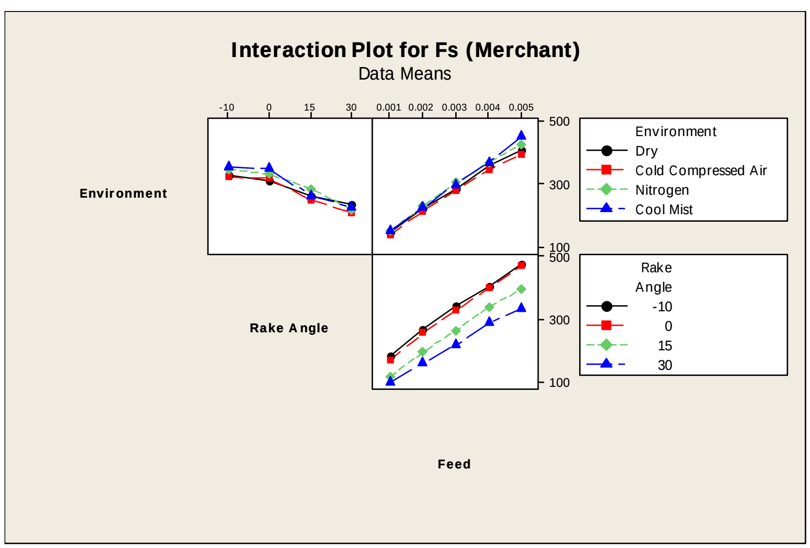

Figure 43: Interaction Plot for Shear Force along Shear Plane (Minitab 15)

General Linear Model: Fs (Merchant) versus Environment, Rake Angle, Feed

Factor	Type	Levels	Values
Environment	fixed	4	Dry, Cold Compressed Air, Nitrogen, Cool Mist
Rake Angle	fixed	4	-10, 0, 15, 30
Feed	fixed	5	0.001, 0.002, 0.003, 0.004, 0.005

Analysis of Variance for Fs (Merchant), using Adjusted SS for Tests

Source	DF	Seq SS	Adj SS	Adj MS	F	P
Environment	3	36379	36379	12126	21.64	0.000
Rake Angle	3	878195	878195	292732	522.42	0.000
Feed	4	3785829	3785829	946457	1689.08	0.000
Environment*Rake Angle	9	26975	26975	2997	5.35	0.000
Environment*Feed	12	16441	16441	1370	2.45	0.005
Rake Angle*Feed	12	30081	30081	2507	4.47	0.000
Environment*Rake Angle*Feed	36	29863	29863	830	1.48	0.042
Error	320	179308	179308	560		
Total	399	4983070				

S = 23.6715   R-Sq = 96.40%   R-Sq(adj) = 95.51%

Table 20: ANOVA Table for Shear Force along Shear Plane (Minitab 15)

Analysis of Variance (ANOVA) of the shear force response indicates that feed has a significant main effect of feed upon the force response with an F-statistic of 1689. The tool rake angle is the next most dominant factor with an F-statistic of 522.

Turning at a lower speed is more likely to decrease the shear force than using a sharper tool. Also the effect of interaction between environment, rake angle and feed failed to achieve significance with F-statistic being 1.48 and a p value > 0.001. Negligible drop in shear force is observed between -10^{o} and 0^{o} rake angle where as a drop in nearly 100 N is observed between a 0^{o} and a 30^{o} tool. Environment does have an effect on the shear force but the effect is negligible when compared to individual effects of tool rake angle and feed.

Variation of Normal Force along Shear Plane (F_n) with Environment, Rake an Feed

Statistical analysis of the Normal force along the shear plane (F_n) was conducted using the GLM (general linear module) of MINITAB 15. The main effects plot indicates that the Environment has very little effect on the normal force response. A considerable decrease in normal force is observed with the increasing positive rake angles. The normal force along shear plane increases considerably as the depth of cut or feed is increased.

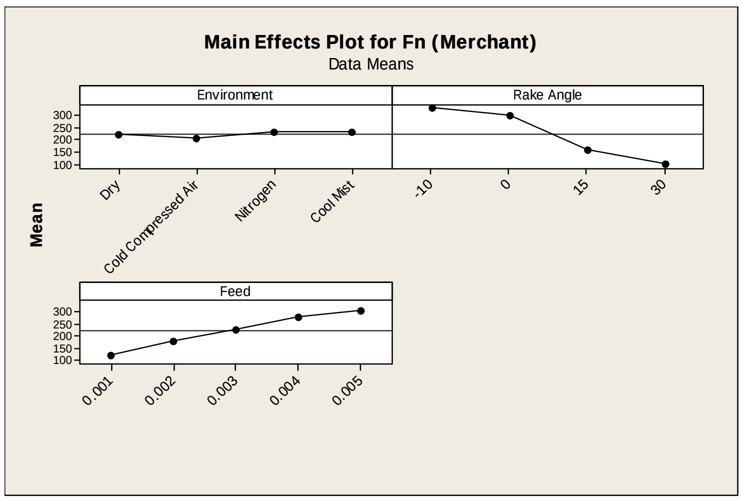

Figure 44: Main Effect Plot of Normal Force along Shear Plane (Minitab 15)

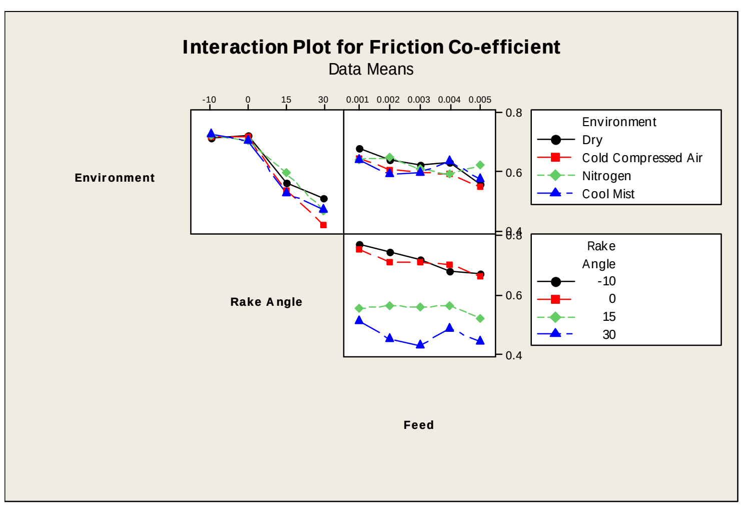

Figure 45: Interaction Plot for Normal Force along Shear Plane (Minitab 15)

General Linear Model: Fn (Merchant) versus Environment, Rake Angle, Feed

Factor	Type	Levels	Values
Environment	fixed	4	Dry, Cold Compressed Air, Nitrogen, Cool Mist
Rake Angle	fixed	4	-10, 0, 15, 30
Feed	fixed	5	0.001, 0.002, 0.003, 0.004, 0.005

Analysis of Variance for Fn (Merchant), using Adjusted SS for Tests

Source	DF	Seq SS	Adj SS	Adj MS	F	P
Environment	3	39001	39001	13000	18.28	0.000
Rake Angle	3	3683843	3683843	1227948	1726.71	0.000
Feed	4	1684883	1684883	421221	592.31	0.000
Environment*Rake Angle	9	34355	34355	3817	5.37	0.000
Environment*Feed	12	42449	42449	3537	4.97	0.000
Rake Angle*Feed	12	176403	176403	14700	20.67	0.000
Environment*Rake Angle*Feed	36	155940	155940	4332	6.09	0.000
Error	320	227568	227568	711		
Total	399	6044442				

S = 26.6674   R-Sq = 96.24%   R-Sq(adj) = 95.31%

Table 21: ANOVA Table for Normal Force along Shear Plane (Minitab 15)

Analysis of Variance of the Normal force along the shear plane indicates that the rake angle has a significant effect on this force with an F-statistic of 1689. The rake angle factor is second in significance with an F-statistic of 592. Environment has an effect on the normal force along the shear plane but is negligible compared to individual effects of rake angle and feed.

Turning using a sharper tool is more likely to reduce the nomal force than just decreasing the feed although a considerable decrease in force is observed with the decrease in feed. Also the effect of cutting environment is prominent for the normal force on the shear plane and is found be the same for nitrogen and spray coolant environment.

Variation of Fs/Fn Ratio with Environment, Rake and Feed

Statistical analysis of the F_s/F_n Ratio was conducted using the GLM (general linear module) of MINITAB 15. The main effects plot indicates that the Environment has varying effect on this force ratio. F_s/F_n ratio is found to increase with the increasing rake angle. A fairly constant response is obtained due to the increase in the feed.

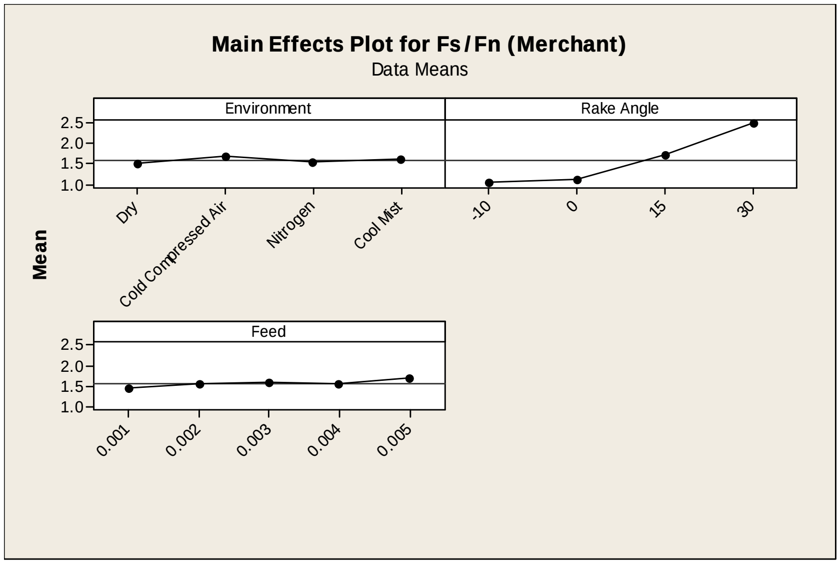

Figure 46: Main Effect Plot for Fs/Fn Ratio (Minitab 15)

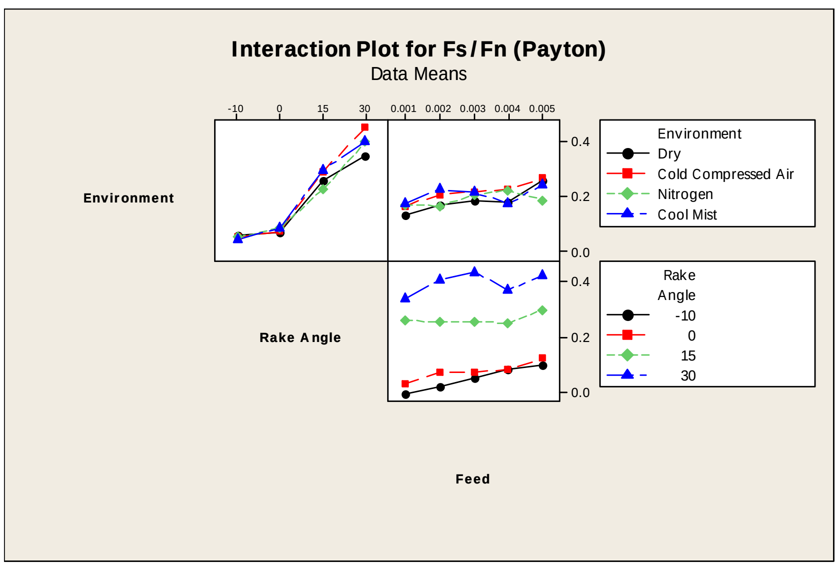

Figure 47: Interaction Plot for Fs/Fn Ratio (Minitab 15)

General Linear Model: Fs/Fn (Merchant) versus Environment, Rake Angle, Feed

Factor	Type	Levels	Values
Environment	fixed	4	Dry, Cold Compressed Air, Nitrogen, Cool Mist
Rake Angle	fixed	4	-10, 0, 15, 30
Feed	fixed	5	0.001, 0.002, 0.003, 0.004, 0.005

Analysis of Variance for Fs/Fn (Merchant), using Adjusted SS for Tests

Source	DF	Seq SS	Adj SS	Adj MS	F	P
Environment	3	1.6244	1.6244	0.5415	4.10	0.007
Rake Angle	3	138.7786	138.7786	46.2595	350.69	0.000
Feed	4	2.6490	2.6490	0.6623	5.02	0.001
Environment*Rake Angle	9	3.0344	3.0344	0.3372	2.56	0.008
Environment*Feed	12	4.1636	4.1636	0.3470	2.63	0.002
Rake Angle*Feed	12	2.4645	2.4645	0.2054	1.56	0.103
Environment*Rake Angle*Feed	36	13.5361	13.5361	0.3760	2.85	0.000
Error	320	42.2117	42.2117	0.1319		
Total	399	208.4623				

S = 0.363196   R-Sq = 79.75%   R-Sq(adj) = 74.75%

Table 22: ANOVA Table for Fs/Fn Ratio (Minitab 15)

Analysis of Variance (ANOVA) of F_s/F_n Ratio indicates that the rake angle has by far the dominant effect on this force ratio with an F-statistic of 350. The environment and feed fail to attain significance on F_s/F_n ratio with their p values being greater than 0.001.

Also the effect of the interaction between environment, rake angle and feed has no significance on the F_s/F_n ratio. The interaction plot obtained shows that with a 30^o rake angle tool a much lower F_s/F_n ratio is obtained than compared to a 0^o, 15^o or a -10^o tool. Also a drastic decrease in F_s/F_n ratio is observed between rake angles of 0^o to 15^o.

Variation of Shear Plane Angle (φ) with Environment, Rake and Feed

Statistical analysis of the Shear angle (φ) was conducted using the GLM (general linear module) of MINITAB 15. The main effects plot indicate that environment and feed has very little effect on the shear angle. Shear angle increases greatly with increasing rake angles. Also an increase in feed results in considerable rise in the shear plane angle value.

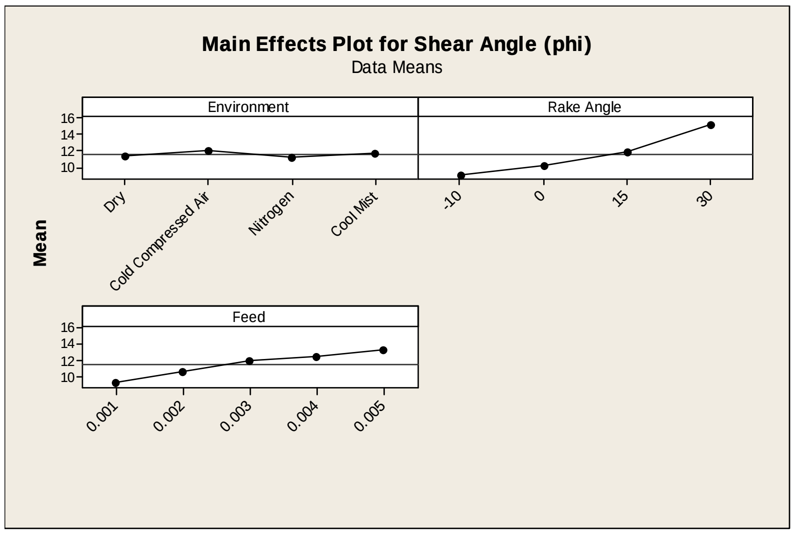

Figure 48: Main Effect Plot for Shear Plane Angle (Minitab 15)

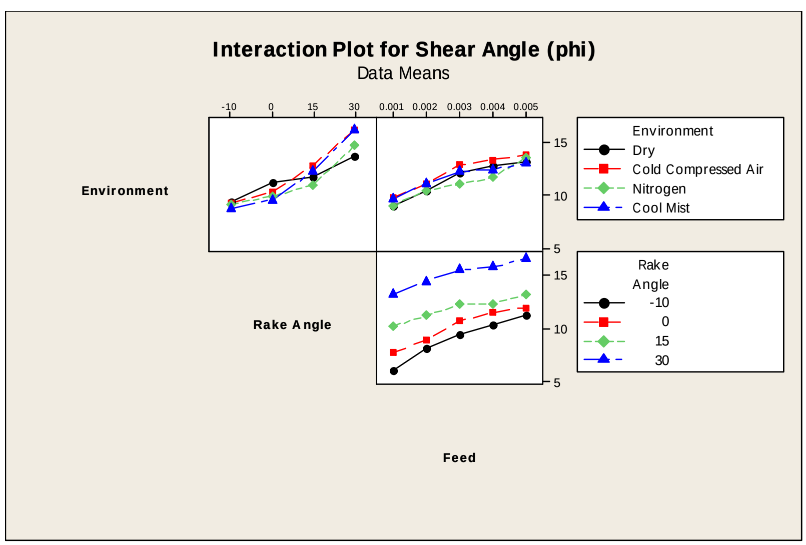

Figure 49: Interaction Plot for Shear Plane Angle (Minitab 15)

General Linear Model: Phi (degrees) versus Environment, Rake Angle, Feed

Factor	Type	Levels	Values
Environment	fixed	4	Dry, Cold Compressed Air, Nitrogen, Cool Mist
Rake Angle	fixed	4	-10, 0, 15, 30
Feed	fixed	5	0.001, 0.002, 0.003, 0.004, 0.005

Analysis of Variance for Phi (degrees), using Adjusted SS for Tests

Source	DF	Seq SS	Adj SS	Adj MS	F	P
Environment	3	42.746	42.746	14.249	86.70	0.000
Rake Angle	3	1921.459	1921.459	640.486	3897.42	0.000
Feed	4	766.450	766.450	191.612	1165.98	0.000
Environment*Rake Angle	9	132.056	132.056	14.673	89.29	0.000
Environment*Feed	12	35.141	35.141	2.928	17.82	0.000
Rake Angle*Feed	12	70.031	70.031	5.836	35.51	0.000
Environment*Rake Angle*Feed	36	126.512	126.512	3.514	21.38	0.000
Error	320	52.588	52.588	0.164		
Total	399	3146.982				

S = 0.405384   R-Sq = 98.33%   R-Sq(adj) = 97.92%

Table 23: ANOVA Table for Shear angle (φ) (Minitab 15)

Analysis of Variance (ANOVA) of Shear angle indicates that the rake angle has by far the dominant effect on this force ratio with an F-statistic of 3,897. The feed factor is second in significance with an F-statistic of 1,165. The individual effect of environment and the interaction effect of environment and rake angle are also found to have appreciable effect on the shear angle with their significant F-statistic values.

The shear plane angle is found to be lowest when machining under a nitrogen atmosphere when compared to other environments and is as shown in the main effects plot in figure 48. It can also be observed that the shear plane angle increases with increase in both rake angle and feed. A 30^o rake angle tool is found to produce higher shear angle than compared to a -10^o, 0^o or a 15^o tool.

Variation of Friction Angle (β) with Environment, Rake and Feed

Statistical analysis of the Friction angle (β) was conducted using the GLM (general linear module) of MINITAB 15. The main effects plot indicates that the effect of environment and feed on the friction angle is nearly a constant. Friction angle decreases appreciably with increasing positive rake angles.

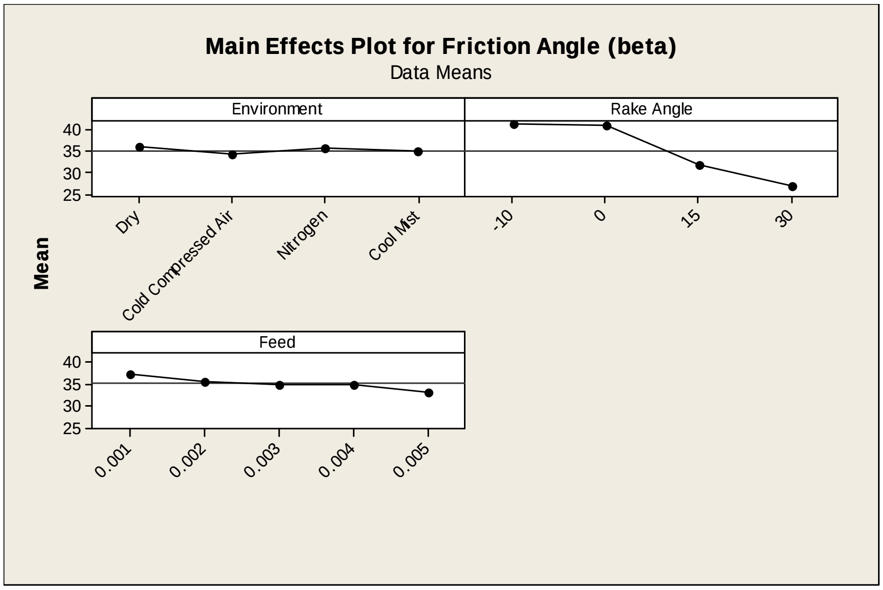

Figure 50: Main Effect Plot for Friction Angle (Minitab 15)

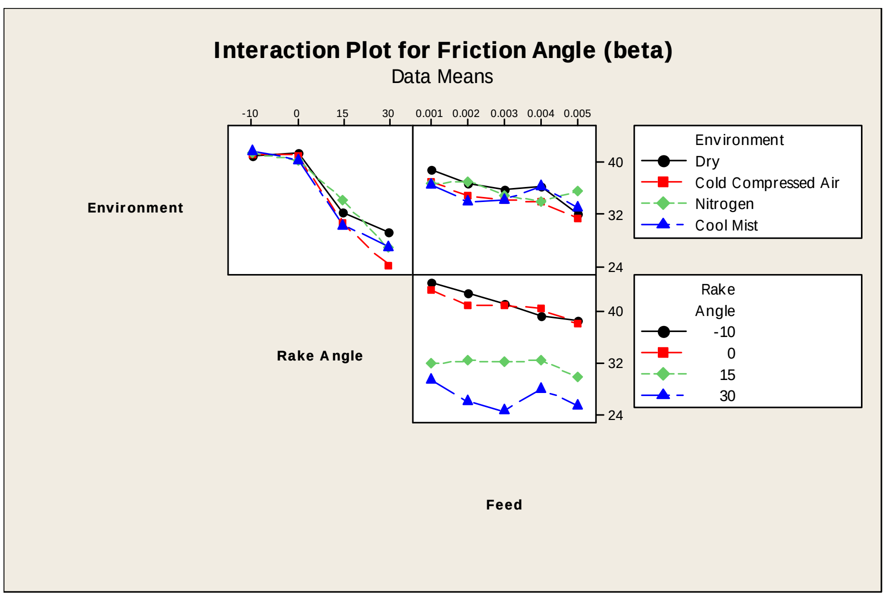

Figure 51: Interaction Plot for Friction Angle (Minitab 15)

General Linear Model: Friction Angle versus Environment, Rake Angle, Feed

Factor	Type	Levels	Values
Environment	fixed	4	Dry, Cold Compressed Air, Nitrogen, Cool Mist
Rake Angle	fixed	4	-10, 0, 15, 30
Feed	fixed	5	0.001, 0.002, 0.003, 0.004, 0.005

Analysis of Variance for Friction Angle (beta), using Adjusted SS for Tests

Source	DF	Seq SS	Adj SS	Adj MS	F	P
Environment	3	173.48	173.48	57.83	0.97	0.405
Rake Angle	3	14983.93	14983.93	4994.64	84.21	0.000
Feed	4	759.27	759.27	189.82	3.20	0.013
Environment*Rake Angle	9	410.15	410.15	45.57	0.77	0.646
Environment*Feed	12	383.82	383.82	31.98	0.54	0.888
Rake Angle*Feed	12	394.25	394.25	32.85	0.55	0.878
Environment*Rake Angle*Feed	36	1423.97	1423.97	39.55	0.67	0.930
Error	320	18979.97	18979.97	59.31		
Total	399	37508.82				

S = 7.70145   R-Sq = 49.40%   R-Sq(adj) = 36.91%

Table 24: ANOVA Table for Friction Angle (Minitab 15)

Analysis of Variance (ANOVA) of Friction angle indicates that the rake angle has by far the dominant effect on this force ratio with an F-statistic of 84. The environment and feed fail to attain significance on friction angle (β) with their p values being greater than 0.001.

The interaction plot obtained shows that with a 30^o rake angle tool a much lower friction angle is obtained than compared to a 0^o, 15^o or a -10^o tool. Also a drastic decrease in friction angle is observed between rake angles of 0^o to 15^o.It is evident from the above exsperiment that the friction angle is soley dependent on rake angle.

Variation of Shear Stress (τ_s) with Environment, Rake and Feed

Statistical analysis of the Shear Stress (τ_s) was conducted using the GLM (general linear module) of MINITAB 15. The main effects plot indicates that machining under nitrogen environment results in reduced shear stress as compared to other environments. The effect of rake angle factor is variable on the shear stress however a decrease in feed causes a significant decrease in the shear stress.

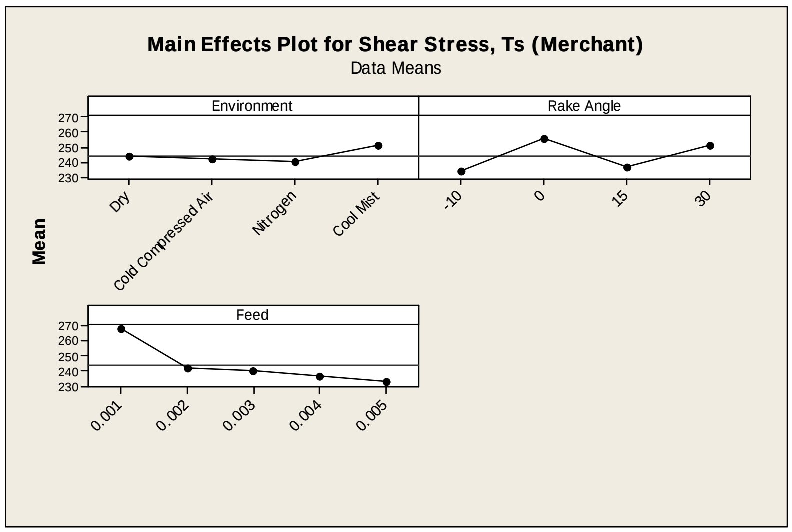

Figure 52: Main Effect Plot for Shear Stress (Minitab 15)

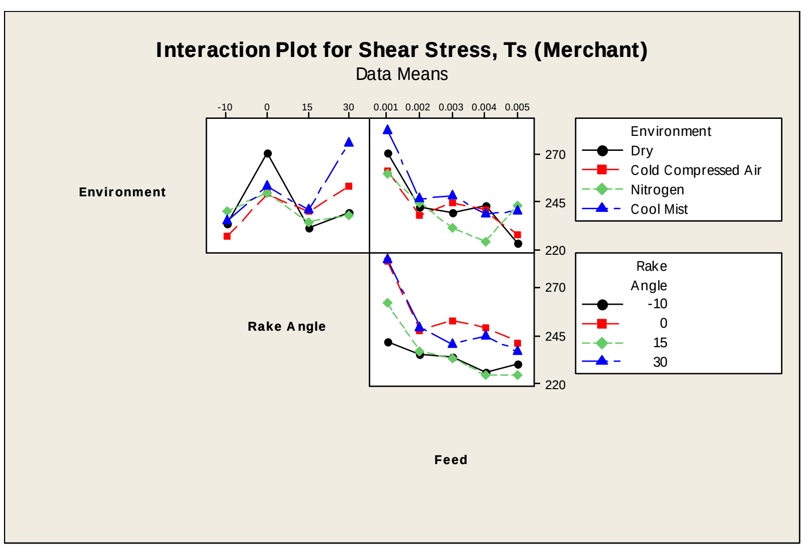

Figure 53: Interaction Plot for Shear Stress (Minitab 15)

General Linear Model: Shear Stress versus Environment, Rake Angle, Feed

Factor	Type	Levels	Values
Environment	fixed	4	Dry, Cold Compressed Air, Nitrogen, Cool Mist
Rake Angle	fixed	4	-10, 0, 15, 30
Feed	fixed	5	0.001, 0.002, 0.003, 0.004, 0.005

Analysis of Variance for Shear Stress, Ts(MPa), using Adjusted SS for Tests

Source	DF	Seq SS	Adj SS	Adj MS	F	P
Environment	3	6467.6	6467.6	2155.9	6.86	0.000
Rake Angle	3	34665.2	34665.2	11555.1	36.78	0.000
Feed	4	61430.8	61430.8	15357.7	48.88	0.000
Environment*Rake Angle	9	27982.0	27982.0	3109.1	9.90	0.000
Environment*Feed	12	13519.3	13519.3	1126.6	3.59	0.000
Rake Angle*Feed	12	11712.5	11712.5	976.0	3.11	0.000
Environment*Rake Angle*Feed	36	52191.2	52191.2	1449.8	4.61	0.000
Error	320	100543.9	100543.9	314.2		
Total	399	308512.5				

S = 17.7257   R-Sq = 67.41%   R-Sq(adj) = 59.36%

Table 25: ANOVA Table for Shear Stress (Minitab 15)

Analysis of Variance (ANOVA) of the shear stress response indicates that feed has a significant main effect upon the response with an F-statistic of 48. The tool rake angle is the next most dominant factor with an F-statistic of 36.

The interaction between the environment, rake angle and feed is found to have prominence over the shear stress. Also the shear stress is found to decrease with the increase in feed due to the decrease in shear force and increase in shear area leading to increase in shear plane angle [23].

Variation of Tool Surface Roughness with Environment, Rake and Feed

The visual observations, study and literature, all states that the variation of environment, rake angle and feed will have an influence on the tool surface. It can be observed from the main effects plot that the tool wear is found to be the least under nitrogen environment than compared to dry, cold compressed air or spray coolant environment.

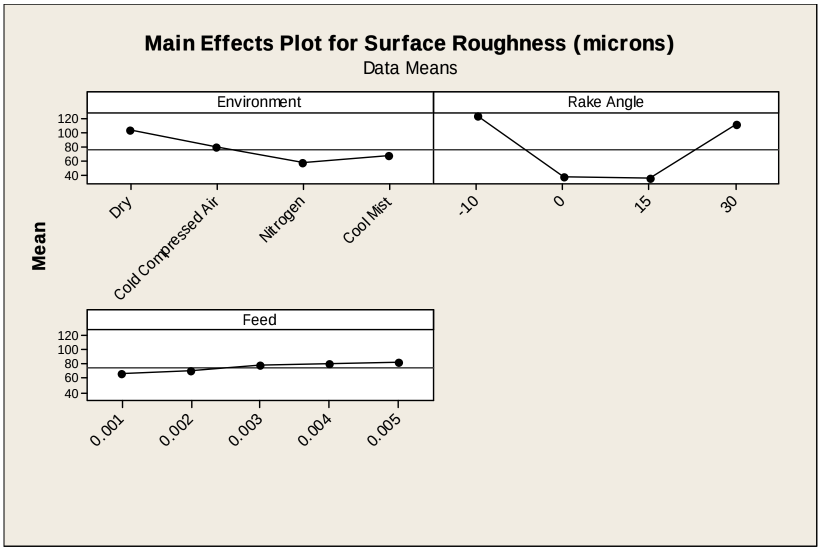

Figure 54: Main Effect Plot for Tool Surface Roughness (Minitab 15)

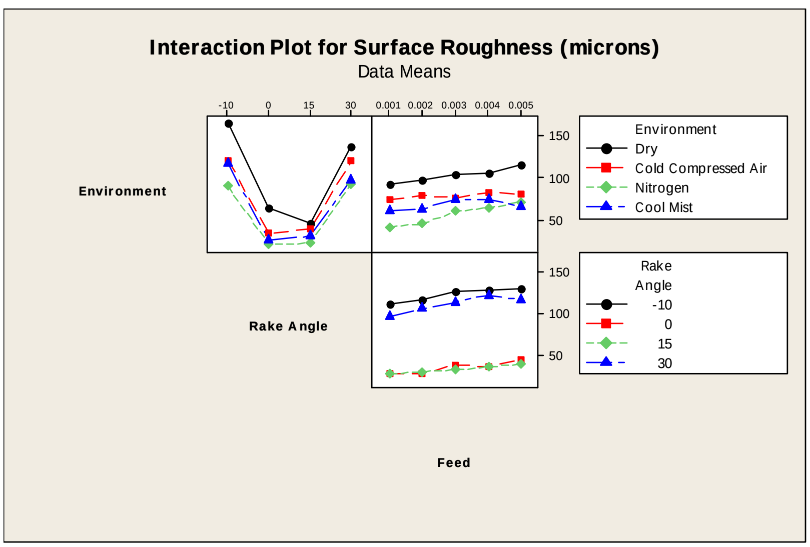

Figure 55: Interaction Plot for Tool Surface Roughness (Minitab 15)

The dry cutting environment produced an average surface roughness of 102 microns, with cold compressed air environment producing a surface roughness of 75 microns. The spray coolant environment resulted in a tool surface roughness of 70 microns as against nitrogen environment resulting in an average tool surface roughness of 55 microns.

Tool surface roughness is also found to be higher for the -10^o and 30^o tool when compared to a 0^o or a 15^o tool which showed significantly less surface roughness under all environments. Increase in tool surface roughness is observed with the increase in feed and is highest for a 0.005 inch feed. Also it is to be noted that the tool surface roughness is found to increase with the increase in thrust force and cutting force.

Appendix G provides detailed examples of each calculated value which was discussed in the chapter.

Variation of Tool Surface Roughness with Normal Force

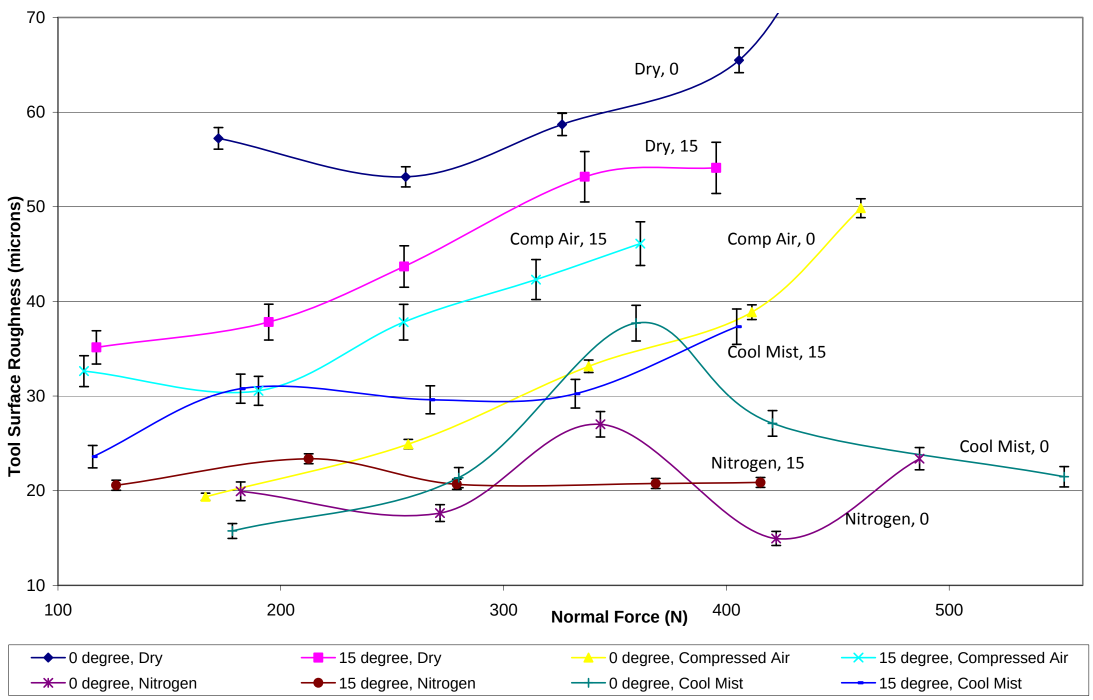

Figure 56: Variation of Tool surface roughness with Normal Force

The plot of variation of Tool surface roughness with normal force as shown in Figure 56 for a 0^{o} and a 15^{o} tool under all cutting environment shows that tool surface roughness increases with the increase in normal force. It is also to be noted that a 15^{o} tool has always generated less force compared to a 0^{o} tool under all four cutting environments. The tool surface roughness in the case of Nitrogen environment is less than the cool mist environment for both 0^{o} and 15^{o} tool rake angles. It is evident that nitrogen environment showed reduced tool surface roughness due to the decrease in shear angle and reduction in tool chip contact length. During the experiments it was also observed that the gases applications generally proved better results than dry machining.

CHAPTER 9

CONCLUSIONS

Based on a through analysis of the experimental results and observations the following conclusions are made about the variation of tool forces, tool surface roughness and the behavior of the shear angle with the change in input parameters.

1. The cutting force and the thrust force increases significantly with increase in feed. This can be explained by the fact that a feed rate increase will increase the amount of energy required to cause the plastic deformation of the material, resulting in increased tool forces.
2. The cutting force and thrust force decreases marginally with the increase in rake angle from -10^{o} to 0^{o} but decreases rapidly with the increase in rake angle from 0^{o} to 30^{o}. This can be explained by the fact that the tool chip contact area decreases with the increase in rake angle leading to the decrease in tool forces.
3. Reduced cutting force and thrust force are achieved using cold compressed air environment as compared to dry environment. The nitrogen environment produced a marginal decrease in forces as compared to spray coolant environment. It can be concluded that a tube turning set up with a nitrogen environment is the best environment for prolonging tool life at 500 sfpm during Orthogonal Tube Turning of AL 6061-T6.

4. Onset of Shear angle is found to be influenced by all the factor levels and is found to be the least at nitrogen environment. An increase in onset of shear angle is observed with an increase in rake angle and feed.
5. Tool surface roughness increases with the increase in feed from 0.001 inch to 0.005 inch.The surface roughness is also found to be significantly less when using a 0^o or a15^o rake angle tool when compared to a -10^o or a 30^0 tool.
6. Environment is found to have a significant effect on the tool surface roughness. The surface roughness in the nitrogen environment is found to be significantly less than all the other machining environments. The dry cutting environment produced an average surface roughness of 102 microns, with cold compressed air environment producing a surface roughness of 75 microns. The spray coolant environment resulted in a tool surface roughness of 70 micros as against nitrogen environment resulting in a average tool roughness of 55 microns.

CHAPTER 10

SCOPE FOR FUTURE WORK

A recent CIRP working paper reports the survey by a leading tool manufacturer indicating the following factors

- A correct cutting tool is selected less than 50% of the time.
- A tool is used at the rated cutting speed only 58% of the time.
- Only 38% of tools are used up to their full life capability

Viktor P Astakhov [24] states that today's Industry is completely dependent on empirical data provided by cutting tool and machine tool manufacturers as well as data provided through handbooks and workshops by Professional Engineering Associations. There is a lack of agreement in the data as it does not originate from the same source and there is no unified Metal Cutting Theory. Non availability of reliable tool life and optimum cutting parameters data for various tool and work material combinations leads to the reduced life of cutting tool and machine tools, so it is of prime importance to develop a realistic theory that governs the mechanism of metal cutting more deterministically and more accurately.

1. Additional models, other than the 1945 Merchant Model, can be compared to the data obtained in this thesis.

2. Cryogenic nitrogen is being investigated routinely as a cutting enviorment. It was not done during this experiment due to time and cost constraints. The forces, shear angle and tool surface roughness data under the various environments carried out can be compared with the cryogenic environment to more accurately determine the variation of responses with environment.
3. The complete insight of the behavior of the cutting forces, onset of shear plane angle, friction angle, shear stress and tool surface roughness with the variation in the feed, rake angle, cutting speed and environment is yet to be established by providing correction factors to the classical equations if necessary.
4. A simulation of the orthogonal tube turning can be carried out using an analysis package like ANSYS or NASTRAN to develop an optimum cutting condition in terms of tool forces and tool surface roughness.

REFERENCES

1. Merchant, M.E., "Mechanics of the Metal Cutting process," *Journal of Applied Physics*, Vol. 16, pp 267-275, 1945.
2. Paul Degarmo, E., Black, J.T., Kosher, R A., "Materials and Processes in Manufacturing," 10th Edition, Prentice Hall, Inc.
3. Payton, L.N., "A Correction to the 20th Century Orthogonal Metal Cutting Models," *Proceedings of the 2009 Industrial Engineering Research Conference.*
4. Lee, E.H., Shaffer, B.W., "The Theory of Plasticity Applied to a Problem of Machining," *Journal of Applied Mechanics*, Trans. ASME, Vol.73, 1951.
5. Rowe, G.W., SMART, E.F., "The Importance of Oxygen in Dry Machining of Metal on a Lathe," British Journal of Applied Physics, Vol.14, 1963.
6. Kovacevic, R., Cherukuthota, C., Mazurkiewicz, M., "High Pressure Water jet Cooling/Lubrication to Improve Machining Efficiency in Milling," *Journal of Machine Tools Manufacturing*, Vol.35, No. 10, 1995, pp 1459 – 1473.
7. Klocke, F., Eisenblatter, G., "Keynote Papers," RWTH Aachen, Germany.
8. Huang, L.H., Chen J.C., Chang, T., "Effect of Tool/Chip Contact Length on Orthogonal Tube Turning Performance," *Journal of Industrial Technology*, Vol.15, No. 2, February 1999 to April 1999.
9. Sreejith, P.S., Ngoi, B.K.A., "Dry machining: machining of the Future," *Journal of Materials Processing Technology*, Vol. 101, 2000, pp 287-291

10. Margitu, D.B., Ciocirlan, B.O., Craciunoiu, N., "Non-linear Dynamics in Orthogonal Turning Process," Department of Mechanical Engineering, Auburn University, 202, Ross Hall, Auburn, AL 36849, 2000.

11. Grzesik, W., "The Influence of Thin Hard Coatings on Frictional Behavior in the Orthogonal Cutting Process" Technical University of Opole, Department of Manufacturing Engineering and Automation, Opole, Poland, 2000.

12. Vieira, J.M., Machado, A.R., Ezugwu, E.O., 'Performance of Cutting Fluids during Face Milling of Steels," *Journal of Materials Processing Technology*, Vol.116, 2001, pp 244-251.

13. Paul, S., Dhar, N.R., Chattopadhyay, A.B., "Beneficial effects of Cryogenic Cooling over Dry and Wet Machining on Tool Wear and Surface Finish in Turning AISI 1060 Steel," *Journal of Materials Processing Technology*, 2007.

14. Diniz, A.E., Micaroni, R., "Cutting Conditions for Finish Turning Process Aiming the use of Dry Cutting," *International Journal of Machine Tools and Manufacture*, Vol.42, 2002, pp 899-904.

15. Cakir, O., Kiyak, M., Altan, E., "Comparison of Gases Applications to Wet and Dry Cuttings in Turning," *Journal of Materials Processing Technology*, Vol.153-154, 2004, pp 35-41.

16. M'Saoubi, R., Chandrasekaran, H., "Investigation of the Effects of Tool Micro-geometry and Coating on Tool Temperature during Orthogonal Turning of Quenched and Tempered Steel," *International Journal of Machine Tool and Manufacture*, Vol.44, No.2, pp213-224, 2004.

17. Salgam, H., Yaldiz, S., Unsarcar, F., "The Effect of Tool Geometry and Cutting Speed on Main Cutting Force and Tool Tip Temperature," Mechanical Engineering department, Technical Science College, Selcuk University, Konya, Turkey, 2005.

18. Kalyankumar, K.V.B.S., Choudry, S.K., "Investigation of Tool Wear and Cutting Force in Cryogenic Machining using Design of Experiments," *Journal of Materials Processing Technology*, Vol.203, 2007, pp 95-101.

19. Pujana, J., Azarolla, P.J., Villar, J.A., "In-process High Speed Photography Applied to Orthogonal Turning," *Journal of Materials Processing Technology*,Vol.202, 2008, pp 475-485.

20. Stanford, M., Lister, P.M., Morgan, C., Kibble, K.A., "Investigation into the use of Gaseous and Liquid Nitrogen as a Cutting Fluid when Turning BS 970-80A15 (En32b) Plain Carbon Steel using WC-Co uncoated tooling," *Journal of Materials Processing Technology*, Vol.209, Issue 2, 2009, pp 961-97

21. William H Cubberly., "Metals Handbook by American Society for Metals, ASM Handbook Committee, ASM International, Bruce P Bardes Edition: 9, illustrated".

22. Payton, L.N., "Orthogonal Machining of Copper using a Virtual Quick Stop Device", June 2000.

23. Kobayashi, S., Thomsen, E.G., "Role of Friction in Metal Cutting," *Journal of Engineering for Industry*, Transactions of the ASME, 1960, pp324-332.

24. Astakhov, V.P., "Metal Cutting Mechanics," Boca Raton: CRC Press, c1999.

APPENDIX A

The calibration certificate for the Kistler 9257 A dynamometer is given below.

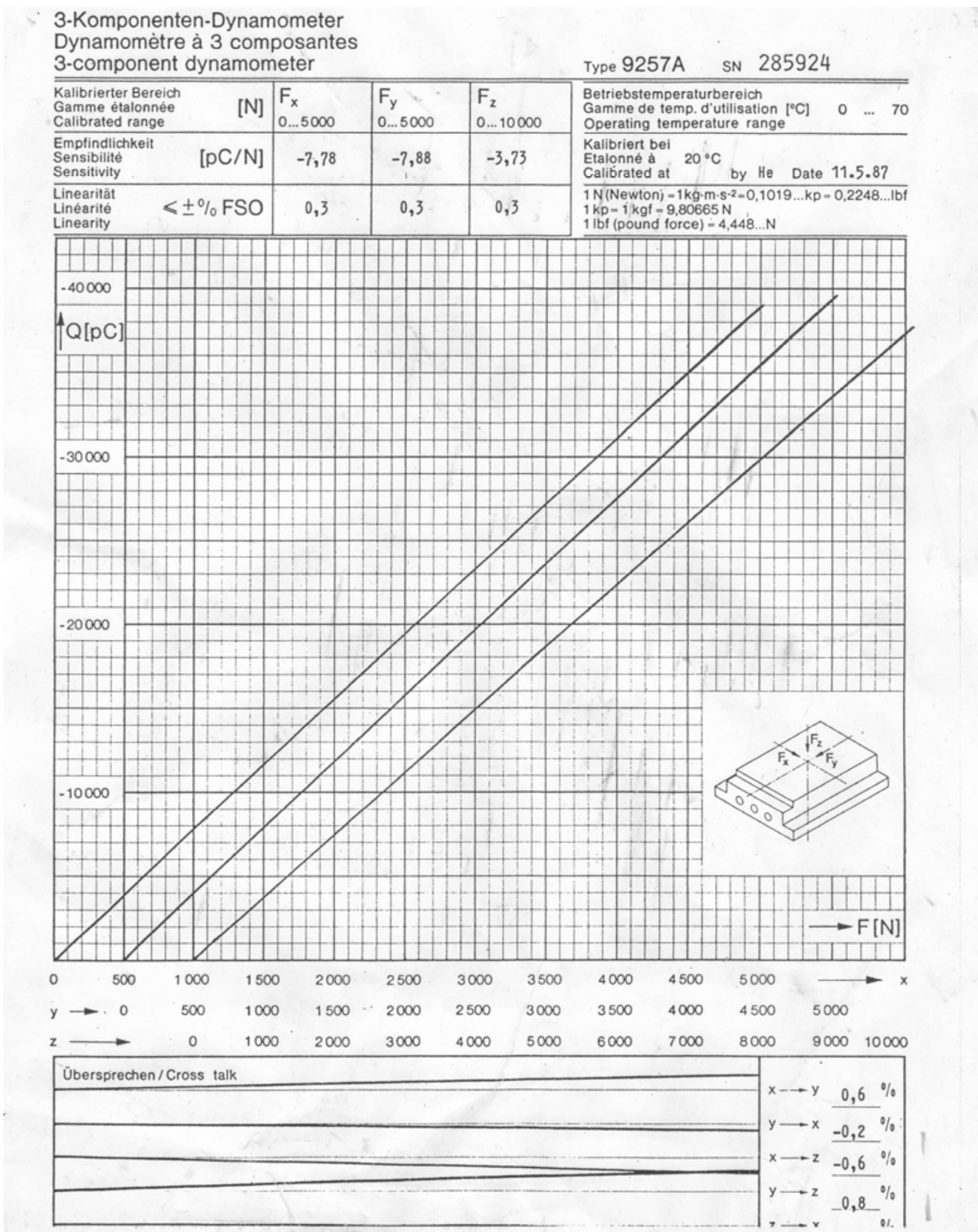

APPENDIX B

The spindle speed was calculated considering the material hardness and the geometrical dimensions of the alloy as shown below.

Alloy: Aluminum 6061

Hardness: 54.5 HRB

Diameter: 3 inches

Wall thickness: 0.125 inches

Considering a feed of 0.002 inch/rev to 0.005 inch/rev from "Machinery's Handbook" 27th Edition, pp 1038 for an Aluminum 6061 alloy being machined by a HSS tool the speed is 500 feet/minute.

Volume Swept by the tool in 1 revolution = 2 x π x 1.5 = 9.426 inches

= 0.7855 feet.

$$\text{RPM} = \frac{\text{Cutting Speed}}{\text{Volume Swept by the tool in 1 revolution}}$$

$$= \frac{500\,\frac{feet}{\min ute}}{0.7855\,\frac{feet}{rev}} = \mathbf{636.5372\ RPM}$$

The spindle speed was approximated as 640 RPM for the ease of calculations.

APPENDIX C

The below table gives the Thrust Force, Cutting Force and Cut Chip thickness data for all the 80 different factor level combinations.

Run No.	Environment	α	Feed	Run	Ft	Fc	tc
1	Dry	-10	0.001	Run 1	177.7517	175.993	0.0079
2	Dry	-10	0.001	Run 2	184.1773	177.2929	0.00833
3	Dry	-10	0.001	Run 3	177.9254	180.9517	0.00834
4	Dry	-10	0.001	Run 4	189.0791	181.1614	0.00808
5	Dry	-10	0.001	Run 5	194.356	185.0437	0.00837
6	Dry	-10	0.002	Run 1	251.7904	263.4748	0.01248
7	Dry	-10	0.002	Run 2	257.8228	268.7747	0.01263
8	Dry	-10	0.002	Run 3	258.6709	267.5613	0.01207
9	Dry	-10	0.002	Run 4	262.6206	272.2441	0.01229
10	Dry	-10	0.002	Run 5	264.2924	277.1065	0.01216
11	Dry	-10	0.003	Run 1	310.3103	335.1369	0.0177
12	Dry	-10	0.003	Run 2	327.1769	341.8487	0.01766
13	Dry	-10	0.003	Run 3	304.3356	340.2505	0.01742
14	Dry	-10	0.003	Run 4	313.9446	347.0742	0.0176
15	Dry	-10	0.003	Run 5	301.7063	335.4178	0.01719
16	Dry	-10	0.004	Run 1	356.3264	412.3702	0.02054
17	Dry	-10	0.004	Run 2	350.0089	402.2674	0.02122
18	Dry	-10	0.004	Run 3	370.2052	419.0703	0.02041
19	Dry	-10	0.004	Run 4	364.9769	409.6705	0.02143
20	Dry	-10	0.004	Run 5	375.6279	424.4903	0.02065
21	Dry	-10	0.005	Run 1	407.1834	474.696	0.02355
22	Dry	-10	0.005	Run 2	410.9808	475.7449	0.02417
23	Dry	-10	0.005	Run 3	404.456	467.8064	0.02412
24	Dry	-10	0.005	Run 4	415.8704	479.9004	0.02454
25	Dry	-10	0.005	Run 5	416.2005	483.9898	0.02425
26	Dry	0	0.001	Run 1	178.7172	172.4828	0.00647
27	Dry	0	0.001	Run 2	175.5777	171.1007	0.00624
28	Dry	0	0.001	Run 3	175.7445	174.1149	0.0063
29	Dry	0	0.001	Run 4	173.5154	170.2533	0.00651
30	Dry	0	0.001	Run 5	170.9717	172.3044	0.00647
31	Dry	0	0.002	Run 1	223.7989	255.7188	0.01126
32	Dry	0	0.002	Run 2	218.0048	250.2855	0.01114

Run No.	Environment	α	Feed	Run	Ft	Fc	tc
33	Dry	0	0.002	Run 3	219.3895	254.1104	0.01158
34	Dry	0	0.002	Run 4	226.1762	264.9091	0.01145
35	Dry	0	0.002	Run 5	220.2374	255.4329	0.01138
36	Dry	0	0.003	Run 1	293.5401	323.8849	0.01375
37	Dry	0	0.003	Run 2	304.5111	329.6172	0.0141
38	Dry	0	0.003	Run 3	297.467	329.553	0.01405
39	Dry	0	0.003	Run 4	292.9392	325.1263	0.01384
40	Dry	0	0.003	Run 5	292.05	323.1182	0.01385
41	Dry	0	0.004	Run 1	360.526	414.8286	0.01746
42	Dry	0	0.004	Run 2	363.5965	399.0163	0.01774
43	Dry	0	0.004	Run 3	377.5881	399.5048	0.01746
44	Dry	0	0.004	Run 4	361.6405	411.0423	0.01735
45	Dry	0	0.004	Run 5	373.5652	403.9943	0.0179
46	Dry	0	0.005	Run 1	319.7004	460.565	0.02348
47	Dry	0	0.005	Run 2	327.1955	450.0505	0.02348
48	Dry	0	0.005	Run 3	327.1843	459.6015	0.02314
49	Dry	0	0.005	Run 4	329.8673	448.3882	0.02324
50	Dry	0	0.005	Run 5	323.936	458.4112	0.02357
51	Dry	15	0.001	Run 1	58.8858	127.9112	0.00547
52	Dry	15	0.001	Run 2	65.4667	120.879	0.00556
53	Dry	15	0.001	Run 3	69.0838	114.2018	0.00562
54	Dry	15	0.001	Run 4	66.4581	122.6205	0.00522
55	Dry	15	0.001	Run 5	66.4237	120.155	0.00527
56	Dry	15	0.002	Run 1	107.4316	201.9459	0.01054
57	Dry	15	0.002	Run 2	113.0798	200.5681	0.0106
58	Dry	15	0.002	Run 3	114.3104	199.1714	0.01055
59	Dry	15	0.002	Run 4	118.0056	204.2604	0.01019
60	Dry	15	0.002	Run 5	118.1204	201.6331	0.01074
61	Dry	15	0.003	Run 1	131.4321	261.1614	0.01455
62	Dry	15	0.003	Run 2	142.362	262.1011	0.01446
63	Dry	15	0.003	Run 3	153.4347	268.9463	0.01457
64	Dry	15	0.003	Run 4	148.8125	262.3391	0.01459
65	Dry	15	0.003	Run 5	151.5232	265.1171	0.01466
66	Dry	15	0.004	Run 1	199.523	355.5064	0.01961
67	Dry	15	0.004	Run 2	201.9163	354.7528	0.01952
68	Dry	15	0.004	Run 3	207.3945	347.9605	0.0196
69	Dry	15	0.004	Run 4	201.1935	339.4066	0.0194
70	Dry	15	0.004	Run 5	212.3329	348.3219	0.0195
71	Dry	15	0.005	Run 1	214.2508	410.0906	0.02203
72	Dry	15	0.005	Run 2	224.6541	411.051	0.02271
73	Dry	15	0.005	Run 3	227.3489	405.2153	0.02242
74	Dry	15	0.005	Run 4	223.9582	407.5608	0.02251
75	Dry	15	0.005	Run 5	233.539	412.6333	0.02249
76	Dry	30	0.001	Run 1	63.2424	116.0273	0.00565
77	Dry	30	0.001	Run 2	63.6391	116.4696	0.00554
78	Dry	30	0.001	Run 3	63.6573	117.28	0.00562
79	Dry	30	0.001	Run 4	64.9941	118.6791	0.00552

Run No.	Environment	α	Feed	Run	Ft	Fc	tc
80	Dry	30	0.001	Run 5	62.9518	115.4918	0.00545
81	Dry	30	0.002	Run 1	81.252	188.0265	0.00951
82	Dry	30	0.002	Run 2	81.1605	176.7414	0.0096
83	Dry	30	0.002	Run 3	88.0791	178.6659	0.00958
84	Dry	30	0.002	Run 4	90.344	181.2736	0.00927
85	Dry	30	0.002	Run 5	91.9134	182.55	0.00933
86	Dry	30	0.003	Run 1	92.8429	236.4955	0.01134
87	Dry	30	0.003	Run 2	99.4893	239.5004	0.01155
88	Dry	30	0.003	Run 3	98.1772	238.2484	0.01113
89	Dry	30	0.003	Run 4	98.0449	242.13	0.01143
90	Dry	30	0.003	Run 5	100.0638	239.2623	0.01156
91	Dry	30	0.004	Run 1	136.5777	316.4789	0.0115
92	Dry	30	0.004	Run 2	140.2462	323.6529	0.01152
93	Dry	30	0.004	Run 3	143.6655	315.2217	0.01569
94	Dry	30	0.004	Run 4	141.0172	322.3968	0.01583
95	Dry	30	0.004	Run 5	141.963	316.2296	0.0156
96	Dry	30	0.005	Run 1	90.2882	333.6152	0.01761
97	Dry	30	0.005	Run 2	93.9447	333.7997	0.01768
98	Dry	30	0.005	Run 3	91.8477	339.6543	0.01733
99	Dry	30	0.005	Run 4	101.1709	335.6297	0.01756
100	Dry	30	0.005	Run 5	99.2913	343.7709	0.01766
101	Compressed Air	-10	0.001	Run 1	197.7884	182.1416	0.00933
102	Compressed Air	-10	0.001	Run 2	201.2496	185.7809	0.00958
103	Compressed Air	-10	0.001	Run 3	199.8761	184.3276	0.00919
104	Compressed Air	-10	0.001	Run 4	199.5928	186.4235	0.00951
105	Compressed Air	-10	0.001	Run 5	200.8335	187.2002	0.00975
106	Compressed Air	-10	0.002	Run 1	256.1353	262.1515	0.01296
107	Compressed Air	-10	0.002	Run 2	259.7657	260.5958	0.01365
108	Compressed Air	-10	0.002	Run 3	261.4814	264.5966	0.01346
109	Compressed Air	-10	0.002	Run 4	268.5294	271.2766	0.01356
110	Compressed Air	-10	0.002	Run 5	269.8701	274.0365	0.01359
111	Compressed Air	-10	0.003	Run 1	293.3559	324.7656	0.0165
112	Compressed Air	-10	0.003	Run 2	296.6442	324.1789	0.0164
113	Compressed Air	-10	0.003	Run 3	302.8356	329.6997	0.01657
114	Compressed Air	-10	0.003	Run 4	299.3754	331.8196	0.01632
115	Compressed Air	-10	0.003	Run 5	310.1497	340.834	0.01661
116	Compressed Air	-10	0.004	Run 1	339.8878	395.3502	0.01964
117	Compressed Air	-10	0.004	Run 2	347.7198	397.9039	0.01972
118	Compressed Air	-10	0.004	Run 3	354.7987	405.5534	0.01951
119	Compressed Air	-10	0.004	Run 4	358.8273	405.5811	0.01965
120	Compressed Air	-10	0.004	Run 5	359.2857	410.5226	0.01973
121	Compressed Air	-10	0.005	Run 1	402.3728	459.5607	0.02311
122	Compressed Air	-10	0.005	Run 2	396.068	466.8819	0.02345
123	Compressed Air	-10	0.005	Run 3	407.5286	474.8292	0.02309
124	Compressed Air	-10	0.005	Run 4	402.6982	477.0524	0.0237
125	Compressed Air	-10	0.005	Run 5	399.2012	472.631	0.02363
126	Compressed Air	0	0.001	Run 1	162.9359	165.2332	0.00768

Run No.	Environment	α	Feed	Run	Ft	Fc	tc
127	Compressed Air	0	0.001	Run 2	162.1041	165.1499	0.00737
128	Compressed Air	0	0.001	Run 3	162.9914	165.581	0.00727
129	Compressed Air	0	0.001	Run 4	165.6891	166.338	0.00737
130	Compressed Air	0	0.001	Run 5	166.8184	168.7141	0.00771
131	Compressed Air	0	0.002	Run 1	219.5647	261.0481	0.01325
132	Compressed Air	0	0.002	Run 2	213.2506	254.2292	0.01335
133	Compressed Air	0	0.002	Run 3	215.2732	254.5406	0.01311
134	Compressed Air	0	0.002	Run 4	220.1807	259.7471	0.01298
135	Compressed Air	0	0.002	Run 5	213.1102	256.4842	0.01278
136	Compressed Air	0	0.003	Run 1	306.661	331.6338	0.01537
137	Compressed Air	0	0.003	Run 2	304.5306	333.9596	0.01518
138	Compressed Air	0	0.003	Run 3	298.4483	337.417	0.01564
139	Compressed Air	0	0.003	Run 4	309.4737	345.7519	0.01527
140	Compressed Air	0	0.003	Run 5	302.9238	342.2661	0.01543
141	Compressed Air	0	0.004	Run 1	371.3089	412.5695	0.02037
142	Compressed Air	0	0.004	Run 2	379.8773	415.9003	0.02058
143	Compressed Air	0	0.004	Run 3	378.5803	417.6269	0.01986
144	Compressed Air	0	0.004	Run 4	374.1755	407.4259	0.02045
145	Compressed Air	0	0.004	Run 5	377.5255	403.7149	0.0196
146	Compressed Air	0	0.005	Run 1	322.9589	463.6449	0.02241
147	Compressed Air	0	0.005	Run 2	328.9528	459.787	0.02253
148	Compressed Air	0	0.005	Run 3	337.3287	459.4949	0.02239
149	Compressed Air	0	0.005	Run 4	328.9954	454.964	0.02239
150	Compressed Air	0	0.005	Run 5	337.7602	463.6962	0.02234
151	Compressed Air	15	0.001	Run 1	61.5124	113.1831	0.00548
152	Compressed Air	15	0.001	Run 2	63.2416	114.0435	0.00556
153	Compressed Air	15	0.001	Run 3	64.4127	116.2906	0.00542
154	Compressed Air	15	0.001	Run 4	65.1112	117.1496	0.0053
155	Compressed Air	15	0.001	Run 5	66.058	117.3281	0.00537
156	Compressed Air	15	0.002	Run 1	105.2246	197.447	0.00976
157	Compressed Air	15	0.002	Run 2	104.2617	190.4033	0.01001
158	Compressed Air	15	0.002	Run 3	112.199	195.5409	0.00965
159	Compressed Air	15	0.002	Run 4	114.3065	199.6868	0.00969
160	Compressed Air	15	0.002	Run 5	119.2931	200.8401	0.00975
161	Compressed Air	15	0.003	Run 1	134.4895	254.2782	0.0138
162	Compressed Air	15	0.003	Run 2	143.1355	265.2779	0.01368
163	Compressed Air	15	0.003	Run 3	142.515	265.0369	0.01354
164	Compressed Air	15	0.003	Run 4	144.0262	265.7019	0.0135
165	Compressed Air	15	0.003	Run 5	145.1991	268.8831	0.01379
166	Compressed Air	15	0.004	Run 1	167.0502	323.9666	0.01654
167	Compressed Air	15	0.004	Run 2	163.5994	323.5697	0.01638
168	Compressed Air	15	0.004	Run 3	165.446	323.5697	0.01631
169	Compressed Air	15	0.004	Run 4	172.0612	329.7176	0.01671
170	Compressed Air	15	0.004	Run 5	167.4072	326.1765	0.01645
171	Compressed Air	15	0.005	Run 1	159.3689	363.3295	0.01976
172	Compressed Air	15	0.005	Run 2	167.9498	372.6552	0.01953
173	Compressed Air	15	0.005	Run 3	169.5887	372.6489	0.01964

Run No.	Environment	α	Feed	Run	Ft	Fc	tc
174	Compressed Air	15	0.005	Run 4	167.1795	376.4682	0.01979
175	Compressed Air	15	0.005	Run 5	170.1	375.4764	0.01981
176	Compressed Air	30	0.001	Run 1	29.9759	89.3659	0.00359
177	Compressed Air	30	0.001	Run 2	33.7425	91.2695	0.00387
178	Compressed Air	30	0.001	Run 3	32.2379	95.873	0.00374
179	Compressed Air	30	0.001	Run 4	35.996	95.9412	0.00373
180	Compressed Air	30	0.001	Run 5	38.689	94.1467	0.00381
181	Compressed Air	30	0.002	Run 1	44.4358	149.7706	0.00755
182	Compressed Air	30	0.002	Run 2	47.7565	152.4468	0.00754
183	Compressed Air	30	0.002	Run 3	50.2597	155.6077	0.00705
184	Compressed Air	30	0.002	Run 4	50.2975	155.8898	0.00742
185	Compressed Air	30	0.002	Run 5	51.8714	156.5935	0.00704
186	Compressed Air	30	0.003	Run 1	63.5885	215.6585	0.00967
187	Compressed Air	30	0.003	Run 2	61.2472	210.745	0.00965
188	Compressed Air	30	0.003	Run 3	64.6666	211.8868	0.00977
189	Compressed Air	30	0.003	Run 4	69.2517	216.0162	0.0097
190	Compressed Air	30	0.003	Run 5	70.628	217.1014	0.00964
191	Compressed Air	30	0.004	Run 1	92.6672	285.7289	0.01352
192	Compressed Air	30	0.004	Run 2	88.1638	279.4771	0.01333
193	Compressed Air	30	0.004	Run 3	86.1354	277.423	0.01349
194	Compressed Air	30	0.004	Run 4	86.2464	281.964	0.01342
195	Compressed Air	30	0.004	Run 5	91.2761	287.9853	0.01348
196	Compressed Air	30	0.005	Run 1	109.3864	328.9997	0.01762
197	Compressed Air	30	0.005	Run 2	107.6019	325.5716	0.01754
198	Compressed Air	30	0.005	Run 3	108.0435	331.8501	0.01757
199	Compressed Air	30	0.005	Run 4	112.4562	336.0007	0.01767
200	Compressed Air	30	0.005	Run 5	102.807	322.619	0.01777
201	Nitrogen	-10	0.001	Run 1	206.6564	195.5815	0.00968
202	Nitrogen	-10	0.001	Run 2	207.1426	192.6893	0.0095
203	Nitrogen	-10	0.001	Run 3	202.68	194.1392	0.00924
204	Nitrogen	-10	0.001	Run 4	217.7624	200.6148	0.00938
205	Nitrogen	-10	0.001	Run 5	214.5732	198.1373	0.00967
206	Nitrogen	-10	0.002	Run 1	287.6712	281.1819	0.01354
207	Nitrogen	-10	0.002	Run 2	287.13	282.1961	0.01346
208	Nitrogen	-10	0.002	Run 3	292.2072	285.1416	0.01364
209	Nitrogen	-10	0.002	Run 4	284.7899	279.5205	0.01352
210	Nitrogen	-10	0.002	Run 5	289.2702	279.558	0.01318
211	Nitrogen	-10	0.003	Run 1	383.9224	395.708	0.01845
212	Nitrogen	-10	0.003	Run 2	373.3497	398.0761	0.01843
213	Nitrogen	-10	0.003	Run 3	382.5961	385.8474	0.01838
214	Nitrogen	-10	0.003	Run 4	382.5391	391.1423	0.01855
215	Nitrogen	-10	0.003	Run 5	379.7901	396.6776	0.01825
216	Nitrogen	-10	0.004	Run 1	368.9621	439.3335	0.0205
217	Nitrogen	-10	0.004	Run 2	373.8964	424.6515	0.02083
218	Nitrogen	-10	0.004	Run 3	381.3443	437.8459	0.02043
219	Nitrogen	-10	0.004	Run 4	390.1037	439.4337	0.02089
220	Nitrogen	-10	0.004	Run 5	377.0451	433.2095	0.02045

Run No.	Environment	α	Feed	Run	Ft	Fc	tc
221	Nitrogen	-10	0.005	Run 1	395.6619	495.5847	0.02189
222	Nitrogen	-10	0.005	Run 2	373.1608	478.6916	0.02219
223	Nitrogen	-10	0.005	Run 3	378.8455	472.3057	0.02183
224	Nitrogen	-10	0.005	Run 4	382.9149	474.1717	0.02223
225	Nitrogen	-10	0.005	Run 5	392.4226	487.8136	0.02217
226	Nitrogen	0	0.001	Run 1	164.5504	184.5599	0.00813
227	Nitrogen	0	0.001	Run 2	163.1026	182.9984	0.00817
228	Nitrogen	0	0.001	Run 3	159.9201	178.6047	0.00812
229	Nitrogen	0	0.001	Run 4	161.9422	182.6511	0.00825
230	Nitrogen	0	0.001	Run 5	163.0827	181.1829	0.00806
231	Nitrogen	0	0.002	Run 1	233.1829	271.1694	0.01107
232	Nitrogen	0	0.002	Run 2	234.9983	266.0591	0.01385
233	Nitrogen	0	0.002	Run 3	242.5081	275.9159	0.01366
234	Nitrogen	0	0.002	Run 4	236.4188	270.1852	0.01361
235	Nitrogen	0	0.002	Run 5	237.9905	274.003	0.01357
236	Nitrogen	0	0.003	Run 1	279.5769	346.4283	0.01688
237	Nitrogen	0	0.003	Run 2	279.0627	343.8411	0.01675
238	Nitrogen	0	0.003	Run 3	281.6154	342.3731	0.01656
239	Nitrogen	0	0.003	Run 4	275.8128	342.3738	0.01689
240	Nitrogen	0	0.003	Run 5	279.2154	342.2708	0.01653
241	Nitrogen	0	0.004	Run 1	334.6459	425.5195	0.01958
242	Nitrogen	0	0.004	Run 2	331.8301	416.7075	0.01971
243	Nitrogen	0	0.004	Run 3	335.0354	424.1981	0.01964
244	Nitrogen	0	0.004	Run 4	328.8234	420.35	0.01964
245	Nitrogen	0	0.004	Run 5	326.9944	424.9836	0.0197
246	Nitrogen	0	0.005	Run 1	430.5991	484.6631	0.02352
247	Nitrogen	0	0.005	Run 2	427.0402	488.0082	0.02404
248	Nitrogen	0	0.005	Run 3	417.6366	483.0138	0.02342
249	Nitrogen	0	0.005	Run 4	424.0487	490.4496	0.02468
250	Nitrogen	0	0.005	Run 5	417.0269	487.2506	0.02383
251	Nitrogen	15	0.001	Run 1	78.6877	132.4233	0.00646
252	Nitrogen	15	0.001	Run 2	77.7225	130.8423	0.00596
253	Nitrogen	15	0.001	Run 3	78.8442	129.2723	0.00632
254	Nitrogen	15	0.001	Run 4	76.9546	133.4419	0.00612
255	Nitrogen	15	0.001	Run 5	77.8638	129.4782	0.00641
256	Nitrogen	15	0.002	Run 1	150.1096	221.7002	0.01123
257	Nitrogen	15	0.002	Run 2	152.0043	220.2428	0.01148
258	Nitrogen	15	0.002	Run 3	156.324	228.9791	0.01119
259	Nitrogen	15	0.002	Run 4	149.3831	219.0391	0.01152
260	Nitrogen	15	0.002	Run 5	149.2316	219.1011	0.01164
261	Nitrogen	15	0.003	Run 1	167.8966	291.6661	0.01467
262	Nitrogen	15	0.003	Run 2	163.8237	284.3597	0.01483
263	Nitrogen	15	0.003	Run 3	166.1155	286.7002	0.01511
264	Nitrogen	15	0.003	Run 4	169.8913	290.2186	0.01501
265	Nitrogen	15	0.003	Run 5	170.3016	295.5275	0.01529
266	Nitrogen	15	0.004	Run 1	241.7012	380.6288	0.02117
267	Nitrogen	15	0.004	Run 2	243.4664	381.1891	0.02134

Run No.	Environment	α	Feed	Run	Ft	Fc	tc
268	Nitrogen	15	0.004	Run 3	236.7358	376.3736	0.02151
269	Nitrogen	15	0.004	Run 4	240.0703	388.8308	0.02168
270	Nitrogen	15	0.004	Run 5	247.0985	389.9095	0.02121
271	Nitrogen	15	0.005	Run 1	223.7015	430.0145	0.02171
272	Nitrogen	15	0.005	Run 2	222.2084	427.8287	0.02216
273	Nitrogen	15	0.005	Run 3	229.9665	428.6029	0.02209
274	Nitrogen	15	0.005	Run 4	230.929	429.1843	0.02194
275	Nitrogen	15	0.005	Run 5	233.4081	433.5332	0.02206
276	Nitrogen	30	0.001	Run 1	34.2568	91.7117	0.00406
277	Nitrogen	30	0.001	Run 2	34.379	93.6644	0.00414
278	Nitrogen	30	0.001	Run 3	36.4733	95.4205	0.00396
279	Nitrogen	30	0.001	Run 4	37.0401	96.0515	0.00403
280	Nitrogen	30	0.001	Run 5	31.39	92.8399	0.00367
281	Nitrogen	30	0.002	Run 1	57.6798	158.8456	0.00755
282	Nitrogen	30	0.002	Run 2	58.8684	169.1589	0.00755
283	Nitrogen	30	0.002	Run 3	64.8787	166.0229	0.00761
284	Nitrogen	30	0.002	Run 4	64.8416	167.4373	0.00754
285	Nitrogen	30	0.002	Run 5	54.8339	171.6381	0.00753
286	Nitrogen	30	0.003	Run 1	70.0972	213.5992	0.01228
287	Nitrogen	30	0.003	Run 2	74.4158	219.5313	0.01212
288	Nitrogen	30	0.003	Run 3	76.2422	218.8497	0.01257
289	Nitrogen	30	0.003	Run 4	74.3471	217.4577	0.01227
290	Nitrogen	30	0.003	Run 5	83.6924	224.6447	0.01268
291	Nitrogen	30	0.004	Run 1	76.5872	261.6407	0.01532
292	Nitrogen	30	0.004	Run 2	76.7912	262.8484	0.01655
293	Nitrogen	30	0.004	Run 3	82.3925	270.9511	0.01568
294	Nitrogen	30	0.004	Run 4	85.1815	271.8372	0.0167
295	Nitrogen	30	0.004	Run 5	83.8936	269.3505	0.01676
296	Nitrogen	30	0.005	Run 1	195.738	376.7756	0.01659
297	Nitrogen	30	0.005	Run 2	191.2584	369.0897	0.01658
298	Nitrogen	30	0.005	Run 3	198.9184	369.0897	0.01651
299	Nitrogen	30	0.005	Run 4	197.3296	364.3208	0.01687
300	Nitrogen	30	0.005	Run 5	186.2928	369.2408	0.01652
301	Cool Mist	-10	0.001	Run 1	195.7094	196.7856	0.00929
302	Cool Mist	-10	0.001	Run 2	196.3354	192.175	0.00955
303	Cool Mist	-10	0.001	Run 3	204.0934	201.2071	0.00931
304	Cool Mist	-10	0.001	Run 4	201.2784	193.76	0.00956
305	Cool Mist	-10	0.001	Run 5	208.4875	202.2933	0.00952
306	Cool Mist	-10	0.002	Run 1	297.3487	290.4151	0.01465
307	Cool Mist	-10	0.002	Run 2	300.1617	291.3465	0.01463
308	Cool Mist	-10	0.002	Run 3	289.5194	286.3318	0.01472
309	Cool Mist	-10	0.002	Run 4	289.8274	286.5597	0.01462
310	Cool Mist	-10	0.002	Run 5	287.2581	293.0959	0.01475
311	Cool Mist	-10	0.003	Run 1	359.714	375.0335	0.01655
312	Cool Mist	-10	0.003	Run 2	359.7902	373.8692	0.01676
313	Cool Mist	-10	0.003	Run 3	349.0415	367.1384	0.01673
314	Cool Mist	-10	0.003	Run 4	356.6663	364.5413	0.01685

Run No.	Environment	α	Feed	Run	Ft	Fc	tc
315	Cool Mist	-10	0.003	Run 5	349.8105	362.813	0.01679
316	Cool Mist	-10	0.004	Run 1	375.2386	428.8634	0.0223
317	Cool Mist	-10	0.004	Run 2	386.0774	429.459	0.02259
318	Cool Mist	-10	0.004	Run 3	373.0587	428.976	0.02229
319	Cool Mist	-10	0.004	Run 4	374.3297	435.5474	0.02246
320	Cool Mist	-10	0.004	Run 5	376.0092	429.0622	0.02241
321	Cool Mist	-10	0.005	Run 1	483.7339	534.68	0.02549
322	Cool Mist	-10	0.005	Run 2	490.7619	544.2519	0.02545
323	Cool Mist	-10	0.005	Run 3	491.3546	544.1311	0.02561
324	Cool Mist	-10	0.005	Run 4	491.4266	546.3741	0.02552
325	Cool Mist	-10	0.005	Run 5	491.3052	547.4965	0.02548
326	Cool Mist	0	0.001	Run 1	152.4772	175.133	0.0075
327	Cool Mist	0	0.001	Run 2	152.2068	180.9133	0.00764
328	Cool Mist	0	0.001	Run 3	156.0352	179.9308	0.00743
329	Cool Mist	0	0.001	Run 4	158.5667	179.1254	0.00756
330	Cool Mist	0	0.001	Run 5	156.9991	176.181	0.00763
331	Cool Mist	0	0.002	Run 1	247.4289	279.3266	0.0135
332	Cool Mist	0	0.002	Run 2	243.5632	275.3585	0.0136
333	Cool Mist	0	0.002	Run 3	246.5875	278.1679	0.01361
334	Cool Mist	0	0.002	Run 4	252.9061	282.2953	0.01338
335	Cool Mist	0	0.002	Run 5	252.7687	284.098	0.01361
336	Cool Mist	0	0.003	Run 1	307.5088	364.4924	0.01765
337	Cool Mist	0	0.003	Run 2	304.3039	358.126	0.01779
338	Cool Mist	0	0.003	Run 3	299.7853	355.6117	0.01761
339	Cool Mist	0	0.003	Run 4	298.1503	356.1509	0.01764
340	Cool Mist	0	0.003	Run 5	306.4602	362.9809	0.01773
341	Cool Mist	0	0.004	Run 1	335.8497	421.2274	0.0214
342	Cool Mist	0	0.004	Run 2	335.8612	418.2116	0.02153
343	Cool Mist	0	0.004	Run 3	334.4233	418.9726	0.02152
344	Cool Mist	0	0.004	Run 4	338.8065	422.3275	0.0217
345	Cool Mist	0	0.004	Run 5	338.8065	422.8405	0.02106
346	Cool Mist	0	0.005	Run 1	462.9319	556.5036	0.02455
347	Cool Mist	0	0.005	Run 2	463.8574	554.134	0.02461
348	Cool Mist	0	0.005	Run 3	461.594	546.7876	0.02471
349	Cool Mist	0	0.005	Run 4	456.2306	559.0695	0.02474
350	Cool Mist	0	0.005	Run 5	454.8527	541.429	0.02464
351	Cool Mist	15	0.001	Run 1	61.4443	117.727	0.00528
352	Cool Mist	15	0.001	Run 2	61.1567	117.5025	0.00547
353	Cool Mist	15	0.001	Run 3	62.3705	120.783	0.00518
354	Cool Mist	15	0.001	Run 4	63.5301	120.5455	0.00548
355	Cool Mist	15	0.001	Run 5	64.199	121.12	0.00558
356	Cool Mist	15	0.002	Run 1	85.1025	187.8264	0.00956
357	Cool Mist	15	0.002	Run 2	86.1069	189.8	0.00932
358	Cool Mist	15	0.002	Run 3	86.883	189.432	0.00938
359	Cool Mist	15	0.002	Run 4	82.936	185.5118	0.00963
360	Cool Mist	15	0.002	Run 5	82.9105	185.8108	0.00946
361	Cool Mist	15	0.003	Run 1	153.7815	277.4535	0.01353

Run No.	Environment	α	Feed	Run	Ft	Fc	tc
362	Cool Mist	15	0.003	Run 2	151.4303	274.1256	0.01328
363	Cool Mist	15	0.003	Run 3	156.5936	276.4732	0.0136
364	Cool Mist	15	0.003	Run 4	157.1355	277.2494	0.01309
365	Cool Mist	15	0.003	Run 5	159.999	279.3632	0.01303
366	Cool Mist	15	0.004	Run 1	187.335	341.0167	0.01809
367	Cool Mist	15	0.004	Run 2	181.2863	342.5107	0.01822
368	Cool Mist	15	0.004	Run 3	188.967	347.3744	0.01788
369	Cool Mist	15	0.004	Run 4	181.3638	342.7891	0.01809
370	Cool Mist	15	0.004	Run 5	186.9441	347.3383	0.01775
371	Cool Mist	15	0.005	Run 1	202.7457	419.7883	0.0236
372	Cool Mist	15	0.005	Run 2	209.5801	414.2354	0.02362
373	Cool Mist	15	0.005	Run 3	209.4235	415.6389	0.02341
374	Cool Mist	15	0.005	Run 4	211.2018	416.244	0.02326
375	Cool Mist	15	0.005	Run 5	212.4995	423.9621	0.02362
376	Cool Mist	30	0.001	Run 1	51.8232	111.6602	0.00384
377	Cool Mist	30	0.001	Run 2	50.7544	109.552	0.00388
378	Cool Mist	30	0.001	Run 3	51.1189	112.6215	0.00383
379	Cool Mist	30	0.001	Run 4	49.955	108.7509	0.00388
380	Cool Mist	30	0.001	Run 5	50.6559	110.5263	0.00382
381	Cool Mist	30	0.002	Run 1	55.3825	166.1258	0.007
382	Cool Mist	30	0.002	Run 2	57.7285	169.0374	0.00692
383	Cool Mist	30	0.002	Run 3	45.0762	158.2031	0.00705
384	Cool Mist	30	0.002	Run 4	47.4462	161.4845	0.007
385	Cool Mist	30	0.002	Run 5	46.0538	157.6917	0.00701
386	Cool Mist	30	0.003	Run 1	60.3193	218.0873	0.01036
387	Cool Mist	30	0.003	Run 2	63.5088	220.3345	0.01041
388	Cool Mist	30	0.003	Run 3	66.2184	223.8298	0.01045
389	Cool Mist	30	0.003	Run 4	67.4257	224.4799	0.01022
390	Cool Mist	30	0.003	Run 5	69.5599	224.3973	0.01055
391	Cool Mist	30	0.004	Run 1	189.3965	327.3907	0.01382
392	Cool Mist	30	0.004	Run 2	183.8052	324.5705	0.01378
393	Cool Mist	30	0.004	Run 3	187.4379	329.6599	0.01391
394	Cool Mist	30	0.004	Run 4	193.1028	328.3061	0.01384
395	Cool Mist	30	0.004	Run 5	187.2169	329.0382	0.01342
396	Cool Mist	30	0.005	Run 1	103.1147	345.305	0.01649
397	Cool Mist	30	0.005	Run 2	101.9503	346.1842	0.01632
398	Cool Mist	30	0.005	Run 3	94.5451	333.1663	0.01572
399	Cool Mist	30	0.005	Run 4	95.4506	334.7357	0.01666
400	Cool Mist	30	0.005	Run 5	97.1873	341.0194	0.01643

APPENDIX D

The classical metal cutting equations generally used in the study of the mechanics are as given below.

Chip Thickness ratio, $r_c = \frac{t}{t_c}$

Onset of Shear Plane Angle, $\phi = \tan^{-1}\left[\frac{r_c \times \cos\alpha}{1 - r_c \times \sin\alpha}\right]$

Friction Force, $F = F_c \times \sin\alpha + F_t \times \cos\alpha$

Normal Force, $N = F_c \times \cos\alpha + F_t \times \sin\alpha$

Friction Co-efficient, $\mu = \frac{F}{N}$

Resultant Force, $R = \sqrt{F_c^2 + F_t^2}$

Friction Angle, $\beta = \tan^{-1}\left[\frac{F}{N}\right]$

Shear Force along the onset of Shear Plane, $F_s = F_c \times \cos\phi - F_t \times \sin\phi$

Normal Force along the onset of Shear Plane, $F_n = F_c \times \sin\phi - F_t \times \cos\phi$

Shear Area, $A_s = \frac{t \times w}{\sin\phi}$

Shear Stress, $\tau_s = \frac{F_s}{A_s} = \frac{F_s \times \sin\phi}{t \times w}$

Horse Power, $HP = \frac{F_c \times V}{33{,}000}$

Material removal Rate, $MRR = \frac{\pi(D^2 - D_1^2)}{4} \times t \times w$

Specific Horse Power, $HP_s = \frac{HP}{MRR}$

Root Mean Square Deviation, $Rq = \sqrt{\frac{z_1^2 + z_2^2 + z_3^2 \ldots\ldots\ldots\ldots z_n^2}{n}}$

$\Delta R_q = (R_q)_{new} - (R_q)_{used}$

APPENDIX E

The Force Ratios calculated from the classical Metal Cutting equations using the raw data obtained from the experiments are tablulated below.

Run No.	F	N	F/N Ratio	Fs	Fn	Fs/Fn
1	144.4904	204.1855	0.7076	154.0374	197.0830	0.7816
2	184.1773	177.2929	1.0388	177.2929	184.1773	0.9626
3	177.9254	180.9517	0.9833	180.9517	177.9254	1.0170
4	189.0791	181.1614	1.0437	181.1614	189.0791	0.9581
5	194.356	185.0437	1.0503	185.0437	194.3560	0.9521
6	202.2132	303.195	0.6669	221.6816	289.2657	0.7664
7	257.8228	268.7747	0.9593	268.7747	257.8228	1.0425
8	258.6709	267.5613	0.9668	267.5613	258.6709	1.0344
9	262.6206	272.2441	0.9647	272.2441	262.6206	1.0366
10	264.2924	277.1065	0.9538	277.1065	264.2924	1.0485
11	247.4001	383.9302	0.6444	280.5633	360.4074	0.7785
12	327.1769	341.8487	0.9571	341.8487	327.1769	1.0448
13	304.3356	340.2505	0.8944	340.2505	304.3356	1.1180
14	313.9446	347.0742	0.9045	347.0742	313.9446	1.1055
15	301.7063	335.4178	0.8995	335.4178	301.7063	1.1117
16	279.3057	467.9808	0.5968	341.5569	424.6841	0.8043
17	350.0089	402.2674	0.8701	402.2674	350.0089	1.1493
18	370.2052	419.0703	0.8834	419.0703	370.2052	1.1320
19	364.9769	409.6705	0.8909	409.6705	364.9769	1.1225
20	375.6279	424.4903	0.8849	424.4903	375.6279	1.1301
21	318.5673	538.191	0.5919	387.0387	491.2592	0.7879
22	410.9808	475.7449	0.8639	475.7449	410.9808	1.1576
23	404.456	467.8064	0.8646	467.8064	404.4560	1.1566
24	415.8704	479.9004	0.8666	479.9004	415.8704	1.1540
25	416.2005	483.9898	0.8599	483.9898	416.2005	1.1629
26	178.7172	172.4828	1.0361	142.8156	203.2089	0.7028
27	175.5777	171.1007	1.0262	171.1007	175.5777	0.9745
28	175.7445	174.1149	1.0094	174.1149	175.7445	0.9907
29	173.5154	170.2533	1.0192	170.2533	173.5154	0.9812
30	170.9717	172.3044	0.9923	172.3044	170.9717	1.0078
31	223.7989	255.7188	0.8752	213.049	264.7417	0.8047
32	218.0048	250.2855	0.871	250.2855	218.0048	1.1481

Run No.	F	N	F/N Ratio	Fs	Fn	Fs/Fn
33	219.3895	254.1104	0.8634	254.1104	219.3895	1.1583
34	226.1762	264.9091	0.8538	264.9091	226.1762	1.1713
35	220.2374	255.4329	0.8622	255.4329	220.2374	1.1598
36	293.5401	323.8849	0.9063	254.7618	355.1952	0.7172
37	304.5111	329.6172	0.9238	329.6172	304.5111	1.0824
38	297.467	329.553	0.9026	329.553	297.4670	1.1079
39	292.9392	325.1263	0.901	325.1263	292.9392	1.1099
40	292.05	323.1182	0.9038	323.1182	292.0500	1.1064
41	360.526	414.8286	0.8691	324.5147	443.5673	0.7316
42	363.5965	399.0163	0.9112	399.0163	363.5965	1.0974
43	377.5881	399.5048	0.9451	399.5048	377.5881	1.0580
44	361.6405	411.0423	0.8798	411.0423	361.6405	1.1366
45	373.5652	403.9943	0.9247	403.9943	373.5652	1.0815
46	319.7004	460.565	0.6941	383.5295	408.9421	0.9379
47	327.1955	450.0505	0.727	450.0505	327.1955	1.3755
48	327.1843	459.6015	0.7119	459.6015	327.1843	1.4047
49	329.8673	448.3882	0.7357	448.3882	329.8673	1.3593
50	323.936	458.4112	0.7066	458.4112	323.9360	1.4151
51	89.9852	108.312	0.8308	114.9185	81.3790	1.4121
52	65.4667	120.879	0.5416	120.879	65.4667	1.8464
53	69.0838	114.2018	0.6049	114.2018	69.0838	1.6531
54	66.4581	122.6205	0.542	122.6205	66.4581	1.8451
55	66.4237	120.155	0.5528	120.155	66.4237	1.8089
56	156.0384	167.2594	0.9329	177.9194	143.7650	1.2376
57	113.0798	200.5681	0.5638	200.5681	113.0798	1.7737
58	114.3104	199.1714	0.5739	199.1714	114.3104	1.7424
59	118.0056	204.2604	0.5777	204.2604	118.0056	1.7309
60	118.1204	201.6331	0.5858	201.6331	118.1204	1.7070
61	194.5472	218.2454	0.8914	228.55	182.3310	1.2535
62	142.362	262.1011	0.5432	262.1011	142.3620	1.8411
63	153.4347	268.9463	0.5705	268.9463	153.4347	1.7528
64	148.8125	262.3391	0.5673	262.3391	148.8125	1.7629
65	151.5232	265.1171	0.5715	265.1171	151.5232	1.7497
66	284.7362	291.7525	0.976	307.181	268.0188	1.1461
67	201.9163	354.7528	0.5692	354.7528	201.9163	1.7569
68	207.3945	347.9605	0.596	347.9605	207.3945	1.6778
69	201.1935	339.4066	0.5928	339.4066	201.1935	1.6870
70	212.3329	348.3219	0.6096	348.3219	212.3329	1.6405
71	313.0896	340.6649	0.9191	352.0655	300.2126	1.1727
72	224.6541	411.051	0.5465	411.051	224.6541	1.8297
73	227.3489	405.2153	0.5611	405.2153	227.3489	1.7823
74	223.9582	407.5608	0.5495	407.5608	223.9582	1.8198
75	233.539	412.6333	0.566	412.6333	233.5390	1.7669
76	112.7831	68.8614	1.6378	103.6847	81.9232	1.2656
77	63.6391	116.4696	0.5464	116.4696	63.6391	1.8302
78	63.6573	117.28	0.5428	117.28	-63.6573	-1.8424
79	64.9941	118.6791	0.5476	118.6791	-64.9941	-1.826

Run No.	F	N	F/N Ratio	Fs	Fn	Fs/Fn
80	62.9518	115.4918	0.5451	115.4918	62.9518	1.8346
81	164.3796	122.2097	1.3451	167.9031	117.3218	1.4311
82	81.1605	176.7414	0.4592	176.7414	81.1605	2.1777
83	88.0791	178.6659	0.493	178.6659	88.0791	2.0285
84	90.344	181.2736	0.4984	181.2736	90.3440	2.0065
85	91.9134	182.55	0.5035	182.55	91.9134	1.9861
86	198.6521	158.3897	1.2542	205.1901	149.8231	1.3695
87	99.4893	239.5004	0.4154	239.5004	99.4893	2.4073
88	98.1772	238.2484	0.4121	238.2484	98.1772	2.4267
89	98.0449	242.13	0.4049	242.13	98.0449	2.4696
90	100.0638	239.2623	0.4182	239.2623	100.0638	2.3911
91	276.5192	205.7899	1.3437	266.3191	218.8299	1.2170
92	140.2462	323.6529	0.4333	323.6529	140.2462	2.3077
93	143.6655	315.2217	0.4558	315.2217	143.6655	2.1941
94	141.0172	322.3968	0.4374	322.3968	141.0172	2.2862
95	141.963	316.2296	0.4489	316.2296	141.9630	2.2275
96	244.9995	243.7751	1.005	295.7011	178.9187	1.6527
97	93.9447	333.7997	0.2814	333.7997	93.9447	3.5531
98	91.8477	339.6543	0.2704	339.6543	91.8477	3.6980
99	101.1709	335.6297	0.3014	335.6297	101.1709	3.3175
100	99.2913	343.7709	0.2888	343.7709	99.2913	3.4622
101	163.155	213.7201	0.7634	161.1101	215.2657	0.7484
102	201.2496	185.7809	1.0833	185.7809	201.2496	0.9231
103	199.8761	184.3276	1.0844	184.3276	199.8761	0.9222
104	199.5928	186.4235	1.0706	186.4235	199.5928	0.9340
105	200.8335	187.2002	1.0728	187.2002	200.8335	0.9321
106	206.7219	302.6463	0.683	223.3055	290.6258	0.7684
107	259.7657	260.5958	0.9968	260.5958	259.7657	1.0032
108	261.4814	264.5966	0.9882	264.5966	261.4814	1.0119
109	268.5294	271.2766	0.9899	271.2766	268.5294	1.0102
110	269.8701	274.0365	0.9848	274.0365	269.8701	1.0154
111	232.5042	370.7724	0.6271	269.7435	344.6286	0.7827
112	296.6442	324.1789	0.9151	324.1789	296.6442	1.0928
113	302.8356	329.6997	0.9185	329.6997	302.8356	1.0887
114	299.3754	331.8196	0.9022	331.8196	299.3754	1.1084
115	310.1497	340.834	0.91	340.834	310.1497	1.0989
116	266.0723	448.3648	0.5934	323.5304	408.8442	0.7913
117	347.7198	397.9039	0.8739	397.9039	347.7198	1.1443
118	354.7987	405.5534	0.8749	405.5534	354.7987	1.1431
119	358.8273	405.5811	0.8847	405.5811	358.8273	1.1303
120	359.2857	410.5226	0.8752	410.5226	359.2857	1.1426
121	316.458	522.4502	0.6057	370.3565	485.7324	0.7625
122	396.068	466.8819	0.8483	466.8819	396.0680	1.1788
123	407.5286	474.8292	0.8583	474.8292	407.5286	1.1651
124	402.6982	477.0524	0.8441	477.0524	402.6982	1.1846
125	399.2012	472.631	0.8446	472.631	399.2012	1.1839
126	162.9359	165.2332	0.9861	142.1853	183.3943	0.7753

Run No.	F	N	F/N Ratio	Fs	Fn	Fs/Fn
127	162.1041	165.1499	0.9816	165.1499	162.1041	1.0188
128	162.9914	165.581	0.9844	165.581	162.9914	1.0159
129	165.6891	166.338	0.9961	166.338	165.6891	1.0039
130	166.8184	168.7141	0.9888	168.7141	166.8184	1.0114
131	219.5647	261.0481	0.8411	224.903	256.4632	0.8769
132	213.2506	254.2292	0.8388	254.2292	213.2506	1.1922
133	215.2732	254.5406	0.8457	254.5406	215.2732	1.1824
134	220.1807	259.7471	0.8477	259.7471	220.1807	1.1797
135	213.1102	256.4842	0.8309	256.4842	213.1102	1.2035
136	306.661	331.6338	0.9247	266.7801	364.4864	0.7319
137	304.5306	333.9596	0.9119	333.9596	304.5306	1.0966
138	298.4483	337.417	0.8845	337.417	298.4483	1.1306
139	309.4737	345.7519	0.8951	345.7519	309.4737	1.1172
140	302.9238	342.2661	0.8851	342.2661	302.9238	1.1299
141	371.3089	412.5695	0.9	332.4675	444.4651	0.7480
142	379.8773	415.9003	0.9134	415.9003	379.8773	1.0948
143	378.5803	417.6269	0.9065	417.6269	378.5803	1.1031
144	374.1755	407.4259	0.9184	407.4259	374.1755	1.0889
145	377.5255	403.7149	0.9351	403.7149	377.5255	1.0694
146	322.9589	463.6449	0.6966	382.1987	416.1649	0.9184
147	328.9528	459.787	0.7154	459.787	328.9528	1.3977
148	337.3287	459.4949	0.7341	459.4949	337.3287	1.3622
149	328.9954	454.964	0.7231	454.964	328.9954	1.3829
150	337.7602	463.6962	0.7284	463.6962	337.7602	1.3729
151	88.7104	93.4059	0.9497	99.9529	81.2626	1.2300
152	63.2416	114.0435	0.5545	114.0435	63.2416	1.8033
153	64.4127	116.2906	0.5539	116.2906	64.4127	1.8054
154	65.1112	117.1496	0.5558	117.1496	65.1112	1.7992
155	66.058	117.3281	0.563	117.3281	66.0580	1.7761
156	152.7422	163.485	0.9343	171.7785	143.3516	1.1983
157	104.2617	190.4033	0.5476	190.4033	104.2617	1.8262
158	112.199	195.5409	0.5738	195.5409	112.1990	1.7428
159	114.3065	199.6868	0.5724	199.6868	114.3065	1.7469
160	119.2931	200.8401	0.594	200.8401	119.2931	1.6836
161	195.7189	210.8054	0.9284	218.5745	187.0027	1.1688
162	143.1355	265.2779	0.5396	265.2779	143.1355	1.8533
163	142.515	265.0369	0.5377	265.0369	142.5150	1.8597
164	144.0262	265.7019	0.5421	265.7019	144.0262	1.8448
165	145.1991	268.8831	0.54	268.8831	145.1991	1.8518
166	245.2068	269.6919	0.9092	273.7338	240.6864	1.1373
167	163.5994	323.5697	0.5056	323.5697	163.5994	1.9778
168	165.446	323.5697	0.5113	323.5697	165.4460	1.9557
169	172.0612	329.7176	0.5218	329.7176	172.0612	1.9163
170	167.4072	326.1765	0.5132	326.1765	167.4072	1.9484
171	247.9751	309.7016	0.8007	311.0038	246.3400	1.2625
172	167.9498	372.6552	0.4507	372.6552	167.9498	2.2188
173	169.5887	372.6489	0.4551	372.6489	169.5887	2.1974

Run No.	F	N	F/N Ratio	Fs	Fn	Fs/Fn
174	167.1795	376.4682	0.4441	376.4682	167.1795	2.2519
175	170.1	375.4764	0.453	375.4764	170.1000	2.2074
176	70.6428	62.4051	1.132	78.6263	51.9876	1.5124
177	33.7425	91.2695	0.3697	91.2695	33.7425	2.7049
178	32.2379	95.873	0.3363	95.873	32.2379	2.9739
179	35.996	95.9412	0.3752	95.9412	35.9960	2.6653
180	38.689	94.1467	0.4109	94.1467	38.6890	2.4334
181	113.3678	107.4873	1.0547	132.6994	82.4417	1.6096
182	47.7565	152.4468	0.3133	152.4468	47.7565	3.1922
183	50.2597	155.6077	0.323	155.6077	50.2597	3.0961
184	50.2975	155.8898	0.3226	155.8898	50.2975	3.0994
185	51.8714	156.5935	0.3312	156.5935	51.8714	3.0189
186	162.8985	154.9715	1.0512	186.3179	125.8480	1.4805
187	61.2472	210.745	0.2906	210.745	61.2472	3.4409
188	64.6666	211.8868	0.3052	211.8868	64.6666	3.2766
189	69.2517	216.0162	0.3206	216.0162	69.2517	3.1193
190	70.628	217.1014	0.3253	217.1014	70.6280	3.0739
191	223.1166	201.1148	1.1094	246.6438	171.4498	1.4386
192	88.1638	279.4771	0.3155	279.4771	88.1638	3.1700
193	86.1354	277.423	0.3105	277.423	86.1354	3.2208
194	86.2464	281.964	0.3059	281.964	86.2464	3.2693
195	91.2761	287.9853	0.3169	287.9853	91.2761	3.1551
196	259.2312	230.2289	1.126	286.2171	195.6679	1.4628
197	107.6019	325.5716	0.3305	325.5716	107.6019	3.0257
198	108.0435	331.8501	0.3256	331.8501	108.0435	3.0714
199	112.4562	336.0007	0.3347	336.0007	112.4562	2.9878
200	102.807	322.619	0.3187	322.619	102.8070	3.1381
201	169.5545	228.4957	0.742	173.6316	225.4131	0.7703
202	207.1426	192.6893	1.075	192.6893	207.1426	0.9302
203	202.68	194.1392	1.044	194.1392	202.6800	0.9579
204	217.7624	200.6148	1.0855	200.6148	217.7624	0.9213
205	214.5732	198.1373	1.083	198.1373	214.5732	0.9234
206	234.4741	326.8637	0.7173	237.7651	324.4777	0.7328
207	287.13	282.1961	1.0175	282.1961	287.1300	0.9828
208	292.2072	285.1416	1.0248	285.1416	292.2072	0.9758
209	284.7899	279.5205	1.0189	279.5205	284.7899	0.9815
210	289.2702	279.558	1.0347	279.558	289.2702	0.9664
211	309.3758	456.3637	0.6779	331.7829	440.3423	0.7535
212	373.3497	398.0761	0.9379	398.0761	373.3497	1.0662
213	382.5961	385.8474	0.9916	385.8474	382.5961	1.0085
214	382.5391	391.1423	0.978	391.1423	382.5391	1.0225
215	379.7901	396.6776	0.9574	396.6776	379.7901	1.0445
216	287.0673	496.7286	0.5779	364.9637	442.6607	0.8245
217	373.8964	424.6515	0.8805	424.6515	373.8964	1.1357
218	381.3443	437.8459	0.871	437.8459	381.3443	1.1482
219	390.1037	439.4337	0.8877	439.4337	390.1037	1.1265
220	377.0451	433.2095	0.8704	433.2095	377.0451	1.1490

Run No.	F	N	F/N Ratio	Fs	Fn	Fs/Fn
221	303.5935	556.7616	0.5453	401.4681	490.8930	0.8178
222	373.1608	478.6916	0.7795	478.6916	373.1608	1.2828
223	378.8455	472.3057	0.8021	472.3057	378.8455	1.2467
224	382.9149	474.1717	0.8075	474.1717	382.9149	1.2383
225	392.4226	487.8136	0.8045	487.8136	392.4226	1.2431
226	164.5504	184.5599	0.8916	163.1351	185.8121	0.8780
227	163.1026	182.9984	0.8913	182.9984	163.1026	1.1220
228	159.9201	178.6047	0.8954	178.6047	159.9201	1.1168
229	161.9422	182.6511	0.8866	182.6511	161.9422	1.1279
230	163.0827	181.1829	0.9001	181.1829	163.0827	1.1110
231	233.1829	271.1694	0.8599	233.0307	271.3002	0.8589
232	234.9983	266.0591	0.8833	266.0591	234.9983	1.1322
233	242.5081	275.9159	0.8789	275.9159	242.5081	1.1378
234	236.4188	270.1852	0.875	270.1852	236.4188	1.1428
235	237.9905	274.003	0.8686	274.003	237.9905	1.1513
236	279.5769	346.4283	0.807	291.6152	336.3575	0.8670
237	279.0627	343.8411	0.8116	343.8411	279.0627	1.2321
238	281.6154	342.3731	0.8225	342.3731	281.6154	1.2157
239	275.8128	342.3738	0.8056	342.3738	275.8128	1.2413
240	279.2154	342.2708	0.8158	342.2708	279.2154	1.2258
241	334.6459	425.5195	0.7864	350.2322	412.7858	0.8485
242	331.8301	416.7075	0.7963	416.7075	331.8301	1.2558
243	335.0354	424.1981	0.7898	424.1981	335.0354	1.2661
244	328.8234	420.35	0.7823	420.35	328.8234	1.2783
245	326.9944	424.9836	0.7694	424.9836	326.9944	1.2997
246	430.5991	484.6631	0.8885	386.2096	520.7264	0.7417
247	427.0402	488.0082	0.8751	488.0082	427.0402	1.1428
248	417.6366	483.0138	0.8646	483.0138	417.6366	1.1565
249	424.0487	490.4496	0.8646	490.4496	424.0487	1.1566
250	417.0269	487.2506	0.8559	487.2506	417.0269	1.1684
251	110.2801	107.5452	1.0254	118.2208	98.7498	1.1972
252	77.7225	130.8423	0.594	130.8423	77.7225	1.6835
253	78.8442	129.2723	0.6099	129.2723	78.8442	1.6396
254	76.9546	133.4419	0.5767	133.4419	76.9546	1.7340
255	77.8638	129.4782	0.6014	129.4782	77.8638	1.6629
256	202.375	175.2947	1.1545	192.0853	186.5131	1.0299
257	152.0043	220.2428	0.6902	220.2428	152.0043	1.4489
258	156.324	228.9791	0.6827	228.9791	156.3240	1.4648
259	149.3831	219.0391	0.682	219.0391	149.3831	1.4663
260	149.2316	219.1011	0.6811	219.1011	149.2316	1.4682
261	237.6644	238.273	0.9974	252.2228	222.8049	1.1320
262	163.8237	284.3597	0.5761	284.3597	163.8237	1.7358
263	166.1155	286.7002	0.5794	286.7002	166.1155	1.7259
264	169.8913	290.2186	0.5854	290.2186	169.8913	1.7083
265	170.3016	295.5275	0.5763	295.5275	170.3016	1.7353
266	331.9794	305.1023	1.0881	328.8548	308.4677	1.0661
267	243.4664	381.1891	0.6387	381.1891	243.4664	1.5657

Run No.	F	N	F/N Ratio	Fs	Fn	Fs/Fn
268	236.7358	376.3736	0.629	376.3736	236.7358	1.5898
269	240.0703	388.8308	0.6174	388.8308	240.0703	1.6197
270	247.0985	389.9095	0.6337	389.9095	247.0985	1.5780
271	327.375	357.4639	0.9158	367.9325	315.5638	1.1660
272	222.2084	427.8287	0.5194	427.8287	222.2084	1.9253
273	229.9665	428.6029	0.5365	428.6029	229.9665	1.8638
274	230.929	429.1843	0.5381	429.1843	230.9290	1.8585
275	233.4081	433.5332	0.5384	433.5332	233.4081	1.8574
276	75.5231	62.2963	1.2123	80.6946	55.4341	1.4557
277	34.379	93.6644	0.367	93.6644	34.3790	2.7245
278	36.4733	95.4205	0.3822	95.4205	36.4733	2.6162
279	37.0401	96.0515	0.3856	96.0515	37.0401	2.5932
280	31.39	92.8399	0.3381	92.8399	31.3900	2.9576
281	129.375	108.7244	1.1899	138.8432	96.3403	1.4412
282	58.8684	169.1589	0.348	169.1589	58.8684	2.8735
283	64.8787	166.0229	0.3908	166.0229	64.8787	2.5590
284	64.8416	167.4373	0.3873	167.4373	64.8416	2.5823
285	54.8339	171.6381	0.3195	171.6381	54.8339	3.1301
286	167.5055	149.9337	1.1172	191.4866	117.7756	1.6259
287	74.4158	219.5313	0.339	219.5313	74.4158	2.9501
288	76.2422	218.8497	0.3484	218.8497	76.2422	2.8705
289	74.3471	217.4577	0.3419	217.4577	74.3471	2.9249
290	83.6924	224.6447	0.3726	224.6447	83.6924	2.6842
291	197.1468	188.2939	1.047	236.0396	136.4065	1.7304
292	76.7912	262.8484	0.2922	262.8484	76.7912	3.4229
293	82.3925	270.9511	0.3041	270.9511	82.3925	3.2885
294	85.1815	271.8372	0.3134	271.8372	85.1815	3.1913
295	83.8936	269.3505	0.3115	269.3505	83.8936	3.2106
296	357.9019	228.4282	1.5668	302.7941	297.6389	1.0173
297	191.2584	369.0897	0.5182	369.0897	191.2584	1.9298
298	198.9184	369.0897	0.5389	369.0897	198.9184	1.8555
299	197.3296	364.3208	0.5416	364.3208	197.3296	1.8463
300	186.2928	369.2408	0.5045	369.2408	186.2928	1.9820
301	158.5647	227.7806	0.6961	175.8309	214.7329	0.8188
302	196.3354	192.175	1.0216	192.175	196.3354	0.9788
303	204.0934	201.2071	1.0143	201.2071	204.0934	0.9859
304	201.2784	193.76	1.0388	193.76	201.2784	0.9626
305	208.4875	202.2933	1.0306	202.2933	208.4875	0.9703
306	242.4013	337.6371	0.7179	249.2924	332.5815	0.7496
307	300.1617	291.3465	1.0303	291.3465	300.1617	0.9706
308	289.5194	286.3318	1.0111	286.3318	289.5194	0.9890
309	289.8274	286.5597	1.0114	286.5597	289.8274	0.9887
310	287.2581	293.0959	0.9801	293.0959	287.2581	1.0203
311	289.1253	431.7996	0.6696	308.9547	417.8412	0.7394
312	359.7902	373.8692	0.9623	373.8692	359.7902	1.0391

Run No.	F	N	F/N Ratio	Fs	Fn	Fs/Fn
313	349.0415	367.1384	0.9507	367.1384	349.0415	1.0518
314	356.6663	364.5413	0.9784	364.5413	356.6663	1.0221
315	349.8105	362.813	0.9642	362.813	349.8105	1.0372
316	295.0665	487.5075	0.6053	359.6964	441.9800	0.8138
317	386.0774	429.459	0.899	429.459	386.0774	1.1124
318	373.0587	428.976	0.8696	428.976	373.0587	1.1499
319	374.3297	435.5474	0.8594	435.5474	374.3297	1.1635
320	376.0092	429.0622	0.8764	429.0622	376.0092	1.1411
321	383.5387	610.5565	0.6282	436.8354	573.6341	0.7615
322	490.7619	544.2519	0.9017	544.2519	490.7619	1.1090
323	491.3546	544.1311	0.903	544.1311	491.3546	1.1074
324	491.4266	546.3741	0.8994	546.3741	491.4266	1.1118
325	491.3052	547.4965	0.8974	547.4965	491.3052	1.1144
326	152.4772	175.133	0.8706	153.6019	174.1474	0.8820
327	152.2068	180.9133	0.8413	180.9133	152.2068	1.1886
328	156.0352	179.9308	0.8672	179.9308	156.0352	1.1531
329	158.5667	179.1254	0.8852	179.1254	158.5667	1.1297
330	156.9991	176.181	0.8911	176.181	156.9991	1.1222
331	247.4289	279.3266	0.8858	240.1728	285.5896	0.8410
332	243.5632	275.3585	0.8845	275.3585	243.5632	1.1305
333	246.5875	278.1679	0.8865	278.1679	246.5875	1.1281
334	252.9061	282.2953	0.8959	282.2953	252.9061	1.1162
335	252.7687	284.098	0.8897	284.098	252.7687	1.1239
336	307.5088	364.4924	0.8437	307.9256	364.1404	0.8456
337	304.3039	358.126	0.8497	358.126	304.3039	1.1769
338	299.7853	355.6117	0.843	355.6117	299.7853	1.1862
339	298.1503	356.1509	0.8371	356.1509	298.1503	1.1945
340	306.4602	362.9809	0.8443	362.9809	306.4602	1.1844
341	335.8497	421.2274	0.7973	352.4936	407.4012	0.8652
342	335.8612	418.2116	0.8031	418.2116	335.8612	1.2452
343	334.4233	418.9726	0.7982	418.9726	334.4233	1.2528
344	338.8065	422.3275	0.8022	422.3275	338.8065	1.2465
345	338.8065	422.8405	0.8013	422.8405	338.8065	1.2480
346	462.9319	556.5036	0.8319	453.3699	564.3208	0.8034
347	463.8574	554.134	0.8371	554.134	463.8574	1.1946
348	461.594	546.7876	0.8442	546.7876	461.5940	1.1846
349	456.2306	559.0695	0.8161	559.0695	456.2306	1.2254
350	454.8527	541.429	0.8401	541.429	454.8527	1.1903
351	89.8206	97.8126	0.9183	104.3512	82.1333	1.2705
352	61.1567	117.5025	0.5205	117.5025	61.1567	1.9213
353	62.3705	120.783	0.5164	120.783	62.3705	1.9365
354	63.5301	120.5455	0.527	120.5455	63.5301	1.8975
355	64.199	121.12	0.53	121.12	64.1990	1.8866
356	130.8158	159.4002	0.8207	165.649	122.8072	1.3489
357	86.1069	189.8	0.4537	189.8	86.1069	2.2042
358	86.883	189.432	0.4587	189.432	86.8830	2.1803

Run No.	F	N	F/N Ratio	Fs	Fn	Fs/Fn
359	82.936	185.5118	0.4471	185.5118	82.9360	2.2368
360	82.9105	185.8108	0.4462	185.8108	82.9105	2.2411
361	220.3518	228.1979	0.9656	235.667	212.3447	1.1098
362	151.4303	274.1256	0.5524	274.1256	151.4303	1.8102
363	156.5936	276.4732	0.5664	276.4732	156.5936	1.7655
364	157.1355	277.2494	0.5668	277.2494	157.1355	1.7644
365	159.999	279.3632	0.5727	279.3632	159.9990	1.7460
366	269.2133	280.911	0.9584	290.9219	258.3626	1.1260
367	181.2863	342.5107	0.5293	342.5107	181.2863	1.8893
368	188.967	347.3744	0.544	347.3744	188.9670	1.8383
369	181.3638	342.7891	0.5291	342.7891	181.3638	1.8901
370	186.9441	347.3383	0.5382	347.3383	186.9441	1.8580
371	304.4865	353.0099	0.8625	367.1155	287.3226	1.2777
372	209.5801	414.2354	0.5059	414.2354	209.5801	1.9765
373	209.4235	415.6389	0.5039	415.6389	209.4235	1.9847
374	211.2018	416.244	0.5074	416.244	211.2018	1.9708
375	212.4995	423.9621	0.5012	423.9621	212.4995	1.9951
376	100.7103	70.789	1.4227	95.1356	78.1208	1.2178
377	50.7544	109.552	0.4633	109.552	50.7544	2.1585
378	51.1189	112.6215	0.4539	112.6215	51.1189	2.2031
379	49.955	108.7509	0.4594	108.7509	49.9550	2.1770
380	50.6559	110.5263	0.4583	110.5263	50.6559	2.1819
381	131.0256	116.1779	1.1278	144.2305	99.3104	1.4523
382	57.7285	169.0374	0.3415	169.0374	57.7285	2.9281
383	45.0762	158.2031	0.2849	158.2031	45.0762	3.5097
384	47.4462	161.4845	0.2938	161.4845	47.4462	3.4035
385	46.0538	157.6917	0.292	157.6917	46.0538	3.4241
386	161.2817	158.7095	1.0162	192.4396	119.0273	1.6168
387	63.5088	220.3345	0.2882	220.3345	63.5088	3.4694
388	66.2184	223.8298	0.2958	223.8298	66.2184	3.3802
389	67.4257	224.4799	0.3004	224.4799	67.4257	3.3293
390	69.5599	224.3973	0.31	224.3973	69.5599	3.2260
391	327.7175	188.8304	1.7355	260.4949	274.2228	0.9499
392	183.8052	324.5705	0.5663	324.5705	183.8052	1.7658
393	187.4379	329.6599	0.5686	329.6599	187.4379	1.7588
394	193.1028	328.3061	0.5882	328.3061	193.1028	1.7002
395	187.2169	329.0382	0.569	329.0382	187.2169	1.7575
396	261.9524	247.4856	1.0585	298.6957	201.6161	1.4815
397	101.9503	346.1842	0.2945	346.1842	101.9503	3.3956
398	94.5451	333.1663	0.2838	333.1663	94.5451	3.5239
399	95.4506	334.7357	0.2852	334.7357	95.4506	3.5069
400	97.1873	341.0194	0.285	341.0194	97.1873	3.5089

APPENDIX F

The effective tool surface roughness calculated using data obtained from the profilometer, the Chip thickness ratio, Shear Plane Angle, Shear Front angle, Friction angle, Shear Area and Shear Stress calculated from the classical Metal Cutting equations using the raw data obtained from the experiments are tablulated below.

Run No.	Roughness(μm)	t/tc	Φ (degrees)	β (degrees)	A_s (inch^2)	τ_s (MPa)
1	154.942318	0.121892	6.704454207	35.2848498	0.0010707	254.35318
2				46.09109792		
3				44.5168538		
4				46.22510005		
5				46.40603269		
6	161.1517652	0.162259	8.83393002	33.70095615	0.0016279	248.96012
7				43.80856404		
8				44.03211179		
9				43.9692226		
10				43.64414797		
11	169.620113	0.171292	9.303365676	32.79725047	0.0023197	219.85956
12				43.74369905		
13				41.81090436		
14				42.13079373		
15				41.9711911		
16	164.004236	0.191847	10.36155416	30.83008201	0.00278	222.69739
17				41.02620866		
18				41.45726363		
19				41.69795712		
20				41.50534539		
21	172.25711	0.207245	11.14494369	30.6222396	0.0032335	219.97836
22				40.82268516		
23				40.84603361		
24				40.91143225		
25				40.69343989		
26	57.234495	0.156299	8.883390955	46.01699116	0.0008095	318.0925
27				45.73987577		
28				45.26687443		
29				45.54367647		
30				44.77756185		

Run No.	Roughness(μm)	t/tc	Φ (degrees)	β (degrees)	A_s (inch^2)	τ_s (MPa)
31				41.19162882		
32				41.05666261		
33	53.159259	0.176025	9.98323796	40.8061092	0.0014421	266.08323
34				40.49030077		
35				40.76831763		
36				42.18632849		
37				42.73275743		
38	58.699539	0.215548	12.16389917	42.07060344	0.0017797	272.10987
39				42.01889115		
40				42.10881411		
41				40.99378438		
42				42.34078987		
43	65.485074	0.227505	12.816942	43.38448966	0.0022539	266.56076
44				41.34174946		
45				42.75892418		
46				34.76638147		
47				36.01788354		
48	84.619697	0.21384	12.07032234	35.44656672	0.0029888	228.18156
49				36.34093095		
50				35.24691529		
51				39.71967382		
52				28.4394782		
53	35.1411615	0.18423	10.58436298	31.17087907	0.0006805	270.02966
54				28.45687613		
55				28.93456114		
56				43.01217718		
57				29.41419657		
58	37.817199	0.190042	10.92721737	29.85279808	0.0013188	231.19109
59				30.01594471		
60				30.36256106		
61				41.71428606		
62				28.50889896		
63	43.691054	0.205959	11.86763239	29.70489255	0.0018235	218.80615
64				29.5641814		
65				29.74939623		
66				44.30271024		
67				29.64743485		
68	53.175756	0.204855	11.80234505	30.79616222	0.0024446	215.28004
69				30.65862121		
70				31.36598967		
71				42.58470373		
72				28.65818527		
73	54.113999	0.222896	12.8701278	29.29491121	0.0028059	219.69272
74				28.78917684		
75				29.50865716		

Run No.	Roughness(μm)	t/tc	Φ (degrees)	β (degrees)	A_s (inch^2)	τ_s (MPa)
76	116.491447	0.179986	9.719680126	58.5932362	0.0007404	239.32775
77				28.65223424		
78				28.49222898		
79				28.70710918		
80				28.59372273		
81	137.235826	0.211461	11.57316922	53.3706542	0.0012461	220.69079
82				24.66481459		
83				26.24246689		
84				26.4909587		
85				26.72512571		
86	142.468258	0.263112	14.70181433	51.43387331	0.0014776	244.27549
87				22.55817056		
88				22.39552793		
89				22.04434714		
90				22.6955593		
91	135.535181	0.285144	16.06656599	53.34280063	0.0018067	264.90069
92				23.42818756		
93				24.50160964		
94				23.62469373		
95				24.17644769		
96	149.38949	0.284608	16.03318923	45.14351729	0.0022629	225.83987
97				15.71874978		
98				15.13175104		
99				16.77470165		
100				16.11029953		
101	118.496228	0.105574	5.829622051	37.35830095	0.0012307	227.92588
102				47.28875955		
103				47.31746222		
104				46.95394022		
105				47.01222052		
106	133.933197	0.148765	8.127782915	34.33494855	0.0017683	226.82207
107				44.90859972		
108				44.66072384		
109				44.70841079		
110				44.56111497		
111	110.688898	0.182039	9.858404852	32.09103038	0.0021902	225.93223
112				42.46048613		
113				42.56808022		
114				42.05751601		
115				42.30134468		
116	126.345719	0.203562	10.95831878	30.68608481	0.0026303	229.01087
117				41.14952263		
118				41.18108185		
119				41.49995673		
120				41.19212386		

Run No.	Roughness(μm)	t/tc	(degrees)	(degrees)	As	Ts
121	113.423296	0.213712	11.47147953	31.20408077	0.0031426	223.10984
122				40.30880414		
123				40.63829025		
124				40.16899295		
125				40.18564309		
126	19.352671	0.13369	7.614711942	44.59891579	0.0009433	265.52076
127				44.46675534		
128				44.54844023		
129				44.88802365		
130				44.6762923		
131	24.915753	0.152742	8.684335384	40.06682403	0.0016557	234.01789
132				39.99034048		
133				40.22227919		
134				40.28705667		
135				39.72285881		
136	33.139799	0.195084	11.03883918	42.7594888	0.0019585	257.40035
137				42.3610167		
138				41.49304171		
139				41.83091193		
140				41.51054659		
141	38.858533	0.198295	11.21595131	41.98693244	0.0025706	238.43237
142				42.40812283		
143				42.19242117		
144				42.56402744		
145				43.08000153		
146	49.853782	0.223095	12.57643961	34.85972652	0.0028704	239.77567
147				35.5816763		
148				36.28348575		
149				35.87159574		
150				36.06990863		
151	32.636596	0.184298	10.58836712	43.5230622	0.0006803	257.36627
152				29.01007802		
153				28.98179965		
154				29.06511571		
155				29.3803564		
156	30.554164	0.204666	11.79118859	43.05430474	0.0012234	242.80984
157				28.70438441		
158				29.8466818		
159				29.7880701		
160				30.70906352		
161	37.8082255	0.219587	12.67416333	42.87467325	0.0017092	232.79172
162				28.34988487		
163				28.26770075		
164				28.46032117		
165				28.36941354		

Run No.	Roughness(µm)	t/tc	(degrees)	(degrees)	As	Ts
166	42.3096365	0.242748	14.04679692	42.27745102	0.00206	237.27695
167				26.82152185		
168				27.08133603		
169				27.55754097		
170				27.16876053		
171	46.1084783	0.25373	14.69812596	38.68392024	0.0024633	227.56587
172				24.26033583		
173				24.46979594		
174				23.94473221		
175				24.37169004		
176	121.240644	0.266809	14.92963965	48.54295922	0.0004852	291.26065
177				20.28945305		
178				18.58555156		
179				20.56549311		
180				22.33990008		
181	125.14415	0.273224	15.32609707	46.52520894	0.0009459	246.87197
182				17.39404798		
183				17.89991409		
184				17.88218123		
185				18.32739056		
186	118.718115	0.309725	17.60841967	46.42855131	0.0012396	260.5954
187				16.2050536		
188				16.97187965		
189				17.77510871		
190				18.0208893		
191	117.246707	0.297442	16.83552537	47.96885199	0.0017264	246.6355
192				17.50838508		
193				17.24873959		
194				17.00767905		
195				17.58585984		
196	113.104302	0.283543	15.96683921	48.39102061	0.0022721	218.61285
197				18.28880409		
198				18.03417339		
199				18.50489775		
200				17.67519805		
201	52.118844	0.10533	5.81644704	36.5771382	0.0012334	241.07724
202				47.0702517		
203				46.23299541		
204				47.34701011		
205				47.28055825		
206	57.687602	0.1485	8.113851469	35.65358416	0.0017713	238.75172
207				45.49652487		
208				45.70115128		
209				45.53499919		
210				45.97817584		

Run No.	Roughness(μm)	t/tc	(degrees)	(degrees)	As	Ts
211	93.959022	0.162937	8.869287411	34.13393102	0.0024322	242.61655
212				43.16413518		
213				44.75758184		
214				44.36290735		
215				43.75406285		
216	110.938971	0.193986	10.47090273	30.02429158	0.0027512	236.63271
217				41.36321563		
218				41.05441531		
219				41.59680663		
220				41.03477238		
221	131.161133	0.226634	12.11963791	28.60295374	0.0029768	241.0205
222				37.93795612		
223				38.73377128		
224				38.92242908		
225				38.81500604		
226	19.937807	0.12276	6.99859315	41.71964144	0.0010259	268.50532
227				41.70994256		
228				41.84081167		
229				41.56085238		
230				41.99037291		
231	17.636055	0.152068	8.646617757	40.69276358	0.0016629	245.92637
232				41.45274501		
233				41.31289647		
234				41.18673587		
235				40.97656697		
236	27.020858	0.179404	10.17091464	38.90445738	0.0021236	242.68349
237				39.06291105		
238				39.43864681		
239				38.85456006		
240				39.20664911		
241	14.950266	0.203521	11.50377489	38.18295517	0.0025071	251.80642
242				38.53080781		
243				38.30199033		
244				38.03468489		
245				37.57570096		
246	23.386262	0.209223	11.81710815	41.61950008	0.0030519	237.1712
247				41.18812113		
248				40.84824563		
249				40.84709285		
250				40.55947967		
251	20.5794515	0.159898	9.152670309	45.71933637	0.0007858	252.96485
252				30.71101543		
253				31.37932982		
254				29.9715998		
255				31.02125831		

Run No.	Roughness(μm)	t/tc	(degrees)	(degrees)	As	Ts
256	23.3734121	0.175254	10.05549407	49.10129007	0.0014318	233.70773
257				34.61215505		
258				34.32134804		
259				34.29370822		
260				34.25910613		
261	20.6853593	0.20024	11.52953691	44.92673638	0.0018762	232.81205
262				29.9468613		
263				30.0882126		
264				30.34431365		
265				29.95326133		
266	20.7577006	0.187073	10.75205775	47.41575244	0.0026801	215.73722
267				32.5664694		
268				32.16954441		
269				31.69183965		
270				32.36378236		
271	20.8684733	0.227355	13.13433213	42.48428541	0.0027505	235.23231
272				27.44675008		
273				28.21574245		
274				28.28313444		
275				28.29738964		
276	71.088548	0.251762	14.00557088	50.48199183	0.0005165	275.29501
277				20.15539787		
278				20.91871662		
279				21.08799022		
280				18.68083078		
281	79.01599	0.26469	14.79902697	49.95691006	0.0009787	257.53574
282				19.18822072		
283				21.3446422		
284				21.16935148		
285				17.71731102		
286	97.07791	0.242248	13.42561044	48.16836424	0.0016151	205.75187
287				18.72541568		
288				19.20715874		
289				18.87515773		
290				20.4331013		
291	106.87934	0.246883	13.70771943	46.31575535	0.00211	192.6175
292				16.28572723		
293				16.9137869		
294				17.39863067		
295				17.30005457		
296	107.649215	0.300951	17.05583469	57.45224505	0.0021309	258.15728
297				27.39271565		
298				28.32214753		
299				28.44161136		
300				26.77228235		

Run No.	Roughness(μm)	t/tc	(degrees)	(degrees)	As	Ts
301	121.806137	0.105865	5.845269409	34.84289847	0.0012274	243.7968
302				45.61353377		
303				45.40801828		
304				46.09032587		
305				45.86390265		
306	115.622348	0.136295	7.470094597	35.67586264	0.0019229	226.76377
307				45.85381127		
308				45.31715513		
309				45.32482235		
310				44.4236793		
311	129.862754	0.179254	9.714966585	33.80555492	0.0022223	247.93154
312				43.90062299		
313				43.55252096		
314				44.37440158		
315				43.95469948		
316	108.54511	0.178492	9.675640327	31.18464826	0.0029749	217.02949
317				41.95508114		
318				41.01183172		
319				40.67729674		
320				41.22974519		
321	103.904811	0.196002	10.57373429	32.13616906	0.003406	238.38043
322				42.04155916		
323				42.08228092		
324				41.96924183		
325				41.90375002		
326	15.744253	0.132415	7.542953922	41.04402325	0.0009522	283.14689
327				40.07472539		
328				40.93168557		
329				41.51613203		
330				41.70499515		
331	21.373276	0.14771	8.402429902	41.53468336	0.0017109	246.44243
332				41.49376414		
333				41.55602605		
334				41.85690719		
335				41.66024506		
336	37.702539	0.169645	9.628268605	40.15309215	0.0022421	240.69029
337				40.35494988		
338				40.13132544		
339				39.9342506		
340				40.17398099		
341	27.113344	0.18655	10.56705068	38.56577913	0.0027265	231.36113
342				38.76756981		
343				38.59681483		
344				38.7378555		
345				38.70391014		

Run No.	Roughness(µm)	t/tc	(degrees)	(degrees)	As	Ts
346	21.472416	0.20284	11.46629484	39.75564374	0.003144	261.76429
347				39.93220429		
348				40.17080691		
349				39.21628381		
350				40.03350653		
351	23.5926107	0.185254	10.64474123	42.56104242	0.0006767	267.67096
352				27.49569151		
353				27.31114832		
354				27.79020572		
355				27.92556918		
356	30.7779982	0.211193	12.17726827	39.37486468	0.0011852	239.64441
357				24.40244384		
358				24.63857018		
359				24.0877774		
360				24.04687895		
361	29.6081105	0.225462	13.02215933	43.99786953	0.0016642	250.13986
362				28.91679199		
363				29.52708703		
364				29.54308487		
365				29.80095548		
366	30.247557	0.222148	12.82583963	43.78186721	0.0022524	229.97571
367				27.89166617		
368				28.5455959		
369				27.88254479		
370				28.28998527		
371	37.3319742	0.212748	12.26926654	40.77920915	0.0029411	214.72721
372				26.83687613		
373				26.74167247		
374				26.90319282		
375				26.62107593		
376	80.090936	0.25974	14.49449315	54.89672427	0.0004994	333.06602
377				24.85781941		
378				24.4132774		
379				24.67182121		
380				24.6226962		
381	81.766506	0.285878	16.1122984	48.43719405	0.0009008	272.08272
382				18.85569715		
383				15.90364506		
384				16.37345565		
385				16.2804337		
386	97.385863	0.288517	16.27697499	45.46054437	0.0013379	251.50532
387				16.07899756		
388				16.48045914		
389				16.71838305		
390				17.22267609		

Run No.	Roughness(μm)	t/tc	(degrees)	(degrees)	As	Ts
391	127.930611	0.290824	16.42113251	60.04950995	0.0017687	275.53886
392				29.52299472		
393				29.62167771		
394				30.46315721		
395				29.63910855		
396	97.068583	0.306297	17.39225545	46.62663458	0.0020909	245.1935
397				16.40955704		
398				15.84274896		
399				15.91561355		
400				15.90704706		

APPENDIX F

The Flow stress and Specific Horse power calculations are as shown below.

Velocity of Cut, V = 500 SFM

Width of cut, w = 0.125 inch

Uncut chip thickness, t = 0.001 inch

Rake Angle, $\alpha = 0^o$

Shear Angle, $\varphi = 8.8834^o$

Cutting Force, Fc = 172.4828 N = 38.7756 lbs

Thrust Force, Ft = 178.7172 N = 40.1772 lbs

Flow Stress, $\tau = \frac{(F_t.\cos(\phi).\sin(\phi) - F_c \sin^2(\phi)}{t.w}$ = 41641.8558 psi

Spindle Horse Power, HP = $\frac{F_c.V}{33,000}$ = 0.58750909

Material Removal Rate, MRR = $\frac{\pi.(D^2 - D_1^2)}{4}.t.N$ = 0.7226 $inch^3$/min.

Specific Horse Power = HP_s = $\frac{SpindleHP}{MRR}$ = 0.8130488 hp/$inch^3$/min.

Rake Angle, $\alpha = 15^o$

Shear Angle, $\varphi = 10.5844^o$

Cutting Force, Fc = 122.6205 N = 27.5661 lbs

Thrust Force, Ft = 66.4581 N = 14.9403 lbs

Flow Stress, $\tau = \dfrac{(F_t.\cos(\phi).\sin(\phi) - F_c \sin^2(\phi)}{t.w}$ = 14140.1440 psi

Spindle Horse Power, HP = $\dfrac{F_c.V}{33{,}000}$ = 0.41766818

Material Removal Rate, MRR = $\dfrac{\pi.(D^2 - D_1^2)}{4}.t.N$ = 0.72266 inch^3/min.

Specific Horse Power = HP$_s$ = $\dfrac{SpindleHP}{MRR}$ = 0.577959 hp/inch^3/min.

APPENDIX G

<u>Sample Calculations</u>:

These sample calculations are provided using the data in Run 1 (or page 88) to illustrate the exact method for data reproduction.

Friction Force, $F = F_c \times \sin\alpha + F_t \times \cos\alpha$

$$F = 175.993 \times \sin(-10) + 177.7517 \times \cos(-10) = 144.4904 \text{ N}$$

Normal Force, $N = F_c \times \cos\alpha - F_t \times \sin\alpha$

$$N = 175.993 \times \cos(-10) - 177.7517 \times \sin(-10) = 204.1855 \text{ N}$$

Shear Force along the onset of Shear Plane, $F_s = F_c \times \cos\phi - F_t \times \sin\phi$

$$F_s = 175.993 \times \cos(6.7) - 177.7517 \times \sin(6.7) = 154.0374 \text{ N}$$

Normal Force along the onset of Shear Plane, $F_n = F_c \times \sin\phi + F_t \times \cos\phi$

$$F_n = 175.993 \times \sin(6.7) + 177.7517 \times \cos(6.7) = 197.0830 \text{ N}$$

Onset of Shear Plane Angle, $\phi = \tan^{-1}\left[\dfrac{r_c \times \cos\alpha}{1 - r_c \times \sin\alpha}\right]$

$$\phi = \tan^{-1}\left[\frac{0.12189 \times \cos(-10)}{1 - 0.12189 \times \sin(-10)}\right] = 6.704454^{\circ}$$

Friction Angle, $\beta = \tan^{-1}\left[\dfrac{F}{N}\right]$

$$\beta = \tan^{-1}\left[\frac{144.4904}{204.1855}\right] = 35.284849^{\circ}$$

Shear Area, $A_s = \frac{t \times w}{\sin\phi}$; $A_s = \frac{0.001 \times 0.125}{\sin(6.704454)}$ = 0.0010707 inch^2

Shear Stress, $\tau_s = \frac{F_s}{A_s} = \frac{F_s \times \sin\phi}{t \times w}$;

$$\tau_s = \frac{154.0374}{0.0010107} = 152406.6489 \text{ N/inch}^2 = \quad 254.35318 \text{ MPa}$$